CALCULATION OF THE STRUCTURE-FORCE RELATIONSHIP IN CORTICAL BONE

by

PATRICIA CANTY
B.A., Emmanuel College, Boston
1971

SUBMITTED IN PARTIAL FULFILLMENT

OF THE REQUIREMENTS FOR THE

DEGREE OF MASTER OF

SCIENCE

at the

MASSACHUSETTS INSTITUTE OF

TECHNOLOGY

February, 1977

Signature of Author_____
Department of Physics,
February 1, 1977

Certified by_____
Thesis Supervisor

Accepted by_____
Chairman, Departmental
Committee

CALCULATION OF THE STRUCTURE-FORCE RELATIONSHIP IN CORTICAL BONE

by

Patricia Canty

Submitted to the Department of Physics on February 1, 1977, in partial fulfillment of the requirements for the degree of Master of Science

ABSTRACT

To determine a muscle-force to bone geometry correlation, forearm (ulna) bone specimens taken from three cadavers were prepared for study. Measurements were made of key geometrical and physical parameters. The bone was mathematically modeled as a hollow cylinder beam of variable cross-section and of perfectly elastic material. Structural analysis of the ulna as a beam under various muscle-force loadings lead to the derivation of force-geometry dependent relationships. The experimental method used is described. The appropriate elastic beam bending theory is discussed and correlation equations are derived. Similarities between the normalized graphs of theoretical predictions and the experimental results are indicative of first order model validity. Results are presented and suggestions for extending the approach adopted are cited.

Thesis Supervisor: Margaret L. A. MacVicar
Title: Associate Professor of Physics

Table of Contents

List of Figures

Page

Page

List of Tables

I. Introduction

Since 1867, the relationship between the form a bone assumes and the bone's function has been the subject of continuing study. Wolff's Law (1892) is a fundamental statement of this relationship and states that bone structure remodels to reflect the forces acting upon the bone.[1] Many researchers have verified this observation qualitatively, among them are Roux, Pauwels, and Kummer. Roux concluded that the Law of Maximal Economy of Building Material is applicable to bone. This law, which is usually applied to the design of machines, states that a machine is constructed with a minimum of material in order to improve its efficiency in work output by reducing energy loss due to friction and weight.[2] The application of this law to the skeletal system implies that the gross shape (volume distribution of material and cross-sectional area) and the internal structure of bone adapt in order to withstand stresses with a minimum of material.

Pauwels verified Roux's Law by applications in design engineering and photoelastic surveys. He found that any building material could be "economized" by two means. The first method is to diminish stresses in a cross section of the material by changing the position of loading on the material.[3] This approach has only theoretical, but no practical value where bone is concerned. The second method is to distribute the material such that there is a greater amount available where known bending stresses exist.[4]

This method was examined in two ways: (1) by allowing the diameter of the cross section to vary so that the peripheral (outer fiber) stresses of the cross section remained a constant, or (2) concentrating material where highest stress occurred and using no material where no stress was present.[5] In applying his two principles to the musculo-skeletal system, Pauwels asserted that bone structure adapts to bending stresses by minimizing the stresses. Although, Roux and Pauwels agreed, in concept, on the functional adaptation of bone to stress, Roux maintained that a axial loading was the only contributor to the process, while Pauwels included the minimization of bending stress in bone as a necessary consideration.[6]

Kummer correlated x-ray picutres (via densitometric survey) with stress trajectories obtained from photoelastic studies of bones. He postulated two levels of bone adaptation to functional forces (i.e. forces acting on bone during normal human activities): (1) "absolute minimum construction", defined where the bone adapts its gross shape and inner structure to maintain stress at a minimum value for a given load; and (2) "relative minimum construction", defined where bone adapts to an actual stress which may not be a minimum for a given load.[7] Both types of minimum construction are just restatements of Roux's Law. Kummer also observed that bone's ability to minimize its structure but sustain the actual stresses present without fracturing implies a certain safety factor. This safety factor is the ratio of the allowable maximum (breaking)

stress to the actual maximum stress under normal conditions.[8] When this safety factor is equally large in all parts of a bone, the bone is considered to be of "uniform strength".[9]

The overall conclusion reached by Roux, Pauwels, and Kummer and supported by extensive photoelastic analysis is that there is a definite correlation between the longitudinal and cross-sectional distributions of bone material and the functional (musculo-skeletal) forces present. The purpose of this thesis is to develop an analytical relationship to express this qualitative observation, thus establishing a criterion for bone remodeling. The central focus of the thesis is the relationship between the cross-sectional area of cortical bone and the local stresses on this area produced by muscular forces. An analytical relationship correlating the structure of bone to its muscular forces is developed for the ulna. The ulna is singled out for special consideration because it plays a major role in flexion, the most common activity of the forearm, and because relatively few major muscles influence its role in this action.

The force contributions due to various forearm flexor muscles are computer analyzed using a biomechanics program formulated for the elbow joint.[10] It has been shown that the ulna incorporated the y-component of the resultant of the muscular forces at the elbow joint.[11] The relative strengths, cross-sectional areas and points of application of the muscles are crucial factors in determining magnitudes of the forces

acting and, consequently, in the degree to which each muscle figures in the stress analysis.

The model used for the ulna is that of a beam in bending and compression:

$$\sigma_{total} = \sigma_{axial} + \sigma_{bending} = F/A + \frac{M\ y}{I}$$

where

σ_{total}	= total stress on a cross section
σ_{axial}	= stress on a cross section due to the axial components of the force.
$\sigma_{bending}$	= stress on a cross section due to the transverse components of the force.
F	= axial force
A	= cross-sectional area
M	= bending moment due to the transverse forces about the neutral axis of the cross section.
y	= displacement from the neutral surface (zero stress) to some point on the cross section.
I	= moment of inertia of the cross-sectional area about its neutral axis.

The stress and inner and outer radii of the cross section are fixed in order to obtain expressions for the variation of the cross-sectional area of the beam as a function of distance down the length of the beam. The variations of other structural parameters are also considered (e.g. distance to outer fiber as a function of x, c(x)). The theoretical approach outlined below was followed:

(a) the initial beam structure chosen so as to be consistent with the minimum material requirement;

(b) the outer fiber stress was taken as constant while variation in the inner and outer radii about the neutral axis of the beam was allowed;

(c) the principal stress was then maximized, minimized and then held constant in order to ascertain what additional information could be secured.

The organization of the thesis is as follows: Chapter II presents physiological background material on bone and muscles as well as a discussion of the biomechanics of the forearm. Chapter III is a presentation of theory and development of the model. In Chapter IV, a discussion of experimental procedures and computer programming particularized to this study is given. Chapters V and VI present the results and data analysis, as well as suggestions for future work.

II. Background

A. Anatomy of the Arm and Forearm

An anatomical discussion of the bones comprising the arm and forearm is necessary before considering their biomechanical behaviors. A list of relevant terminology used throughout this thesis is compiled and defined in Table I.

The skeleton of the forearm consists of two bones, the ulna and the radius. The arm bone is called the humerus. (Figure 1). In the anterior-superior view (favored by most textbooks), the ulna is located medially with respect to the forearm while the radius is lateral to the forearm. The proximal end of the humerus participates in the shoulder articulation while its distal end articulates with both the ulna and radius.

Four key surfaces of the distal humerus should be specifically noted. The lateral and medial epicondyles are origin points, respectively, for the long extensor and flexor muscles. The capitulum is the surface with which the head of the radius articulates, while the trochlea is the surface about which the trochlear notch of the ulna articulates. (Refer to Figure 2).

Proximally, the radius and ulna articulate with each other, the radial notch of the ulna receiving the head of the radius. The ulna is more massive at its proximal end where the olecranon (superior-posterior view) forms the point of the elbow. Two major muscle attachments points on the ulna are the olecra-

TABLE I

GENERAL TERMINOLOGY [12,13]

Surface Positions:	
Anterior	situated on the front of the body, on or nearest the abdominal surface
Posterior	situated on the back of the body
Superior	situated on the upper or higher surface
Inferior	situated on the lower surface
Palmar	situated relative to the palm of the hand
Plane Sections:	
Sagittal plane	vertical plane passing through the body from front to back dividing it into right and left portions
Midsagittal plane	vertical plane at midline, dividing the body into right and left halves
Frontal plane	vertical plane at right angles to the sagittal plane, dividing the body into anterior and posterior halves.
Transverse plane	horizontal plane at right angles to both the sagittal and frontal planes, dividing the body into upper and lower halves
Relative Positions:	
Medial	situated in the middle or nearest to the midsagittal plane
Lateral	situated on the side or farthest from the midsagittal plane
Proximal	situated near the point of attachment of a bone segment (near the center)
Distal	situated away from the point of attachment of a bone segment

Table I (continued)

Movements:	
Flexion	bending to decrease the magnitude of the angle between two adjacent segments of a body
Extension	return from flexion or stretching out to a greater length
Supination	outward (lateral) rotation of the forearm and hand about the longitudinal axis of the forearm so that the palm faces upward
Pronation	inward (medial) rotation of the forearm, palm faces downward
Abduction	sideward movement of a body segment away from the midsagittal plane
Adduction	return from abduction or sideward movement of a body segment towards the midsagittal plane
Supplemental Vocabulary:	
an articulation	a joint or juncture of two or more bones
to articulate	to form a joint
palpable	examinable by touch

Figure 1. Right Humerus, Radius, Ulna - Anterior View.[14]

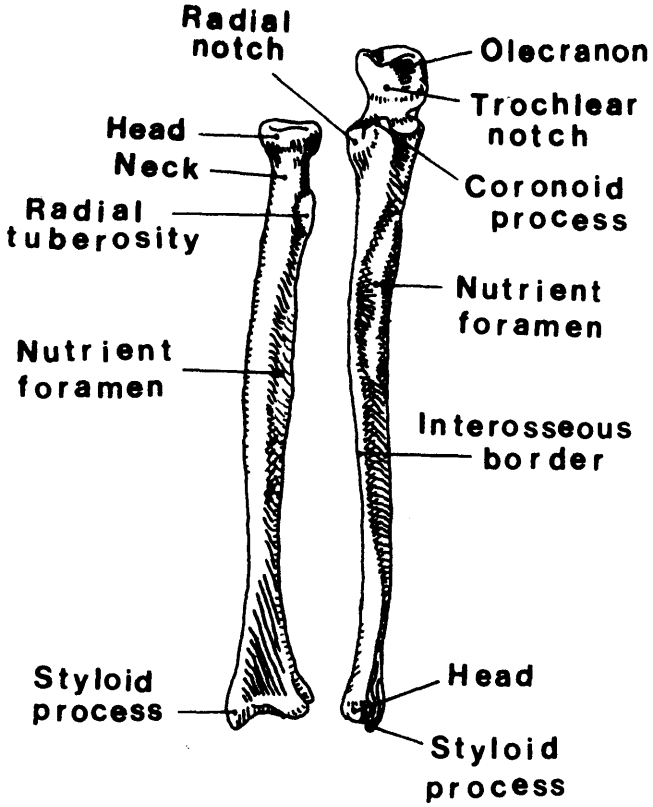

Right radius and Ulna

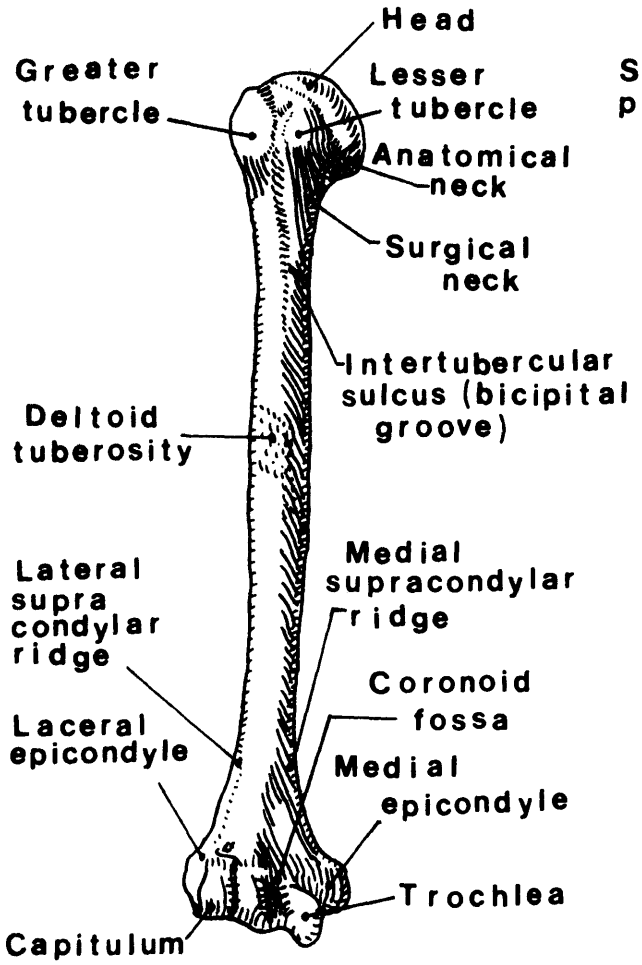

Right humerus

Figure 2. Bones of the Elbow Region - Detail[15,16]

a,c. Anterior View

b,d. Posterior View

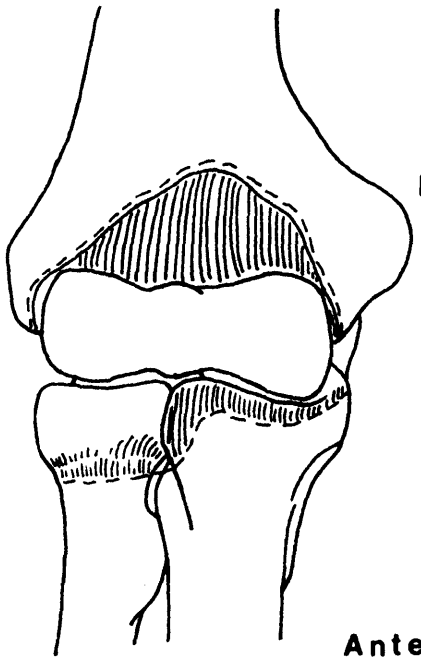

(a)

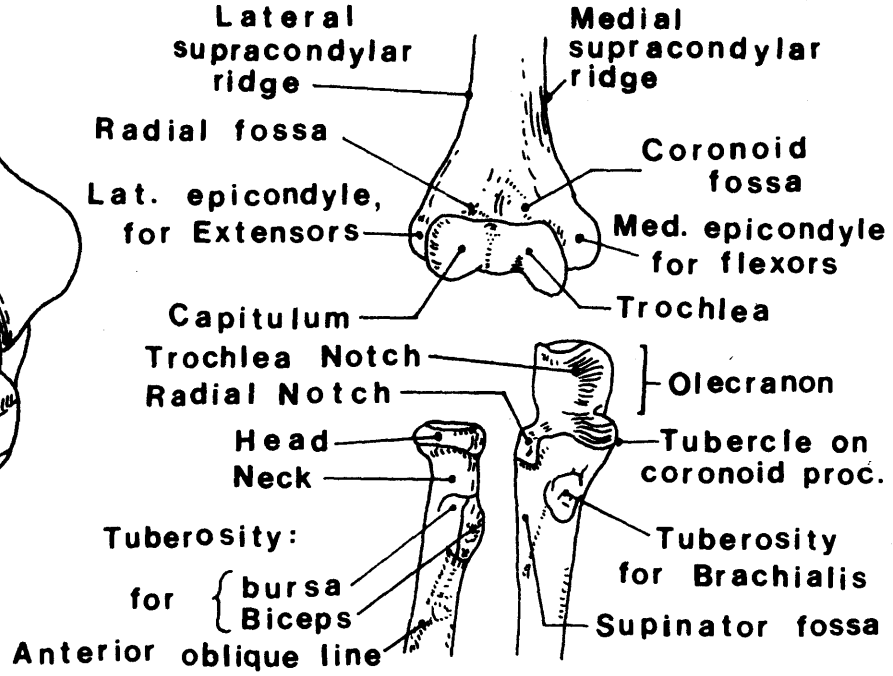

(b)

ANTERIOR VIEW

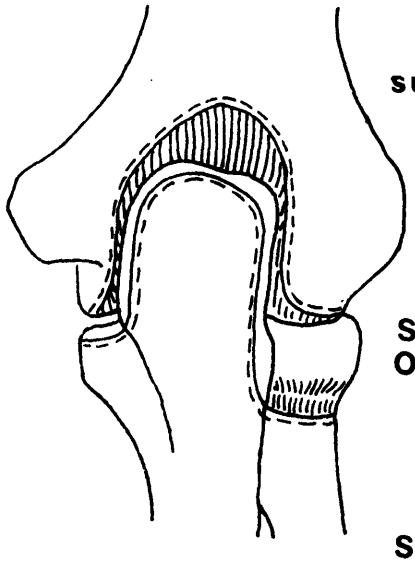

(c)

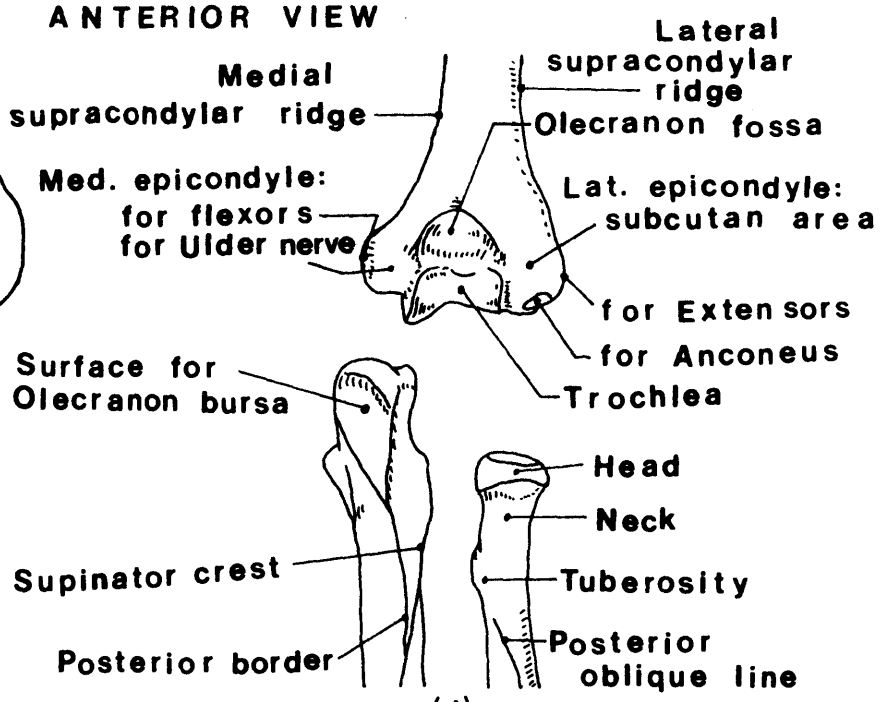

(d)

POSTERIOR VIEW

non and the coronoid process. Distally, the shaft of the ulna, the lateral border of which is known as the interosseous crest, becomes less massive as one approaches the ulnar head. (See Figure 1). The radial shaft progresses from the head into a neck, below which the radial tuberosity protudes medially. The interosseous border begins below the tuberosity, separating into anterior and posterior ridges. Distally, the radius broadens bilaterally for its articulation with the scaphoid and lunate bones of the hand. The styloid processes of both the ulna and radius are easily palpable at the wrist. Figure 3 shows the inferior view of the radius and ulna as well as a palmar view of the left wrist joint. More will be said about the manner of articulation of the humerus, ulna and radius in section IID.

B. Muscles: Their Structure and Function

Before initiating a study of the stresses in a bone, a knowledge of the basic structure of muscles and the mechanics of muscle behavior is essential to understanding the role of muscles as forces.

A skeletal muscle consists of thousands of long, slender fibers, each 10-100μ in diameter, running parallel to each other and surrounded by connective tissue endomysium. (See Figure 4). Myofibrils, sarcoplasm and sarcolemma are the main constituents of the fiber. Myofibrils, .5-1μ in diameter, are arranged in columns with from several hundred to several

Figure 3. a. Inferior View of the Radius and Ulna [17]

b. Palmar View of the Left Wrist Joint

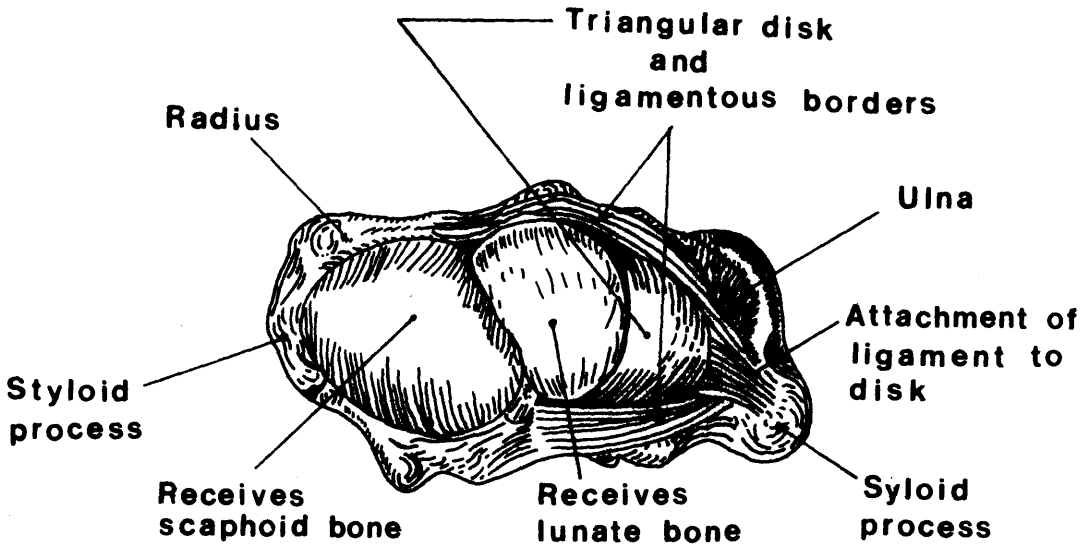
Triangular disk
and
ligamentous borders
Radius
Ulna
Attachment of
ligament to
disk
Styloid
process
Receives
scaphoid bone
Receives
lunate bone
Syloid
process

(a)

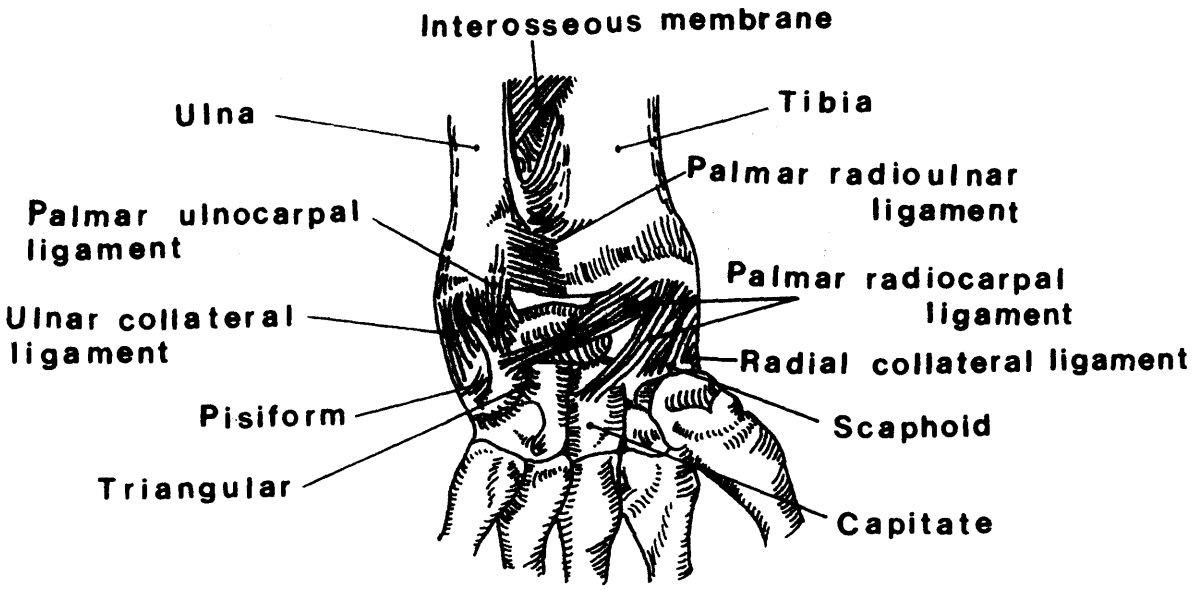
Interosseous membrane
Ulna
Tibia
Palmar radioulnar
ligament
Palmar ulnocarpal
ligament
Palmar radiocarpal
ligament
Ulnar collateral
ligament
Radial collateral ligament
Pisiform
Scaphoid
Triangular
Capitate

(b)

Figure 4. Composition of Skeletal Muscle[18]

a. Cross Section of Muscle

b. Organization of Muscle Tissue

c. A Muscle Fiber

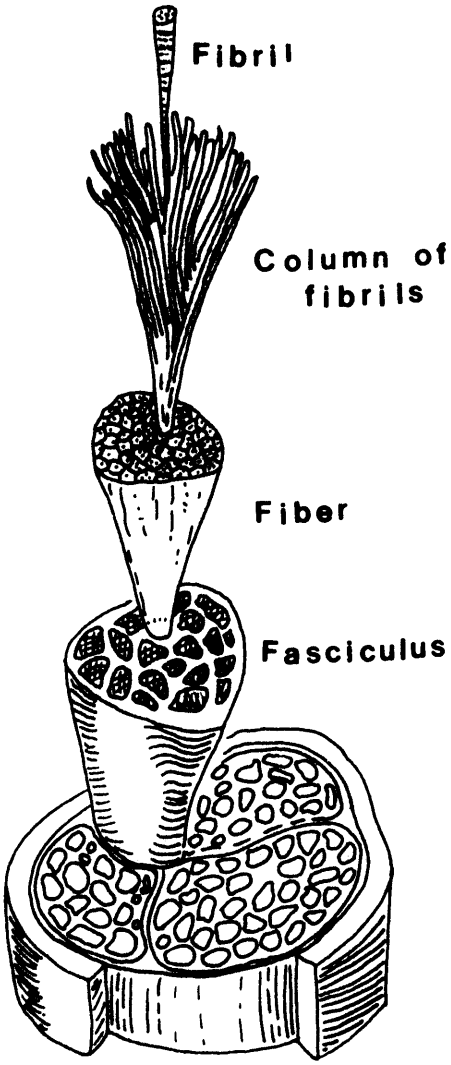
Fibril
Column of fibrils
Fiber
Fasciculus

(b)

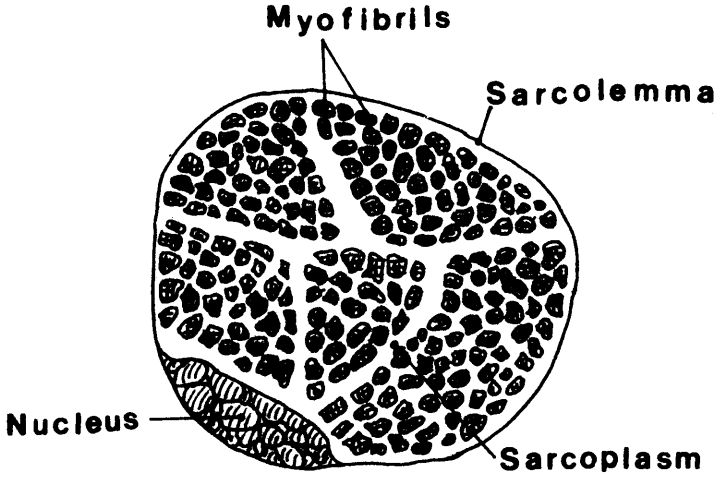
Myofibrils
Sarcolemma
Nucleus
Sarcoplasm

(a)

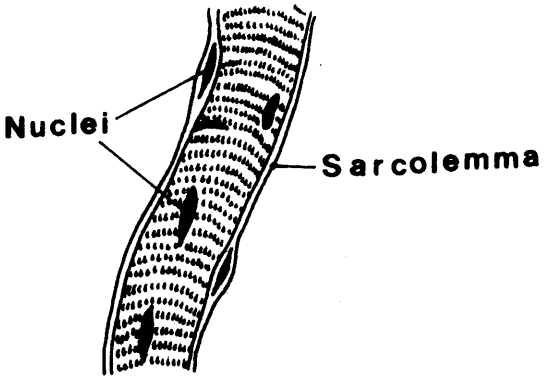
Nuclei
Sarcolemma

(c)

thousand in each muscle fiber. The sarcoplasm is the fluid thorugh which the contractile muscle fiber moves. The sarcolemma, a membrane surrounding the myofibrils and sarcoplasm, conducts the action potential, which is generated during a muscle contraction, throughout the fiber.

All of the muscle fibers of the intact muscle do not contract in a smooth continuous shortening, but by means of many rapid changes. Thus the apparently smooth contraction observed in muscles is actually a summation of all the rapid changes of the fibers. The nerve and chemical considerations in muscles contraction are beyond the scope of this thesis.

The fiber arrangement of a given muscle determine the performance character of the muscle. Muscle contraction is a shortening of the length of the fibers to produce tension. Thus the fiber arrangement is of importance in considering the magnitude of a muscle's contraction and its ability to exert a force. The two main arrangements are called fusiform and penniform. The fusiform muscle has a longitudinal distribution of fibers, running parallel to each other and enabling maximum range of movement of a body segment during contraction. An example of this is the shunt muscle which acts chiefly during rapid movements and acts along the long axis of a bone segment to provide centripetal force helping to stabilize the joint.[19] The penniform (feather-like) arrangement is a diagonal

alignment of short muscle fibers which approach the muscle tendon obliquely from one or more sides, producing a greater force than the fusiform muscles over a shorter range of movement. An example of the "penniform arrangement, the spurt muscle, provides acceleration along the direction of motion of the bone segment about a joint.[20] Various muscle functions and terms are listed and explained in Table II.

The amount of tension a muscle can develop during maximal contraction depends upon the number and size of the muscle fibers as well as their internal fiber arrangement. It has been found that the total force which a muscle can exert is directly proportional to the total cross-sectional area of the muscle at its widest point, including all the muscle's fibers. Since the penniform arrangement has a greater number of fibers within a cross-sectional area, the force of such a muscle will be greater than that of the fusiform type.

C. Muscles of the Ulna and Radius

Figure 5 shows the location of the origin and insertion points of those muscles acting on the arm and forearm about the elbow and wrist. Tables III, IV and V give the names, origins, insertions and functions of these muscles.

D. Biomechanics of the Forearm

(1) The ability to flex, extend abduct or adduct the muscles of the fore arm is dependent upon the degree of articu-

TABLE II [21,22]

TERMINOLOGY SPECIFIC TO MUSCLES

Origin	the attachment end of a muscle on the more stable or stationary bond segment (usually more proximally located in body)
Insertion	the attachment end of a muscle on the more easily moved bone segment (usually more distally located in body)
Agonistic muscle	directly responsible for effecting a particular movement or activity (may be capable of more than one activity)
Antagonistic muscle	causes the opposite movement from that of the agonistic muscle, thus contributing to the smoothness of the action
Shunt muscle	it's origin is situated close to the joint crossed while the insertion is a greater distance away (joint stabilizing function)
Spurt muscle	it's origin is situated further away from the joint crossed than the insertion (provides increased motion about a joint)

Figure 5. Origin and Insertions of Muscles of the Right Upper Extremity - Anterior View [23]

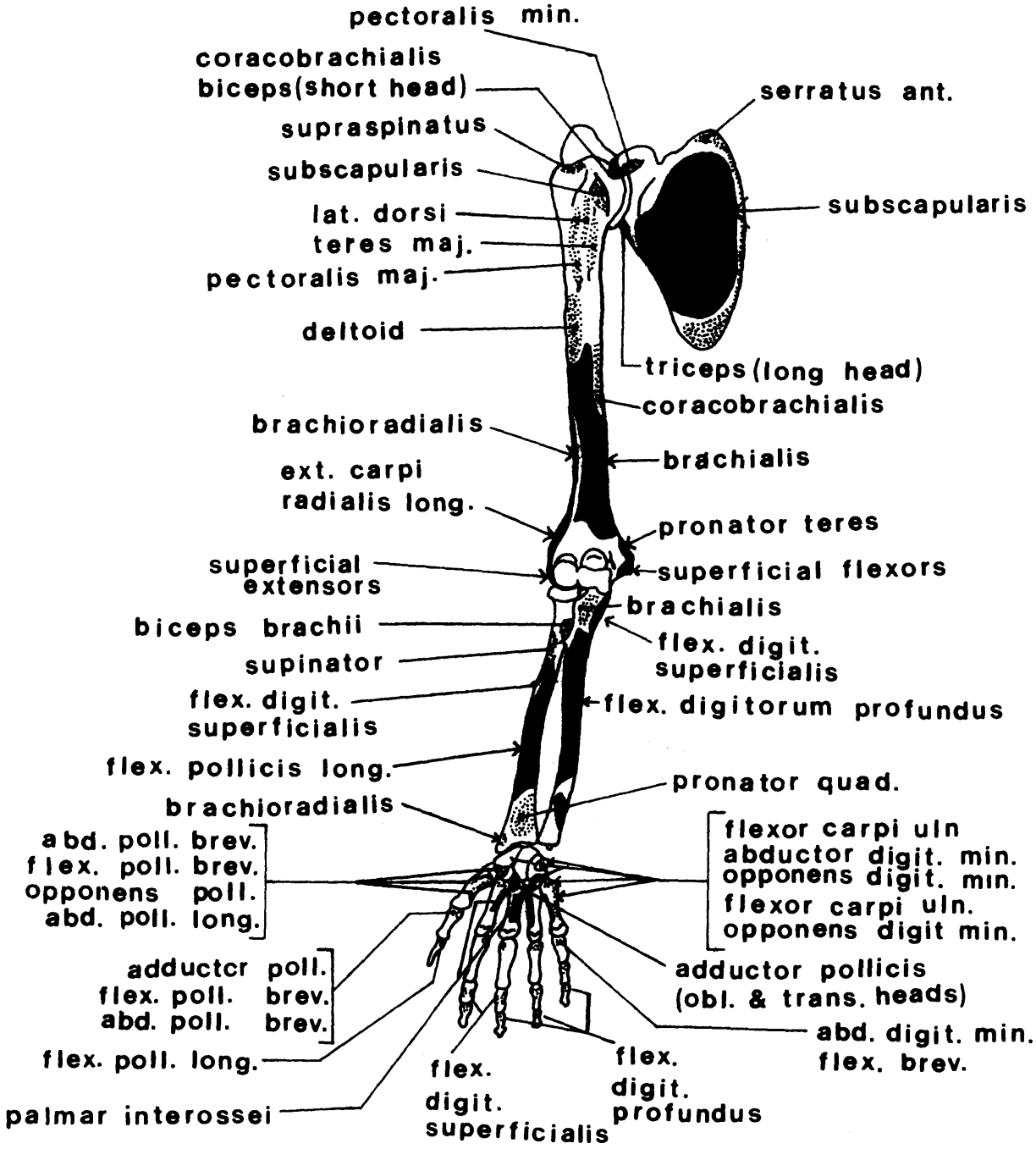
pectoralis min.
coracobrachialis
biceps(short head)
supraspinatus
subscapularis
lat. dorsi
teres maj.
pectoralis maj.
deltoid
serratus ant.
subscapularis
triceps(long head)
coracobrachialis
brachioradialis
brachialis
ext. carpi
radialis long.
pronator teres
superficial
extensors
superficial flexors
brachialis
biceps brachii
flex. digit.
superficialis
supinator
flex. digit.
superficialis
flex. digitorum profundus
flex. pollicis long.
pronator quad.
brachioradialis
abd. poll. brev.
flex. poll. brev.
opponens poll.
abd. poll. long.
flexor carpi uln
abductor digit. min.
opponens digit. min.
flexor carpi uln.
opponens digit min.
adductor poll.
flex. poll. brev.
abd. poll. brev.
adductor pollicis
(obl. & trans. heads)
abd. digit. min.
flex. brev.
flex. poll. long.
flex.
digit.
superficialis
flex.
digit.
profundus
palmar interossei
ORIGINS—SOLID
INSERTIONS—STIPPLED

TABLE III [24]

ARM MUSCLES

Muscle	Origin	Insertion	Actions
The Anterior Group			
1. Biceps brachii			
a. Short head	a. Coracoid process of the scapula	Radial tuberosity of the radius	a. and b. Flexion of the elbow joint; supination of the foreare against resistance; flexion of the shoulder joint
b. Long head	b. Supraglenoid tubercle of the scapula		b. Stabilizes the humeral head in the glenoid fossa
2. Brachialis	Distal half of the anterior aspect of the humerus adjacent to the deltoid tuberosity	Tuberosity of the ulna and the anterior surface of the coronoid process	Flexion of the elbow joint
The Posterior Group			
1. Triceps brachii			
a. Long head	a. Infraglenoid tubercle of the scapula	The olecranon of the ulna	a-c. Extension of the elbow joint
b. Lateral head	b. Posterior surface of the shaft of the humerus proximal to the radial groove		a. Extension and adduction of the shoulder joint
c. Medial head	c. Posterior surface of the shaft of the humerus distal to the radial groove		

TABLE IV [25]

FOREARM MUSCLES - ANTERIOR VIEW

Muscle	Origin	Insertion	Actions
A. Superficial Anterior Group			
1. Brachioradialis	Proximal two thirds of the lateral supracondylar ridge of the humerus	Styloid process of the radius	Flexion of the elbow joint
2. Pronator teres			
a. Humeral head	a. Medial epicondyle of the humerus	Middle of the lateral surface of the shaft of the radius	Assists in elbow flexion against resistance; pronation of the forearm
b. Ulnar head	b. Medial side of the coronoid process of the ulna		
3. Flexor carpi radialis	Medial epicondyle of the humerus	Bases of the 2nd and 3rd metacarpals	Flexion of the wrist joint; assists in radial flexion of the wrist joint
4. Palmaris longus	Medial epicondyle of the humerus	Central part of the flexor retinaculum and palmar aponeurosis	Assists in flexion of the wrist joint
5. Flexor carpi ulnaris			
a. Humeral head	a. Medial epicondyle of the humerus	The pisiform, hamate, and base of the 5th metacarpal	Flexion of the wrist joint; assists in ulnar flexion of the wrist joint
b. Ulnar head	b. Medial margin of the olecranon of the ulna		

Table IV (continued)

Muscle	Origin	Insertion	Actions
6. Flexor digitorum superficialis			
a. Humeral head	a. Medial epicondyle of the humerus	Sides of the shafts of the 2nd phalanges of the four fingers	Assists in flexion of the wrist joint; flexion of the MP and proximal IP joints of the four fingers
b. Ulnar head	b. Medial side of the coronoid process of the ulna		
c. Radial head	c. Oblique line of the radius		
B. Deep Anterior Group			
1. Flexor digitorium profundus	Proximal three fourths of the palmar and medial surfaces of the shaft of the ulna	Bases of the distal phalanges of the four fingers	May assist in flexion of the wrist joint; flexion of the MP and IP joints of the four fingers
2. Flexor pollicis longus	Palmar surface of the shaft of the radius	Base of the distal phalanx of the thumb	May assist in flexion of the wrist joint; flexion of the MP, proximal, and distal IP joints of the thumb; assists in adduction of the thumb
3. Pronator quadratus	Distal fourth of the palmar surface of the ulna	Distal fourth of the palmar surface of the radius	Pronation of the forearm

TABLE V [26]

FOREARM MUSCLES - POSTERIOR VIEW

Muscle	Origin	Insertion	Actions
C. Superficial Posterior Group			
1. Anconeus	Posterior surface of lateral epicondyle of the humerus	Lateral side of the olecranon of the ulna and proximal fourth of the shaft of the ulna	Extension of the elbow joint
2. Extensor carpi radialis longus	Distal third of the lateral supracondylar ridge of the humerus	Base of the 2nd metacarpal	Assists in extension and hyperextention of the wrist joing; radial flexion of the wrist joint
3. Extensor carpi radialis brevis	Lateral epicondyle of the humerus	Base of the 3rd metacarpal	Extension, hyperextension, and radial flexion of the wrist joint
4. Extensor digitorum	Lateral epicondyle of the humerus	Dorsal surface of the bases of the 2nd phalanges and dorsal expansions of the four fingers	Extension and hypertension of the wrist joint and MP joints of the four fingers; extension of the IP joints of the four fingers
5. Extensor digiti minimi	Lateral epicondyle by the common extensor tendon	The extensor expansion and tendon of the extensor digitorum at the proximal phalanx of the little finger	Assists in extension of the wrist joint; extension any hyperextension of the MP joint of the little finger; extension of the IP joints of the little finger
6. Extensor carpi ulnaris	Lateral epicondyle of the humerus by the common extensor tendon	Ulnar side of the base of the 5th metacarpal	Extension, hyperextension, and ulnar flexion of the wrist joint

Table V (continued)

Muscle	Origin	Insertion	Actions
D. Deep Posterior Group			
1. Supinator	Lateral epicondyle of the humerus and adjacent area of the ulna and joint ligaments	Lateral surface of the proximal third of the radius	Supination of the forearm
2. Abductor pollicis longus	Lateral part of the dorsal surface of the shaft of the ulna	Radial side of the base of the first metacarpal	Assists in flexion and radial flexion of the wrist joint; abduction of the CM joint of the thumb
3. Extensor pollicis brevis	Dorsal surface of the shaft of the radius	Base of the first phalanx of the thumb	Assists in radial flexion of the wrist joint; extension of the CM and MP joints of the thumb
4. Extensor pollicis longus	Lateral part of the middle third of the dorsal surface of the shaft of the ulna	Base of the distal phalanx of the thumb	Assists in extension and hyperextension of the wrist joint; extension and adduction of the CM joint of the thumb; extension of the MP and IP joints of the thumb
5. Extensor indicis	Dorsal surface of the shaft of the ulna	The tendon of the extensor digitorum to the little finger	Assists in extension and hyperextension of the wrist joint; extension, hyperextension, and adduction of the MP joint of the index finger; extension of the IP joints of the index finger

lation of the humerus, ulna and radius about the elbow (and to a lesser extent, the wrist).

(2) The elbow joint has two degrees of freedom of motion and is called a throchginglymus; that is, it has hinge motion in one plane and axial rotation in another.[27] The trochlea (humerus), which articulates with the trochlea notch of the ulna, is a hyperboloid. (Refer to Figure 2). Its surface has two curvatures: concave in the frontal plane and convex in the sagittal plane. (Sagitally, it forms almost a complete circle except at the medial edge where the curvature is almost helical). According to Steindler[28] only about 330° of the trochlea is covered with cartilage since the anterior and posterior surfaces are separated by a bony wall--the distal shaft of the humerus and the olecranon fossa. The trochlear notch, which is semicircular in curvature, has a vertical ridge which fits into the neck of the trochlea; the notch is bordered proximally the olecranon and distally by the coronoid process (Figure 2) forming an almost perfect fit. Its angular range of motion 190°, is limited by the olecranon fossa. This joint, the humero-ulnar articulation, forms the hinge motion of the elbow.

(3) The capitulum (humerus) is convex both frontally and sagitally forming half a sphere, although the radius of this sphere is not quite constant. The capitulum also faces forward and downward and is covered with cartilage, indicating a 180° of angular involvement in articulation. The head of the radius

is indented slightly to receive the capitulum and has its thickest covering of cartilage in the middle of the indent. The slight cavity has an angular value of about 40°. This junction, the humeroradial articulation, contributes to the pivot motion of the elbow joint.

(4) The total angular range of motion of the forearm about the elbow is 140°, consistent with the allowed range of motion of each articulation. Although a wide range of movement is possible, the radial and ulnar collateral ligament (Figure 6) attach laterally and medially to the bones blending into the annular ligament which encircles the head of the radius. These ligaments provide added stability to the elbow joint.

(5) The radioulnar articulation (pivot motion) consists of three distinct joints. The proximal radioulnar joint at the elbow is comprised of the head of the radius which is restrained to articulate with the radial notch of the ulnar by the annular ligament. This restraint stabilizes against lateral and distal displacements of the radial head while allowing pivotal motion of the head to occur within the ring of the ligament. The distal radioulnar joint, where the ulnar notch of the radius articulates with the ulnar head, complements the proximal joint allowing axial rotation. The middle radioulnar joint is maintained by the interosseous membrane which runs distally and medially from the radius to the ulna. The fiber arrangement maintains a maximum spatial distance between the two bones during supination while simultaneously restraining

Figure 6. The Left Elbow Joint with Ligaments[29]

a. Lateral View

b. Medial View

c. Anterior View

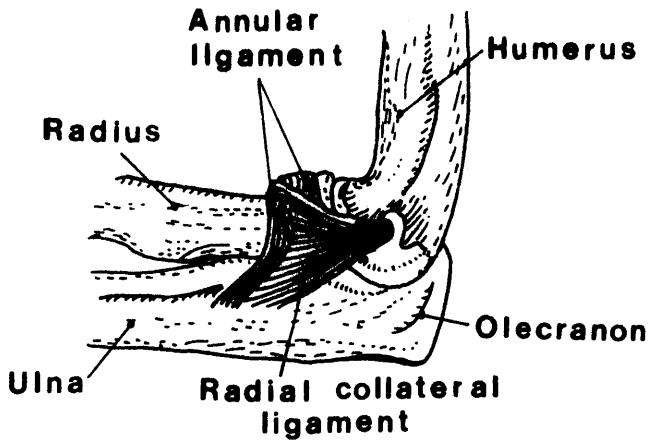
Annular
ligament
Humerus
Radius
Olecranon
Ulna
Radial collateral
ligament

(a)

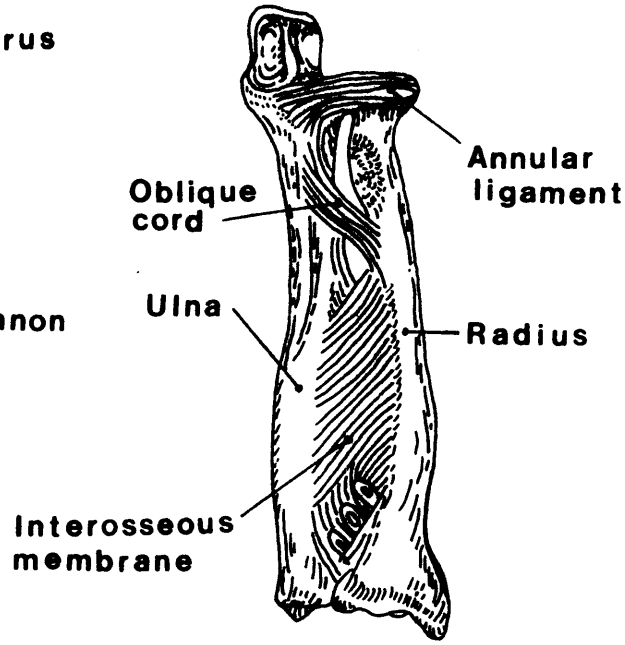
Annular
ligament
Oblique
cord
Ulna
Radius
Interosseous
membrane

(c)

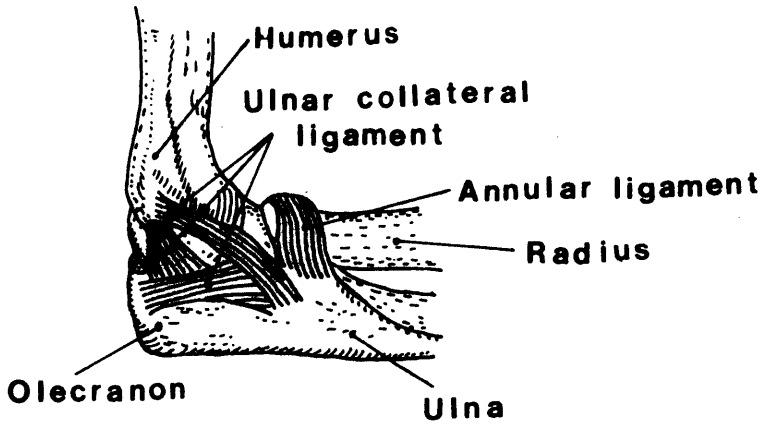
Humerus
Ulnar collateral
ligament
Annular ligament
Radius
Olecranon
Ulna

(b)

the radial head from movements upward against the capitulum. (Figure 6).

(6) The humeroulnar and humeroradial articulations allow for flexion and extension of the forearm with small amounts of abduction and adduction. Maximum flexion (140°-145° depending on researchers) is limited by muscle tissue between the arm and forearm, while maximum extension is limited by those muscles crossing the anterior view of the elbow joint. Hyperextension can occur to about 10°-20°.[30] The radial head, bound closely to the ulna, glides along the proximal surface of the capitulum during flexion-extension. The radioulnar articulations allow for supinated and pronation of the forearm, the radius pivoting about the ulna.

As mentioned in Chapter II, distally the scaphoid, lunate and triangular bones of the hand articulate with the triangular articular disk located distal to the ulna, but connecting with the distal radius. The wrist joint is known as the radiocarpal articulation. It is a very stable joint due to the number of ligaments and muscle tendons which pass over it. (Figure 3b). The wrist is an example of an ellipsoid joint, its two degrees of freedom allowing flexion-extension, hyperextension, radial and ulnar flexions and circumduction. There is no active rotation, although the hand can be passively rotated via the forearm.

The degree of articulation of the forearm about the elbow joint is dependent upon the muscle activity. This ac-

tivity consists of three phases in an excitation-contraction coupling: the latent phase, the contractile phase, and the relaxation phase. The explicit contractile phase is of interest in this work.

An unstretched muscle is considered to be at its rest length. The force due to a muscle contraction is directed along the center line of action of the muscle, usually designated by the direction of the tendon attachment of the muscle on the bone. When a muscle contracts under conditions where little or no shortening occurs, i.e. there is no decrease in length relative to the initial length, this is called isometric contraction. The muscle fibers maintain the same length during contraction, but there is a marked increase in tension in order to counterbalance an external load. No external work is done, but the internal energy produced by the muscle is converted into heat. Examples of an isometric contraction are holding a weight or pressing a wall.

A situation where the muscle fibers maintain a constant tension by changing their length is called isotonic contraction. Shortening of the muscle occurs, thus producing work. An example of isotonic contraction is moving a weight over a certain distance. Pure isotonic contraction is rarely found outside the laboratory. Normal movements require muscle tensions to vary, combining both isometric and isotonic contractions.

The shortening characteristics of isotonic contraction

are dependent on the magnitude of the loads moved. The heavier the load, the less the total shortening. In the limit of no shortening, the state of isometric tension is reached. The velocity of shortening follows the same inverse relationship. Hill[31] and Wilkie[32] established an analytical relationship between the muscular force and its velocity of shortening, i.e.

$$(P+a)(V+b) = \text{constant} = Po\ (a+b)$$

where

P = Force of contraction

V = Velocity of contraction

Po = Force at V=0, isometric contraction

a,b = Constants .

Pertuzon and Bouisset[33] showed that the relationship between a muscle's instantaneous force and its associated velocity of shortening is about the same as the relationship established between maximal values of the force and concurrent velocity.

The literature contains many studies which attempt to determine and/or verify force relationships between various muscle activities and anatomical characteristics. The author found that it is generally difficult to correlate the data due to the variation in initial experimental conditions, however certain generalized observations can be made and substantiated:

1. a definite linear relationship exists between the absolute force, or strength of a muscle, and its effective cross-sectional area;

2. the flexor muscle is stronger than the extensor; and,

3. the muscular force has an angular dependency about a joint.

The absolute force of a muscle is defined as the maximum contractile force during voluntary isometric contraction due to 1 cm^2 of effective cross-sectional area of muscle.[34] The effective cross-sectional area is the area of a section perpendicular to all the fibers of a muscle. For the long, parallel fibers of the fusiform muscle, the effective area is equal to the physiological area; for a penniform muscle, there is a greater number of fibers per cm^2 in its physiological cross-sectional area, and this area may be at an oblique angle to the anatomical cross-sectional area. This difference may account for discrepancies in calculations found in the literature.

Fick (1903) calculated the strength/cm^2 of flexor muscles about the elbow to be 6-10 kg/cm^2.[35,36] Morris'[37] calculation (1948) yielded 9.15 kg/cm^2 for the flexors of males and 7.5 kg/cm^2 for those of females, consistent with Fick's result. On the other hand, Rechlinghausen (1920) obtained 3.6 kg/cm^2,[38] and Ikai and Fukunaga[39] (1968) got 4.7 kg/cm^2, the latter value being independent of sex and age. Going a

step further, deDuca[40] found that the physiological cross-sectional areas of the anterior fibers versus the posterior fibers of the deltoid muscle (penniform) were inversely proportional to each other. This result suggests not only an explanation for the opposing physical function of these two groups of fibers, but also a clear understanding of how the discrepancies, noted above, in strengths of muscles during specific activities could occur.

In considering the relative strength between flexors and extensors, Steindler[41] states that the flexors are one and a half times stronger than the extensors, a result confirmed by Singh and Karpovich.[42]

The angular dependence of the muscle force was established by Wilkie.[43] Jorgensen and Bankov[44] calculated the maximum isometric torque due to all the elbow flexors and determined its dependence on the elbow angles and on the position of the forearm relative to the humerus. This relationship was confirmed by Singh and Karpovich.[45] Wilkie also established the lever ratio, which is constant throughout flexion but varies from muscle to muscle. The lever ratio is defined as the ratio of the moment arm of a muscle about the elbow joint to the moment arm of the resistance force, which is at the hand.

Tables IV and V list all the muscles of the arm and forearm. Of those muscles, five participate in some way in flexion about the elbow joint. They are: brachialis, bicep brachii, brachioradialis, pronator teres, and extensor carpi

radialis longus. The last two muscles are pronator-supinator muscles with minor flexion activity. The first three muscles are considered to be the major flexors of the elbow joint. Many researchers list the biceps brachii as the principal flexor,[46,47] not the brachialis muscle.[48,49] Yet, electromyography (EMG), a technique considered to be the most accurate indicator of which muscles are actively participating in specific movements, shows that the brachialis is the superior flexor under all conditions.[50] The biceps brachii is a strong flexor only when a load is present and the forearm is supinated. The brachioradialis acts as a shunt muscle, supplying a quick force along the long axis of the bone for powerful movements. It functions as a reserve force. Steindler[51] lists the brachialis and biceps brachii (both penniform muscles) as the principal flexors and the brachioradialis and extensor carpi radialis longus (both fusiform muscles) as auxillary muscles. Kelley[52] and Wilkie[53] include the pronator teres as an auxillary flexor when a load is present, while Basmajian[54] states merely that there is no activity in the pronator teres if there is no load or only a minimal load.

III. THEORY

The analytical basis for the prediction of the mechanical response of bone to forces arising from isometric muscle contractions has been extracted from beam bending theory as applied to perfectly elastic media. This development is presented in IIIA. Referenced data, in which the actual mechanical properties of bone are presented, appears in IIIB. Although the anisotropy of bone is evident, the linearity of the stress-strain relation within specified limits is shown. Applicability of the material model of bone as perfectly elastic is thus upheld. Finally section IIIC develops the application of beam bending theory to the ulna. (In Chapter IV, the beam loading is modified to more accurately model the actual muscle forces present.)

A. Theoretical Framework[55,56]

In machine design, one is concerned with the relationship between external forces acting on a structural member, and internal forces and deformation resulting from the external forces. The investigation of this relationship usually begins with the following assumptions concerning material properties:

1. perfect elasticity -- upon the removal of loads, the material completely returns to its original shape;

2. structural and compositional homogeneity;

3. isotropy -- mechanical properties are directionally independent;

4. linearity -- stress and strain are linearly related in accordance with Hooke's Law;

5. elastic properties -- the mechanical response to either tension or compression is the same.

For an elastic body stressed in one direction,

$$\sigma = {}^{F}/A = \varepsilon E \tag{3.1}$$

or, the stress, σ, is equal to the force (F) per unit area (A) and is also linearly proportional to the strain ε by Young's Modulus, E. In general, σ_x, σ_y and σ_z are stresses due to forces acting on surfaces, the normals of which are, respectively, in the x, y and z directions. ε_x, ε_y and ε_z are the strains or increments of deformation per unit length of the beam associated with the respective normal stresses. The resultant strains due to σ_x, σ_y, σ_z are:

$$\begin{aligned} \varepsilon_x &= \frac{1}{E}[\ \sigma_x - \nu(\sigma_y+\sigma_z)\ ] \\ \varepsilon_y &= \frac{1}{E}[\sigma_y - \nu(\sigma_x+\sigma_z)\ ] \\ \varepsilon_z &= \frac{1}{E}[\sigma_z - \nu(\sigma_x+\sigma_y)\ ] \end{aligned} \tag{3.2}$$

where ν = Poisson's ratio, the ratio of the transverse unit strain to the longitudinal unit strain.

A cantilever beam in bending is a horizontal beam fixed at one end and loaded either by vertical point forces or

distributed loads along its length and/or by force couples at its free end. The simplest case is a single force acting at the free end. In order to calculate the internal stresses in the beam resulting from bending, the shear force, V, and bending moment, M_b, acting at various cross sections of the beam must be determined. The vertical shear force at a transverse section of the beam is equal to the resultant of the external forces that lie on either side of the section. In Figure 7, the beam in (a) has been cut, at transverse section mn, into arbitrary portions (b) and (c), the resulting free bodies.

The bending moment at a section is the algebraic sum of the moments due to the applied loads and reactions which lie on either side of the action. The bending moment is related to the shear force and the applied load by the expressions:

$$\frac{dM_b}{dx} = -V(x) \tag{3.3}$$

and

$$\frac{dV}{dx} = -w \tag{3.4}$$

where w = intensity of a continuous load distributed along the beam.

Figure 7. Free Body Diagrams of a Beam in Bending[57]

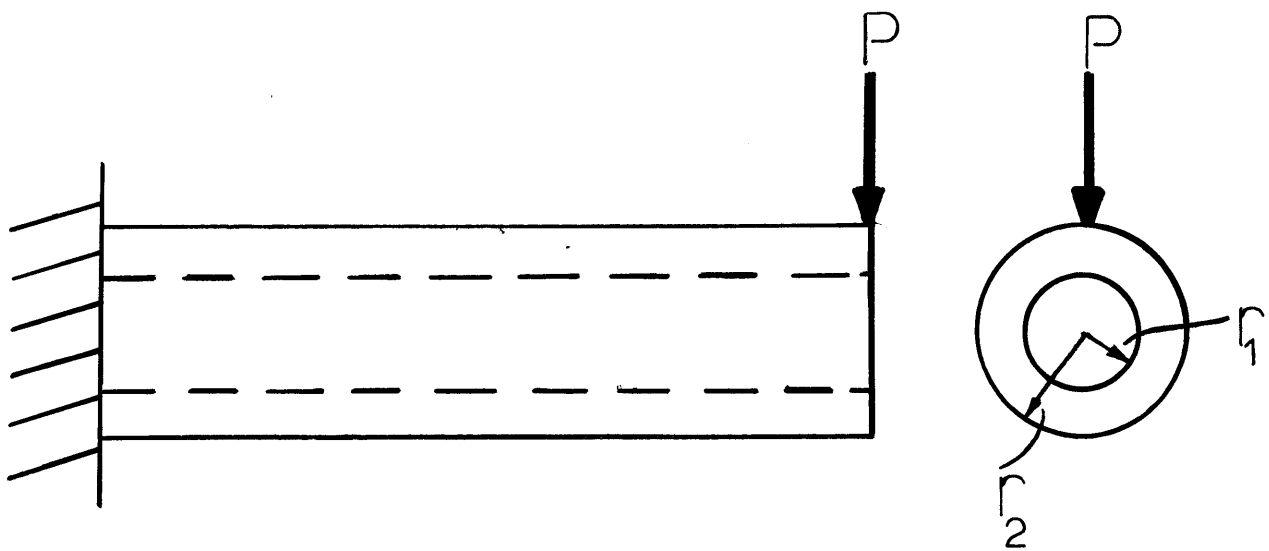
P
P
r_1
r_2

The two types of stresses resulting from bending of a beam, shear stress and bending stress, will be discussed separately. The following assumptions are used in developing the theory for a beam under pure bending and having a longitudinal plane of symmetry:

1. the beam is straight and of uniform planar cross section;

2. the cross section remains planar and normal to the longitudinal fibers* of the beam after bending;

3. the resultant of the applied loads lies in the longitudinal plane of symmetry; and

4. the material structural and compositional properties of the beam are homogeneous along the beam's length and are symmetrical with respect to the plane of loading. The conditions are imposed only to establish a deformation pattern where bending (rather than buckling) is the primary mode of failure.

Application of these assumptions leads to determination of the neutral surface, i.e. that surface on which the fibers do not undergo any strain during bending. The intersection of the neutral surface with any cross section is

---

* The beam is imagined to be composed of thin longitudinal rods or fibers.[58]

called the neutral axis. The radius of curvature (ρ) of the beam is given by

$$\frac{1}{\rho} = \frac{d\phi}{ds} \simeq \frac{\Delta\phi}{\Delta s}$$

where $\Delta\phi$ is the change in slope angle of a curve and Δs is the distance along the curve, and the unit elongation of any fiber is

$$\varepsilon_x = -\frac{y}{\rho} \quad . \tag{3.5}$$

The longitudinal strain is proportional to the distance y from the neutral surface to a given fiber and inversely proportional to the radius of curvature.

From conditions of moment and force equilibrium over a beam cross section, the following equations for a symmetric beam are presented without providing the detailed calculations.[59]

$$\Sigma F_x = \int_A \sigma_x dA = 0 \tag{3.6}$$

$$\Sigma M_y = \int_A z\sigma_x dA = 0 \tag{3.7}$$

$$\Sigma M_z = -\int_A y\sigma_x dA = M_b \tag{3.8}$$

Application of the conditions of stress and deformation (Equations (3.1), (3.2) and (3.5)) to the above equations yields:

$$I_z = \int_A y^2 dA \tag{3.9}$$

and

$$\sigma_x = -\frac{M_b y}{I_z} \tag{3.10}$$

where I_z, the moment of the beam cross section is obtained with respect to the neutral axis. The moment of intertia about an axis is the measure of a section's resistance to bending about that axis. σ_x is the stress distribution along the beam length due to bending, expressed in terms of I_z and the bending moment. Further, σ_x depends on y, which is the distance from the neutral surface to any point on the cross section. Maximum stresses (tensile and compressive) occurring in the outermost fibers are given by

$$\sigma_{MAX} = - \frac{M_b c}{I_z} \tag{3.11}$$

where c is the distance to the outer fiber from the neutral axis. The quantity I_z/c, denoted by Z, is called the section modulus; it is a measure of the bending stress induced in the member due to a bending moment.

The combination of $\Sigma F_x = 0$ with the curvature expression (3.5) yields

$$\int_A y dA = 0, \tag{3.12}$$

which is the first moment of the area with respect to the neutral axis. This implies that the neutral axis must pass through the centroid of the cross-sectional area. The coordinates of the centroid are defined by:

$$\bar{x} = \frac{\int x dA}{\int dA} \quad \text{and} \quad \bar{y} = \frac{\int y dA}{\int dA} \quad . \tag{3.13}$$

The position of the neutral surface depends on the geometry of the cross section; it generally does <u>not</u> include the centroidal axis.

Although it was derived for the case of constant bending, Equation (3.10) is generally assumed to be valid for a bending moment that varies along the length of the beam, i.e. when a shear force is present. The vertical (or longitudinal) shear stress is given by:

$$\tau_{xy} = \frac{VQ}{I_z t} \qquad \text{and} \qquad Q = \int_{A_1} y dA \ , \tag{3.14}$$

where τ_{xy} is the shear stress on the x face of the beam in the y-direction; V is the shear force producing that stress; A_1 is the portion of the area above the layer on which the shear stress acts; Q is the first moment of the area, A_1, about the neutral axis; and t is the width of the cross section at the plane on which the shearing takes place.

For a material in the xy-plane subject to a two-dimensional stress system, the equilibrium requirements of $\Sigma\vec{F} = 0$ at a point leads to the differential equations:

$$\frac{\partial \sigma_x}{\partial x} + \frac{\partial \sigma_{xy}}{\partial y} + \underline{\bar{x}} = 0 \tag{3.14}$$

$$\frac{\partial \sigma_y}{\partial y} + \frac{\partial \tau_{xy}}{\partial x} + \underline{\bar{y}} = 0 \tag{3.15}$$

where $\underline{\bar{x}}$ and $\underline{\bar{y}}$ are body forces distributed over the cross section.

The principal stresses (the maximum and minimum value of the tensile or compressive stresses) and the maximum shear stress are determined by mathematical analysis of the forces acting on an element of the material or by construction of Mohr's circle. The principal stresses due to σ_x, σ_y and τ_{xy} are:

$$\sigma_{1,2} = \frac{\sigma_x+\sigma_y}{2} \pm \left[\left(\frac{\sigma_x-\sigma_y}{2}\right) + \tau_{xy}^2\right]^{1/2} . \tag{3.16}$$

They occur on planes defined by:

$$\tan 2\phi = \frac{2\tau_{xy}}{\pm(\sigma_x-\sigma_y)} \tag{3.17}$$

The maximum shear stress occurs on a plane 45° from the principal stress and is defined as:

$$\tau_{max} = \left[\left(\frac{\sigma_x-\sigma_y}{2}\right)^2 + \tau^2_{xy}\right]^{1/2} . \tag{3.18}$$

For a beam of <u>variable</u> cross section, Equations (3.10) and (3.14) can still be applied. The error is small* if the elastic axis is assumed to be the line of centroids and if the cross sections are taken to be perpendicular to that line. If there is no axis of symmetry in a section, then the location of the principal centroidal axis must be determined

---

* Boley calculates the error to be of the order of $(hm/L)^2$, where h_m is the maximum height of the beam and L is its length.[60]

to calculate stresses correctly. (The principal axes of inertia are axes about which the moment of inertia of any cross section is a maximum or minimum.) The product of inertia is used to calculate the principal axes of asymmetrical sections. For moments of inertia given by:

$$I_{xx} = \int_A y^2 dA \ , \quad I_{yy} = \int_A x^2 dA, \text{ and } I_{xy} = \int_A xy dA \qquad (3.19)$$

from transformation equations, the angle for which the new moment, I, is a maximum or minimum is given by:

$$\tan 2\phi = \frac{2I_{xy}}{I_y - I_x} \ . \qquad (3.20)$$

One then obtains the principal moments I_1, I_2:

$$I_{\substack{1\\2}} = \frac{I_x + I_y}{2} \pm \left[\left(\frac{I_x - I_y}{2}\right)^2 + I_{xy}^2 \right]^{1/2} \ . \qquad (3.21)$$

The parallel axis theorem enables one to calculate the moment of inertia with respect to any arbitrary axis which is parallel to an axis passing through the centroid of the area for which the moment of inertia is known. Restated:

$$I'_x = \bar{I}_x + Ad^2 \ , \qquad (3.22)$$

where

$\bar{I}_x$ = moment of inertia about the centroid

I'_x = moment of inertia with respect to an arbitrary parallel x' axis

d = distance between the axes

A = area of the cross section .

If the cross sections are irregular in shape, integration is not possible and graphical analysis must be performed. Table VI lists the discrete representations of the analytical expressions which were used in this thesis.

B. Mechanical Properties of Bone

The results of work by Yamada[61] and published in a compilation of mechanical properties of bone by Evans[62] show that for strains less than .004, the assumption of perfect elasticity is reasonable for this study. (See Figure 8). Presented next is a summary of research done by these and other investigators[64] on machined samples of cortical bone (compact bone).

The tensile strength of dry bone has been found to vary from 7000 lb./in^2 to 40,000 lb./in^2 depending on the direction of loading, speed of load and geometry of the specimen (cubical vs. planar). The tensile strength of dry bone is less than its compressive strength (in some cases by as much as 1/2). The effect of drying on fresh or embalmed bones is to increase the tensile and compressive characteristics of the samples as well as the modulus of elasticity. As might be expected, strengths also vary in magnitude with the direction of testing (i.e., parallel or perpendicular to the long axis of the bone), thus exhibiting the anisotropic property of bone. (Most mechanical properties are greater in magnitude when tested parallel to the long axis.) Table VII

TABLE VI

ANALYTICAL FUNCTIONS EXPRESSED AS DISCRETE QUANTITIES*

TERM	ANALYTICAL	DISCRETE
Centroidal Coordinates:		
$\bar{x}, \bar{y}$	$= \frac{\int_A x dA}{\int dA}, \frac{\int_A y dA}{\int dA}$	$\rightarrow \frac{\Sigma_A x_i A}{\Sigma A_i}, \frac{\Sigma_A y_i A_i}{\Sigma A_i}$
Moments of Inertia:		
I_{xx}, I_{yy}, I_{xy}	$= \int_A y^2 dA, \int_A x^2 dA, \int_A xy dA$	$\rightarrow \Sigma y_i{}^2 A_i, \Sigma x_i{}^2 A_i, \Sigma x_i y_i A_i$
Moments of Inertia about Centroidal Axis:		
$\bar{I}_{xx}$	$= I'_{xx} - Ad^2 = \int_A y^2 dA - Ad^2$	$\rightarrow \Sigma_A y_i{}^2 A_i - \bar{y}^2 \Sigma A_i$
$\bar{I}_{yy}$	$= I'_{yy} - Ad^2 = \int_A x^2 dA - Ad^2$	$\rightarrow \Sigma_A x_i{}^2 A_i - \bar{x}^2 \Sigma A_i$
$\bar{I}_{xy}$	$= I'_{xy} - Ad^2 = \int_A xy dA - Ad^2$	$\rightarrow \Sigma_A x_i y_i A_i - \overline{xy}\, A_i$
The First Moment of Area, A_1, about Principal Axis:		
Q	$= \int_{y_1}^{c} y dA$	$\rightarrow \Sigma_{y_1}^{c} y_i A_i$

---

*$dA = \Delta A_i$ = amount of area element = A_i.

Figure 8. Stress and Strain in the Human Femur[63]

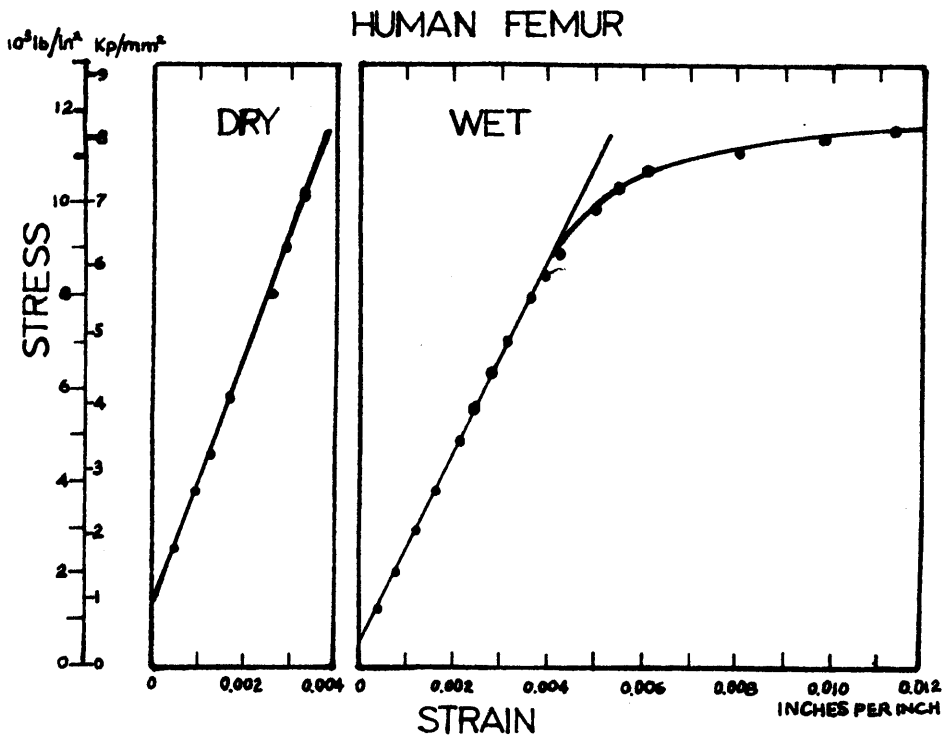
HUMAN FEMUR
10^3 lb/in^2
Kp/mm^2
STRESS
DRY
WET
0
0.002
0.004
0.006
0.008
0.010
0.012
INCHES PER INCH
STRAIN

TABLE VII[65]

DIRECTIONAL DIFFERENCES IN STRENGTHS OF COMPACT BONE

Author	Source	Bone	Condition	Loading Direction	(lb./in.^{2})
	N-Nonhuman H-Human		W-Wet D-Dry	*-Parallel **-Perpendicular	
		TENSILE STRENGTHS			
Hulsen	N	tibia	W	*	16,780
	N	tibia	W	**	12,970
Evans	H	femur	W	*	12,090
	H	tibia	W	*	12,688
	H	femur	W	**	2,326
	H	tibia	W	**	1,910
Sweeney, Byers, Kroon	N	femur	W	*	18,660
	N	femur	W	**	8,135
		COMPRESSIVE STRENGTHS			
Hulsen	H	tibia	W	*	29,760
	H	tibia	W	**	20,590
	H	humerus	W	*	29,040
	H	humerus	W	**	23,460
		BENDING STRENGTHS			
Dempster, Coleman	H	tibia	D	*	36,743
	H	tibia	W	*	27,224
	H	tibia	D	**	6,161
	H	tibia	W	**	4,639
		SHEARING STRENGTHS			
Rauber	H	femur	W	*	14,305
	H	femur	W	**	33,700

compares the ranges of variation in strength measurement due to the factors listed above. Table VIII shows a comparison of different strengths obtained for compact bone and long bone from the ulna. For further comparison, similar strengths for other bones are also tabulated. Measurements on the long bones were based on 5 proportional sections of the shaft. The middle portion of the shaft was generally the strongest for all bones studied. Figure 9 shows the stress-strain curves of the bones referred to in Table VIII.

TABLE VIII [66]

AVERAGE STRENGTHS OF ULNA, RADIUS, HUMERUS AND FEMUR

(WET, UNEMBALMED, LONGITUDINAL DIRECTION)

C: Compact Bone
L: Long Bone

		ULNA	RADIUS	HUMERUS	FEMUR
Tensile Strength (lb./in.^{2})	C:	21,472±213	21,614±199	17,775±114	17,633±156
Compressive Strength (lb./in.^{2})	C:	17,064	16,637	19,197	24,174
	L:	17,064	16,637	18,202	22,325
Bending Strength (lb./in.^{2})	C:	31,426	31,426	27,729	25,169±1564
	L:	32,706	32,990	30,573	30,146
Shearing Strength (_ to long axis) (lb./in.^{2})	C:	11,803±256	10,238±114	10,665±384	11,945±256
Modulus of Elasticity (lb./in.^{2})					
tension.....C:		2.67×10^6	2.69×10^6	2.49×10^6	2.50×10^6
bending.....L:		2.23×10^6	2.3×10^6	1.45×10^6	2.66×10^6

AVERAGE STRAIN					
Tensile (% Elongatron)	C:	1.49	1.50	1.45	1.41
		2.00	2.00	1.90	1.80
Compressive (% Contractron)	C:				

Figure 9. Stress-Strain Curves of Wet Long Bones in Compression[67]

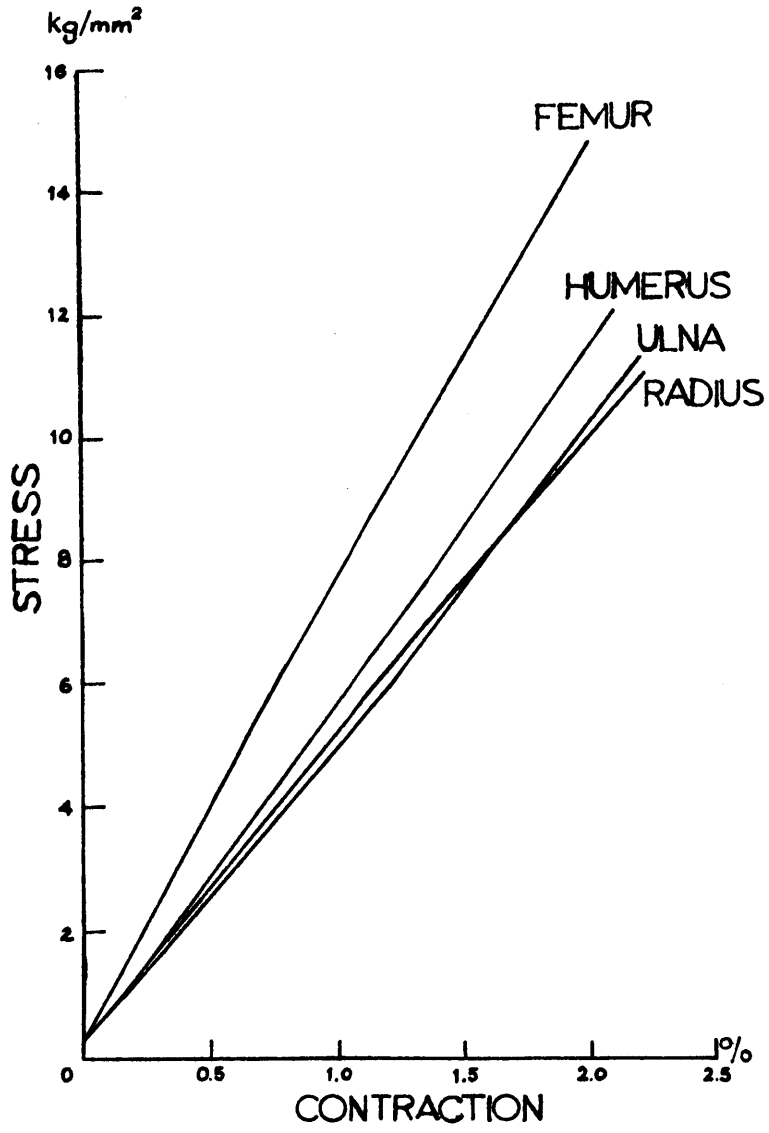
kg/mm²
16
14
12
10
8
6
4
2
0
STRESS
FEMUR
HUMERUS
ULNA
RADIUS
0.5
1.0
1.5
2.0
2.5
%
CONTRACTION

C. Application of Theory

The author's model for the ulna is a cantilever beam fixed at one end and loaded by a concentrated force, $\vec{P}$. The cross section of the beam is cylindrical, with inner radius r_1 and outer radius r_2. (See Figure 10) The problem is to determine analytically how this cross-sectional area responds to the local stresses acting on it, in particular those stresses (forces) pertinent to the ulna. Several approaches to the determination are presented below. Each approach is tested and discussed in Chapter V.

Case 1: $r_2 = r_2(x)$, $r_1 = r_1(x)$

The natural bone remodeling process implies that uniform strength at the outer fiber is necessary to prevent breakdown of the material (i.e. fracture). As given previously,

$$\sigma_x = \pm\frac{P_x}{A} \pm\frac{My}{I} \qquad \text{and } \frac{My}{I} = \frac{P_y xy}{I} \quad . \tag{3.23}$$

For now, let us assume that the positive signs are appropriate. Let σ_x equal a constant outer fiber stress. The distance to the outer fiber of the cross section is r_2. The cross sectional area is $A = \pi(r_2^2 - r_1^2)$ and the moment of inertia is given by $I = \frac{A}{4}(r_2^2 + r_1^2)$. If σ is a constant, then $\frac{\partial\sigma}{\partial x} = 0$. Thus

Figure 10. Forces on the Beam-Bone Model

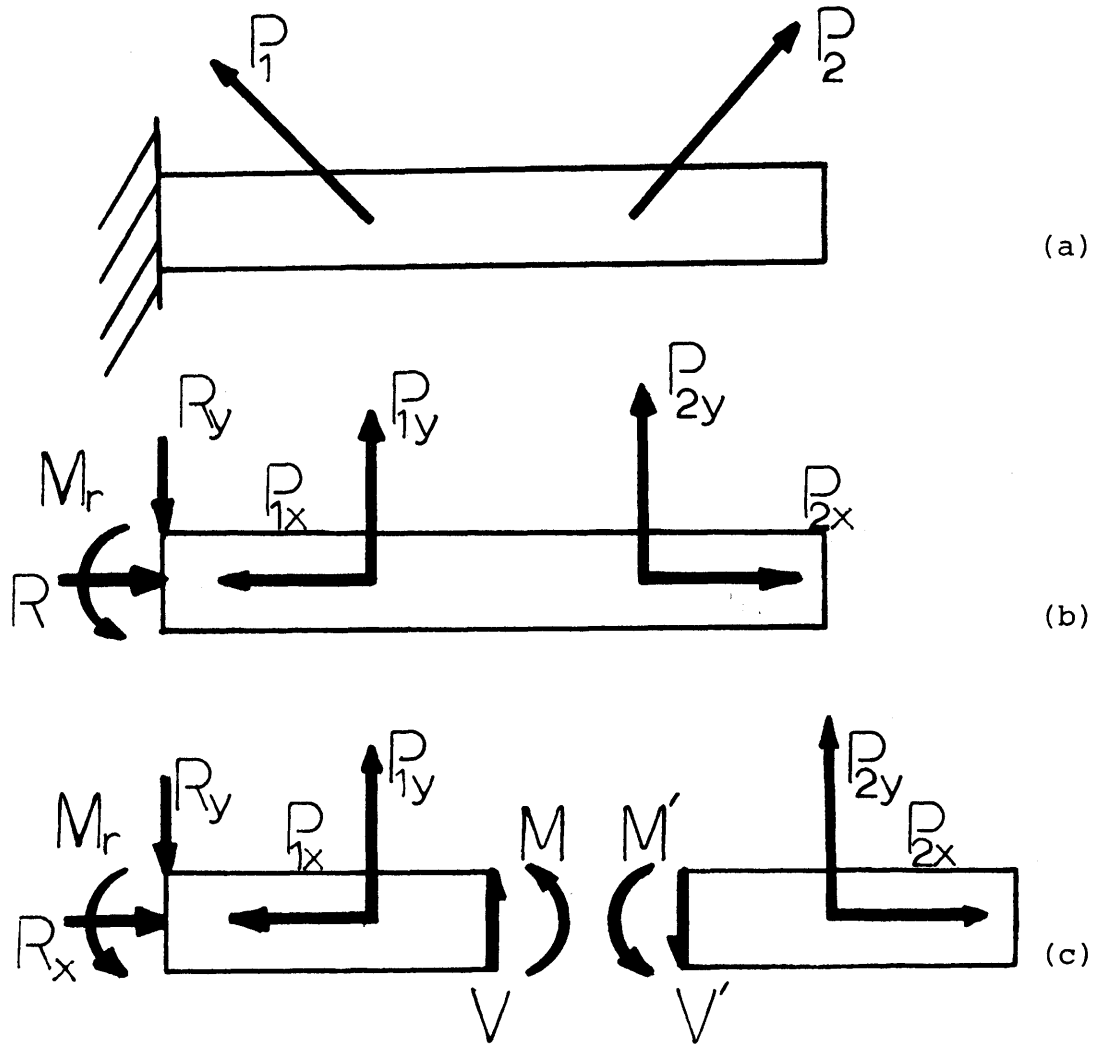

P_1, P_2	=	External Forces
R_x, R_y	=	Reaction Forces
M_R	=	Reaction Moment
V	=	Shear Force
M_b	=	Bending Moment

For the left portion of the beam shown in (c):

⟵ Positive Shear is upward

Positive Bending is counterclockwise

$$\frac{\partial\sigma}{\partial x} = 0 = \frac{P_x}{A}\left(\frac{-dA}{dx}\right) + \left[\frac{P_y x r_2}{I^2}\left(\frac{-dI}{dx}\right) + \frac{P_y x}{I}\frac{dr_2}{dx} + \frac{P_y r_2}{I}\right], \tag{3.24}$$

where $r_2 = r_2(x)$, $r_1 = r_1(x)$, $A = A(x)$, and $I = I(x)$. P_x and P_y are assumed to be constant in the ulnar region considered. Expressing Equations (3.24) in terms of the quantity γ gives (See Appendix I for the details of this and other equations presented in this section):

$$\gamma = \frac{\frac{I}{A^2}\frac{dA}{dx}}{\left[r_2 + \frac{x dr_2}{dx} - \frac{x r_2 A}{2I}\left(r_2\frac{dr_2}{dx} + r_1\frac{dr_1}{dx}\right) - \frac{x r_2}{A}\frac{dA}{dx}\right]} \tag{3.25}$$

where $\gamma = P_y/P_x$ = constant. Each term except γ in Eq. (3.25) can be calculated from experimental data. The components of the forces in γ are obtained from the computer program, to be discussed in Chapter IV, and are derived from consideration of the physical properties of the muscles acting on the bone. It is obvious that convenient simplification of this equation can be achieved by various assumptions. However, for the sake of completeness, this author used the equation in its rigorous form.

The term dA/dx in Eq. (3.25) is similarly assumed to be of some physical significance, since the author's premise is that the cross-sectional area of bone will remodel itself to reflect

the local forces acting upon it. Rearranging expression (3.25) yields:

$$\frac{dA}{dx} = \frac{4I\gamma A^2 \left[r_2 + \frac{xdr_2}{dx} - \frac{xr_2A}{2I}(r_2 \frac{dr_2}{dx} + r_1 \frac{dr_1}{dx}) \right]}{4I^2 + xA^2 r_2 \gamma (r_1^2 + r_2^2)} . \quad (3.26)$$

As can be seen, dA/dx is expressed in terms of the component force ratio, γ, and quantities dependent on the geometry of the cross section. As discussed above, each term except γ can be obtained experimentally.

Case 2: r_2 = constant, $r_1 = r_1(x)$

The next case is simply to fix r_2 and to let r_1 be variable. This condition simulates the effect of the varying inner boundary of cancellous bone relative to the fixed outer boundary of cortical bone. γ and dA/dx then become:

$$\gamma_1 = \left(\frac{r_1^2+r_2^2}{rAr_2}\right) \frac{dA}{dx} \left[1 - \frac{xr_1}{r_1^2+r_2^2} \frac{dr_1}{dx} - \frac{x}{A} \frac{dA}{dx} \right]^{-1} , \quad (3.27)$$

$$\gamma_2 = \frac{2\pi I r_1}{A^2} \frac{dr_1}{dx} \left[r_2 - \frac{xr_1 dr_1}{dx} \left(\frac{r_2 A}{2I} - \frac{2\pi r_2}{A}\right) \right] , \quad (3.28)$$

and

$$\frac{dA}{dx} = \frac{4Ar_2\gamma \left[1 - \frac{2xr_1}{r_1^2+r_2^2} \cdot \frac{dr_1}{dx} \right]}{r_1^2 + r_2^2 + 4xr_2\gamma} . \quad (3.29)$$

γ_2 explicitly allows for the varying r_1 and fixed r_2 while γ_1 allows the area to change with x, but attributes the total change in area to r_1.

Case 3: Exact Calculation of σ_x, Z(x), c(x)

Data for all terms in Eq. (3.23) are substituted into it to establish the true variation of σ_x with x. Comparison of the axial stress component with the component due to bending is made and studied graphically. This information is then used to study the section modulus, Z, and the distance to the outer fiber, c.

The section modulus is an obvious quantity to investigate since, for a beam of uniform strength, each cross section will have only the area necessary to satisfy conditions of strength. Let σ_b = maximum stress due to bending = $\sigma_{max} - P_x/A$. Therefore,

$$Z(x) = \frac{I(x)}{c(x)} = \frac{M_b(x)}{\sigma_b(x)} . \tag{3.30}$$

Experimental results are compared with calculated values of Z.

Since the maximum stress occurs at the outer fiber, then

$$y = c(x) = r_2(x),$$

$$I(x) = \frac{A(x)}{4}(c^2(x) + r_2^{\,2}(x)) , \tag{3.31}$$

and we have

$$\frac{A}{4}\,(c^2 + r_2{}^2) = \frac{M_b c}{\sigma_b} \quad ,$$

or

$$c^2 - \frac{4M_b c}{\sigma_b A} + r_2{}^2 = 0 \quad .$$

Therefore,

$$c(x) = \frac{2M_b(x)}{\sigma_b A(x)} \pm \frac{1}{2}\sqrt{\left(\frac{4M_b}{\sigma_b A}\right)^2 - 4r_2{}^2(x)} \quad . \tag{3.32}$$

<u>Case 4</u>: <u>Shear Stress τ_{xy}</u>

The variation in shear stress is considered graphically via measurements of the specimens and analytically via the shear formula derived from analysis of the beam loading. As indicated in Eq. (3.14)

$$\tau_{xy} = \frac{VQ}{I_z t} \quad , \text{ where } Q = \int_{A_1} y dA. \tag{3.33}$$

The shear force v_y, is just P_y for the model presently being considered and t is $2(r_2-r_1)$. Q will change for $y<r_1$ and $y>r_1$ according to Eqs. (3.34).

$$Q_1 = \frac{2}{3}\left[(r_2-y^2)^{3/2} - (r_1{}^2-y^2)^{3/2}\right] , \quad y<r_1$$

$$Q_2 = \frac{2}{3}\left[r_2{}^2-y^2\right]^{3/2} , \quad y>r_1$$

$$Q = \frac{2}{3}\left[r_2{}^2-r_1{}^2\right]^{3/2} , \quad y=r_1$$

τ_{xy} becomes

$$y<r_1 \qquad \tau_{xy} = \frac{4}{3}\frac{P_y}{A}\frac{(r_2{}^2-y^2)^{3/2}-(r_1{}^2-y^2)^{3/2}}{(r_2-r_1)(r_2{}^2+r_1{}^2)} ,$$

$$y>r_1 \qquad \tau_{xy} = \frac{4}{3}\frac{P_y}{A}\frac{(r_2{}^2-y^2)^{3/2}}{(r_2-r_1)(r_2{}^2+r_1{}^2)} . \tag{3.35}$$

Of interest are the average shear, τ_{avg}, which is the shear force divided by the cross-sectional area; maximum shear, τ_{max}; and intermediate shear, τ_{r_1}, at $y = r_1$. Also of interest is the stress-geometry correlation, as well as information which may be obtained from consideration of these cases. Thus,

$$\tau_{avg} = \frac{V}{A} = \frac{P_y}{A} \tag{3.36}$$

$$\tau_{max} = \frac{4}{3}\frac{P_y}{A}\frac{(r_2{}^2+r_1r_2+r_1{}^2)}{(r_1{}^2+r_2{}^2)} \tag{3.37}$$

$$\tau_{max} = \alpha(x)\ \tau_{avg} \tag{3.38}$$

where

$$\alpha(x) = \frac{4}{3}\ \frac{(r_2^{\ 2}+r_1 r_2+r_1^{\ 2})}{r_1^{\ 2}+r_2^{\ 2}} \tag{3.39}$$

and

$$\tau_{r_1} = \tau_{avg}\ \frac{4}{3}\ \frac{(r_2^{\ 2}-r_1^{\ 2})^{3/2}}{(r_2-r_1)(r_1^{\ 2}+r_2^{\ 2})} \tag{3.40}$$

IV. EXPERIMENTAL PROCEDURE

A. Specimen Characterization

Specimens were obtained by the author from cadavers owned by the Harvard Medical School Gross Anatomy Department. Of seven pair (left and right) of radii and ulnae obtained, two pair were used in establishing investigative procedures; three pair were intensively studied and provided the data used in this thesis; and two pair have been reserved for future analysis. All specimens were taken from male cadavers ranging in age from 49 to 69 years. Since the only specifics provided with each cadaver were sex, age and cause of death, the following criteria for selection of suitable specimens were established:

(1) cause of death should not be related to skeletal tissues or joints;

(2) specimens should show no fractures or growth abnormalities;

(3) cartilage on the articular surfaces of the proximal and distal ends of the radius and ulna, should show no signs of arthritis or joint disease; and

(4) if possible, a complete set of forearm bones from both arms should be taken from a given cadaver.

Each of the seven sets of specimens evidence some degree of articular wear at the joints. Locations of consistently observable surfaces of wear are:

(a) in the trachlear notch perpendicular to the vertical groove at approximately 90°-110° from the coronoid process and

extending medially and laterally to the outer edges of the trachlear notch. (This surface articulates with the concave - convex hyperboloidal surface of the trochlea.-- See Figure 2b);

(b) on the superior surface of the radial head along the slightly convex border (circular in the transverse plane) which articulates with the convex surface of the capitulum; and

(c) on the medial surface of the radial head along the surface of its 80° articulation with the radial notch of the ulna.

Table IX lists specimens obtained, ages of the donors, and overall degree of articular wear observed. Tables X and XI list measurements taken on the radii and ulnar after all muscle tissue was dissected away from the bone. The legend is given below and Figure 11 displays the parameters defined.

TABLE IX

SPECIMEN

Harvard Identification Number	Age (years)	Degree of Articular Wear*			
		L.U.	R.V.	L.R.	R.R.
355	67	3	No Specimen	2	No Specimen
386	59	2	3	2	3
332	55	3	2	2	2
446	69	2	3	2	2
449	49	2	3	2	3
404	**	3	3	2	3
477	53	2	2	1	2

*Degree of Visible Wear:

1 = little or none

2 = moderate

3 = extreme

**no information

L,R = Left, Right

U,R = Ulna, Radius

LEGEND FOR TABLES X AND XI

L_l = length of the radius measured laterally, from the superior surface of the radial head to the distal projection of the styloid process.

L_m = length of the radius measured medially, from the superior surface of the radial head to the distal edge of the ulnar notch

h_l = lateral measurement of the radial head from its superior articular surface to the proximal edge of the radial neck

h_m = medial measurement of the radial head from its superior articular surface to the proximal edge of the radial neck

L_p = length of the ulna measured posteriorly from the proximal surface of the olecranon to the distal projection of the styloid process

L_r = approximate distance over which the interosseous ridge is prominent.

L_c = distance from the anterior projection of the coronoid process to the beginning of the interosseous ridge

d = distance between the proximal projection of the olecranon and the anterior projection of the coronoid process

wt = weight of the long bone.

TABLE X

RADIAL MEASUREMENTS

No.	L_l(in.)	L_m(in.)	h_m(in.)	h_l(in.)	wt(lbs.)
446L	9.85	9.2	.428	.389	.169
446R	10.0	9.18	.427	.377	.169
449L	9.33	8.71	.448	.410	.15
449R	9.22	8.70	.427	.420	.15
332L	10.43	9.83	.533	.513	.20
332R	10.50	9.95	.505	.495	.188
*386L	10.25	9.75	.501	.495	*
*386R	10.40	9.90	.444	.452	*
*355L	9.981	9.188	.453	.524	*
*404L	10.20	9.58	.483	.404	.188
*404R	10.45	9.80	.488	.440	.188
*477L	9.62	9.03	.402	.395	.181
*477R	9.63	9.04	.437	.359	.181

* Specimen used to establish investigative procedures -- no weight measurement obtained.

** Specimen reserved for future analyses.

TABLE XI

ULNAR MEASUREMENTS

No.	L_p(in.)	L_r(in.)	d(in.)	L_c(in.)	wt(lbs.)
446L	10.70	4.0	.95	1.5	.213
446R	10.73	4.0	.95	1.5	.213
449L	9.99	4.0	.90	2.0	.163
449R	9.96	3.5	.90	2.0	.163
332L	11.20	5.0	1.05	1.6	.213
332R	11.36	5.56	.99	1.6	.213
*386L	11.125	5.2	.94	---	*
*386R	11.30	5.1	.96	---	*
*355L	10.45	5.4	.92	---	*
**404L	10.85	4.0	.88	---	.206
**404R	11.15	3.5	.95	---	.219
**477L	10.32	3.0	.85	---	.231
**477R	10.34	3.0	.85	---	.219

* Specimen used to establish investigative procedures -- no weight measurement obtained

** Specimen reserved for future analyses

--- Measurements were not obtained

Figure 11. Length Measurements of the Radius and Ulna

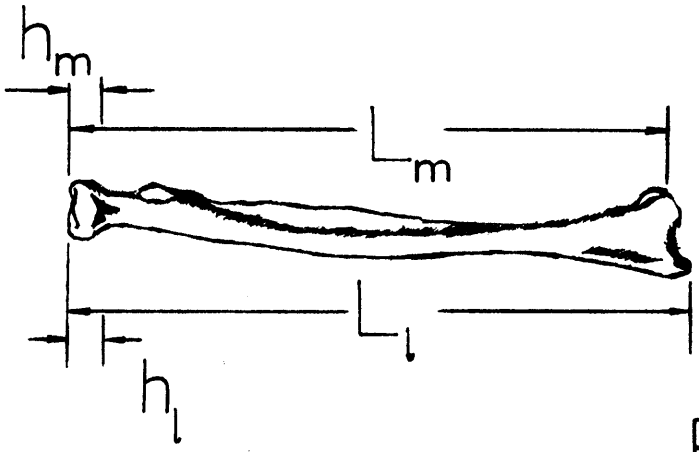

RADIUS

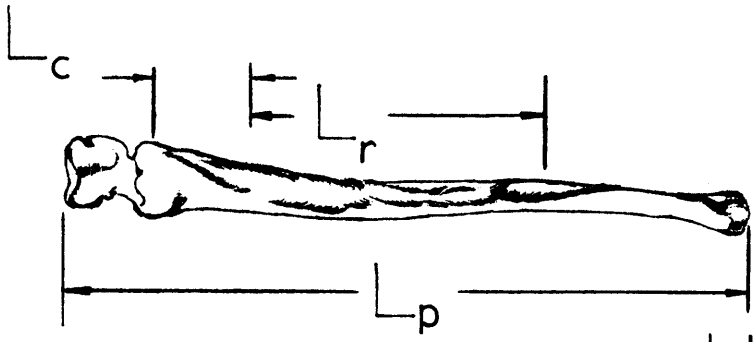

ULNA

B. Orientation Procedure

The specific orientation of the ulna in space relative to the radius and the humerus had to be ascertained for each specimen and a method developed to reproduce the orientation for subsequent studies. A procedure was developed for referencing each ulna-radius set in a consistent manner from specimen to specimen. A reference plane was determined with respect to which bone sections were cut. The construction of this plane is described below (refer to figs. 12 and 13 during this discussion).

The ulna and radius were loosely bound together in an anterior-supine position approximating 90° flexion. The distal radius was not allowed to rotate about the ulnar head. The position of the distal radius was established by the intersection of two lines: (1) the bisector of the ulnar head and distal styloid process of the ulna and (2) the line joining the bisectors of the ulnar notch and the distal styloid process on the radius. Thread was used to indicate the lines and their intersection point, and adhesive tape was used to maintain the position. The radial head was then stabilized against the radial notch. These steps define articular surfaces restrained to be in contact with one another in a specified orientation. A 1/4-inch hole* was drilled through back and proximal and

* The length of the 1/8-inch drill bits available did not permit continuous drilling from the distal end to the proximal end of the taped set of bones. To avoid the buckling of a longer thin bit, a 1/4-inch bit was used to drill inward from each end of the bones toward the center. The diameter of the larger bit allowed insertion of the 1/8-inch glass rod through both holes despite the fact that the direction of the holes was generally nonaligned.

Figure 12. Detailed Views of Prepared Specimen

Distal Articular Surface of Radius

DISTAL VIEW

Anterior View of Radius, Ulna & Rod

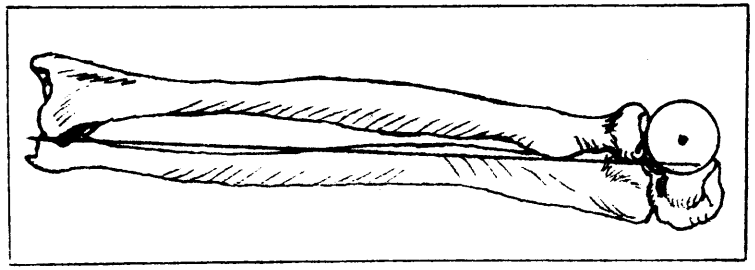

ANTERIOR VIEW

Glass Cylinder

Radial Head

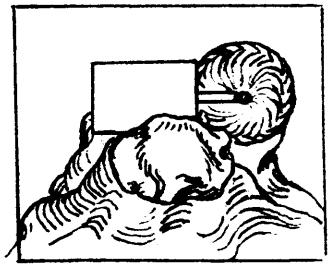

PROXIMAL VIEW

Figure 13. Construction of the Reference Plane

Anterior View:

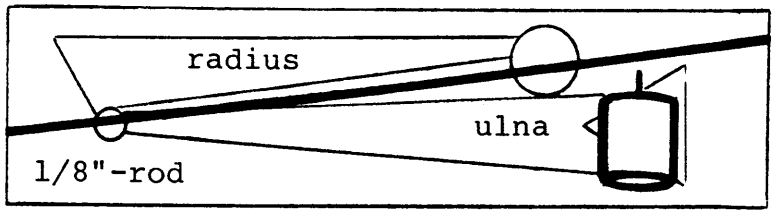

Proximal View:

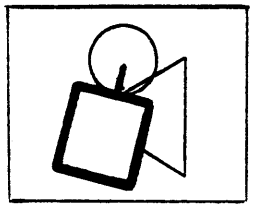

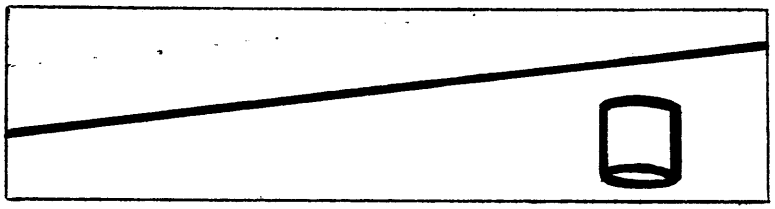

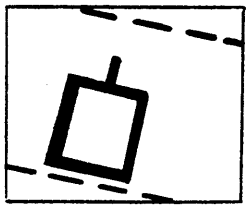

Medial View:

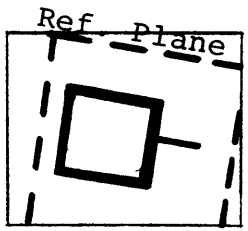

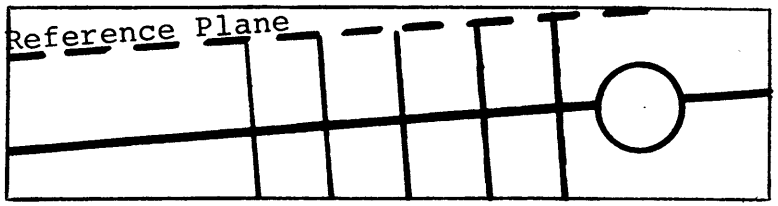

transverse cuts

distal contact points and a glass rod, 1/8-inch in diameter, was inserted and stabilized in the holes using Duco Cement. This reference rod fixed the orientation of the ulna relative to the radius. The reference plane was later cut so as to be parallel to the reference rod.

An 1/8-inch hole was drilled in the center of the superior surface of the radial head and a 2-3 inch segment of copper wire, gauge 13, was set vertically in place, approximately parallel to the long bone of the radius. A glass cylinder, 1-inch in length and 3/4-inch in diameter, was used to approximate the transverse axis through the distal humerus. A hole, ∿1/16-inch in diameter and 1/16-inch in depth was drilled at the center of one planar end surface of the cylinder and a segment of copper wire, ∿1/2-inch in length was inserted with good fit. The cylinder was then placed in the olecranon and electrical tape was used as a filler, providing contact between the cylindrical surface and the inner curvature of the trochlear notch of the ulna. Refer to Figure 12. Plasticine provided added stability. The cylinder was positioned so that the protruding wire intersected the wire extending from radial head at approximately 90°. The orientation of the smooth surface of the glass cylinder perpendicular to the wire simulating the trochlea's axis defined a second plane, thus completing the orientation process.

A small amount of plasticine was placed on the posterior surface of the set of bones and the entire configuration

(bones, rod, cylinder, wires, plasticine) was placed in a glass container 3-1/2 x 4 x 12-1/2 inches in outer dimension. Clear cast, liquid plastic, was used to fix the total configuration. It was found that the best molds were obtained when 36 drops of catalyst* were gradually added to 1.4 litres of Clear Cast. The average curing time at room temperature was approximately 18 hours. Since the purpose of the mold was to fix all components of the oriented specimen in place, attention was not given to cracks in the casting which occurred at locations of extreme curvature during the curing process. Penetration of the plastic into the shaft of the long bones also was not a concern since emphasis of this study was only on the structure of cortical bone.

C. Sectioning

The sample (mold) was then machined to obtain the reference plane for the direction of sectioning. (Refer to Figure 13.) Using a flycutter on a milling machine, the sides of the sample were cut parallel to the oriented plane of the cylinder. The machined sides were polished with metallographic grinding and polishing papers to improve transparency. The sample was then mounted and aligned parallel to the long 1/8-inch glass rod. The final plane was machined above the rod and parallel to it.

---

* methyl ethyl ketone peroxide in dimethyl phthalate.

This reference plane became the surface against which transverse sectioning of the sample was undertaken. Any cut taken perpendicular to this plane is also perpendicular to the circular cross-section of the glass rod.

Sectioning was accomplished using a diamond band saw .04-.05-inches thick. The sample was placed flat on the reference plane and the first cut made at the proximal superior surface of the radial head. Each sample was normalized to obtain seventeen serial sections between the first cut and the last at the distal tip of the radius. Table XII shows the resulting thickness of each section. Initially the faces of each section were ground and polished to remove the lines produced by the serrated teeth of the diamond band saw. It was later found that the lines proved useful in quickly depicting the direction of cut relative to the cross-sections of the rod, ulna and radius; and the perpendicular plane against which the cut was made.

The sections were labeled accordingly:

Identification Number	Left or Right	Number of the Section, counting from the proximal end.		
446	L	12	⟶	446L12

Section numbers 4 through 15 correspond to the long bone shaft of each sample. It is data from these sections which was analyzed in detail according to the following procedures.

TABLE XII

THICKNESS OF SECTIONS (inches)

Section Number	446L	449L	332L	446R	449R	332R
4	.543	.545	.583	.562	.531	.595
5	.542	.510	.585	.545	.522	.594
6	.542	.503	.584	.543	.521	.594
7	.542	.509	.585	.547	.521	.594
8	.539	.510	.587	.545	.506	.595
9	.539	.504	.587	.544	.515	.597
10	.540	.505	.588	.542	.515	.595
11	.539	.506	.588	.544	.516	.595
12	.539	.505	.588	.543	.521	.591
13	.542	.506	.589	.542	.511	.593
14	.535	.505	.583	.544	.523	.591
15	.554	.513	.587	.545	.546	.591
Average	.541	.510	.586	.546	.521	.594

D. Photographic and Tracing Procedure

Each section was placed on a black surface for greater contrast of the bone structure and rod components. Polaroid photographs were taken with appropriate combinations of filters and exposure times and the negatives were enlarged to enable prints to be made, as in Figure 14.

A tracing was made of each enlargement: the inner boundary of each cross section was drawn so as to encompass all cancellous bone regardless of the extent to which the transitory state from cancellous to cortical bone had occurred. The 1/8-inch glass rod cross-section was indicated on the tracing also. The difference between the true 1/8-inch diameter of the actual rod and its photographic dimension allowed computation of a scale factor for each enlargement. Two of the many parallel texture lines in the section caused by the band saw were also traced for reference and for orientational purposes. The final tracings, depicting cross-sections of the ulna, radius, and glass rod, and two parallel lines, became the prototypes from which all gross numerical data were obtained. The tracing corresponding to Figure 14 is shown in Figure 15 and the data obtained from it is also listed. Details of the markings on the tracing are discussed in the next section.

Figure 14. An Enlargement of Section 332L8

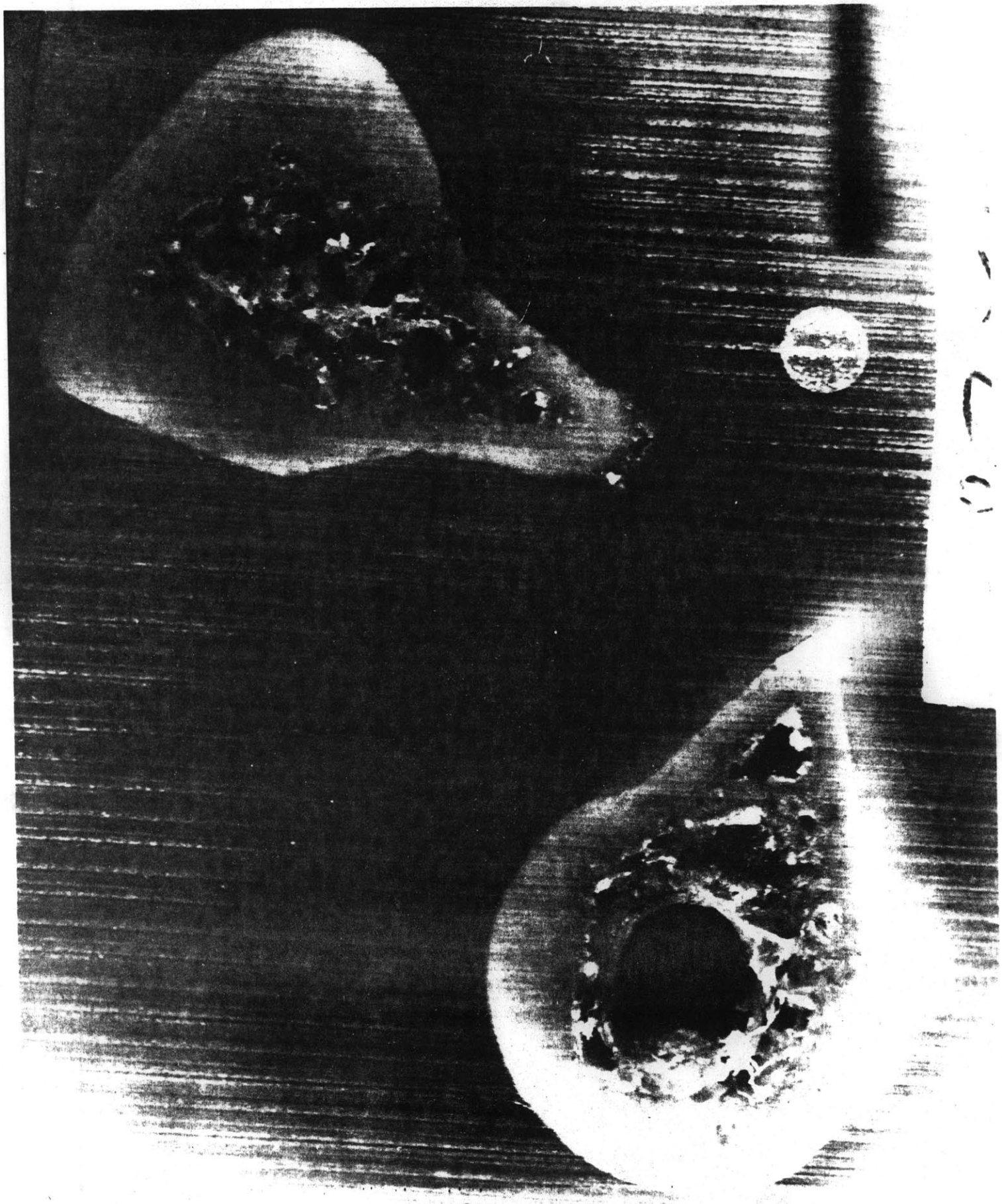

Figure 15. A Tracing of the Enlargement in Figure 13 - 332L8

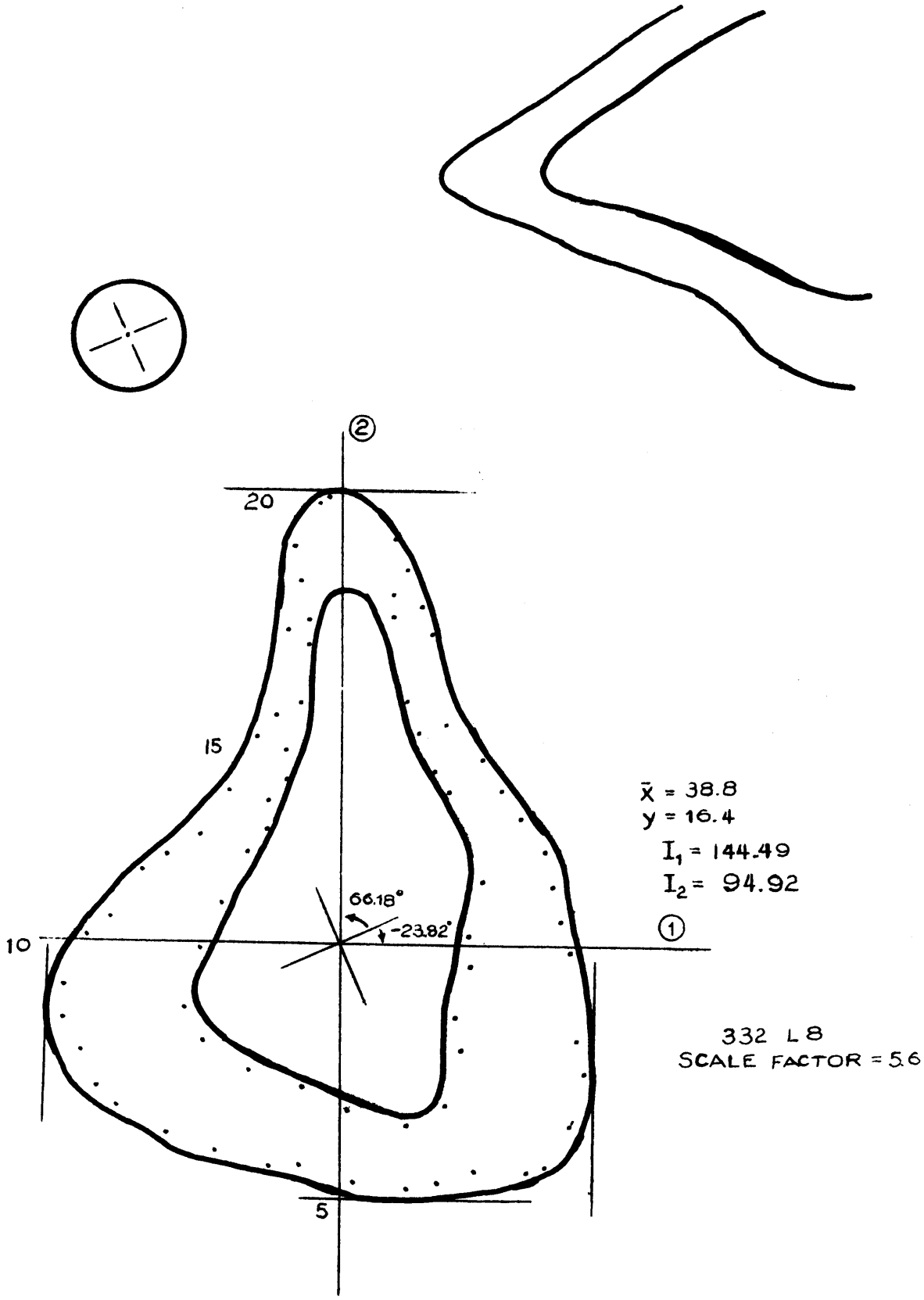
②
20
15
10
5
66.18°
-23.82°
①
$\bar{x}$ = 38.8
y = 16.4
I_1 = 144.49
I_2 = 94.92
332 L 8
SCALE FACTOR = 5.6

E. Compilation of Data

During preliminary data analysis, two approaches were attempted which were subsequently discarded. The first involved the use of a planimeter to obtain area measurements. The planimeter gave relative numbers which could be calibrated to yield absolute numbers, however area was the only quantity obtainable. The second approach utilized the M.I.T. Architecture Department's CADDS3 computer graphics system to obtain digitized data with which to perform the necessary calculations. Major problems were encountered both because of the limited storage capacity of the system, and because of the system's inherent arbitrary positioning of zero. Time, however, became the overwhelming drawback: the system searches all the data stored to verify that the coordinate it assigns are correct for each entity that the user indicates. The greater the number of entities, the longer it takes for the system to verify the point and assign a value to it. The three dimensional nature of CADDS3 is ideal for quantitatively investigating a structure's orientation in space, but inefficient for this study in the current stage of development. Having eliminated the planimeter and computer graphics techniques, manual compilation of the data was finally undertaken.

A 1/4-inch square grid, 18 inches in length and 12 inches wide, was prepared. The abscissae and ordinates were numbered with consecutive integers with (0,0) located in the lower left

hand corner of the grid. Coordinate (40,33) was arbitrarily taken as the common reference point. Each tracing was placed on the grid, simultaneously aligning the two band saw texture lines parallel to the y-axis and centering the 1/8-inch glass rod cross-section on point (40,33). The rod and lines established the tracing's orientation in space for reference to subsequent tracings involving other sections of the same specimen.

Data was obtained from the ulna alone, proceeding horizontally along the x-axis of the grid and completing a row before incrementing in the y-direction. The amount of each 1/4-inch square area element (A_i) contained within the cross section and the x-, y-coordinates of the centroid of each of these elements (x_i,y_i) were tabulated. See Figure 16a. There was an average of 150 sets of data (x_i, y_i, A_i) per cross section (72 total).

With this data as a base, computer programs were then written by the author to calculate the following quantities based on the equations presented in Table VI:

1. the total area of the cross section, (A);

2. the coordinates of the centroid of the cross-section relative to the origin of the grid, ($\bar{x}$,$\bar{y}$);

3. the moments of inertia about the centroid, (I_{xx}, I_{yy}, (I_{xy}); and

4. the principal moments of inertia (I_1,I_2) and their orientation relative to the centroid (Θ_1,Θ_2).

Figure 16. Data Compilation Process

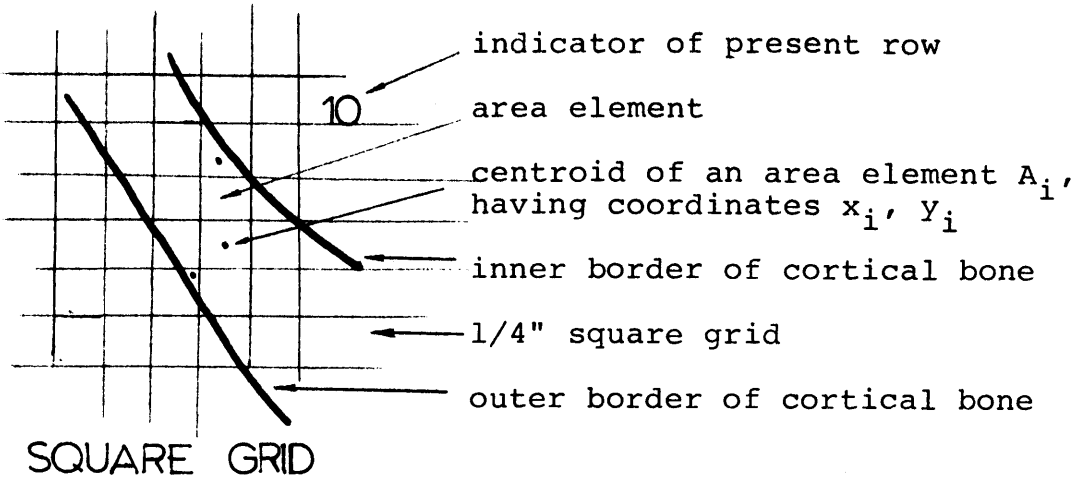

$$\frac{\sum_{j=1}^{36} r_j(\text{outer})}{36} = \bar{r}_{outer}$$

$$\frac{\sum_{j=1}^{36} r_j(\text{inner})}{36} = \bar{r}_{inner}$$

$$\bar{r} = \bar{r}_{outer} - \bar{r}_{inner}$$

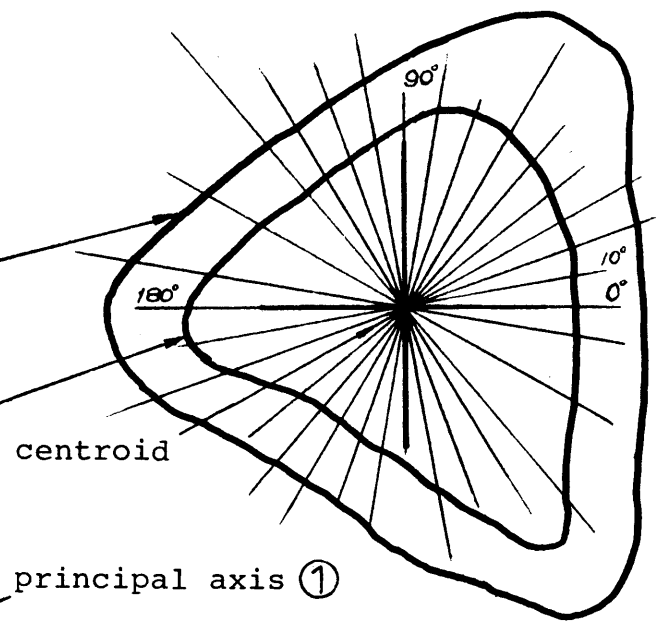

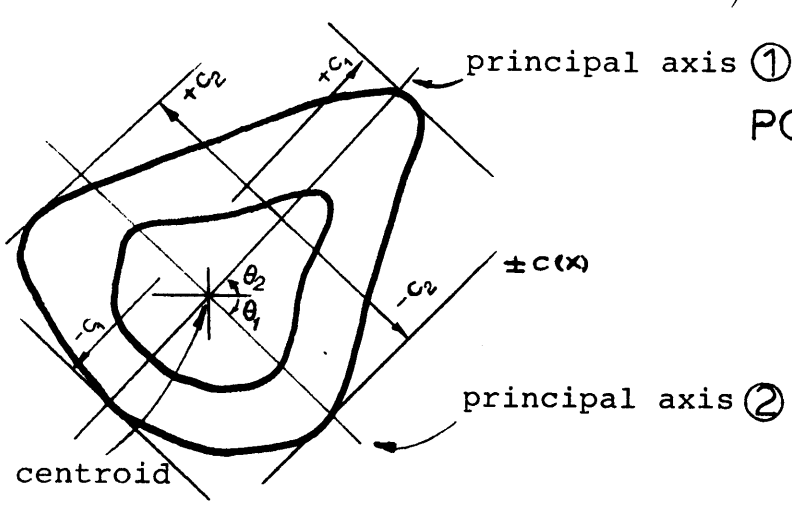

On each tracing, after realignment, the location of the centroid was indicated.

Next, the tracing was placed on a polar grid, matching the centroid with the origin of the grid. (Figure 16b) Radial measurements of the distance to the inner and outer boundaries of the cross section were taken in increments of 10° counter-clockwise relative to the centroid (36 measurements per boundary). Average inner and outer radii were calculated from this data and their difference, i.e., $r_{outer} - r_{inner}$, as a function of displacement was noted. Differences between the radii of adjacent sections at a fixed angular orientation were also obtained and studied. The polar grid was also employed to construct the axes of the principal moments relative to the centroid. Figure 14 shows these axes, labeled 1 and 2 as well as the location of the centroid and 30° indicators used in obtaining the radial data. Markings were drawn on the periphery of the cross section parallel to the appropriate principal axis. (Figure 15c) The distance between each marking and its respective axis was recorded as $\pm c(x)$, the distance from the neutral surface to the outermost fiber of the bone.

The tracing was then positioned on the rectangular grid so that the principal axis-2- was aligned parallel to the x-axis. The area elements and the y-coordinate of the centroid of each element were tabulated above and below the 2-axis. From this data, Q was obtained. The results of the above calculations will be presented in Chapter V.

F. Data Obtained from the Literature

The data discussed in the preceding section was used to test the cylindrical-beam model of the bone. A decision as to muscle participation and numerical information about the forces was necessary. The flow chart in Figure 17 shows the computer program manipulation of the data (Section IVA.) obtained from the literature and theory, and the data obtained by the author.

Calculation of the muscular forces acting on the ulna was initially based on a computer program designed to investigate the biomechanics of the elbow joint.* Since flexion against resistence is the most important activity of the forearm, the resultant of the flexor muscles at the elbow joint was computed for varying degrees of flexion. Townsend obtained the relative magnitude of the forces since experimental data in the literature did not yield information on individual muscles. The major assumptions of this program were:

(1) all muscles are alike in fiber arrangement (fusiform versus penniform) and are considered to be straight during flexion;

(2) the cross-sectional areas of the muscles are assumed to remain constant for all degrees of flexion;

(3) each muscle attachment point lies along the bone axis

---

* Townsend, while a graduate student at M.I.T., developed this program as he investigated the function of cancellous bone in the elbow joint.

Figure 17

FLOW CHART OF DATA SOURCES

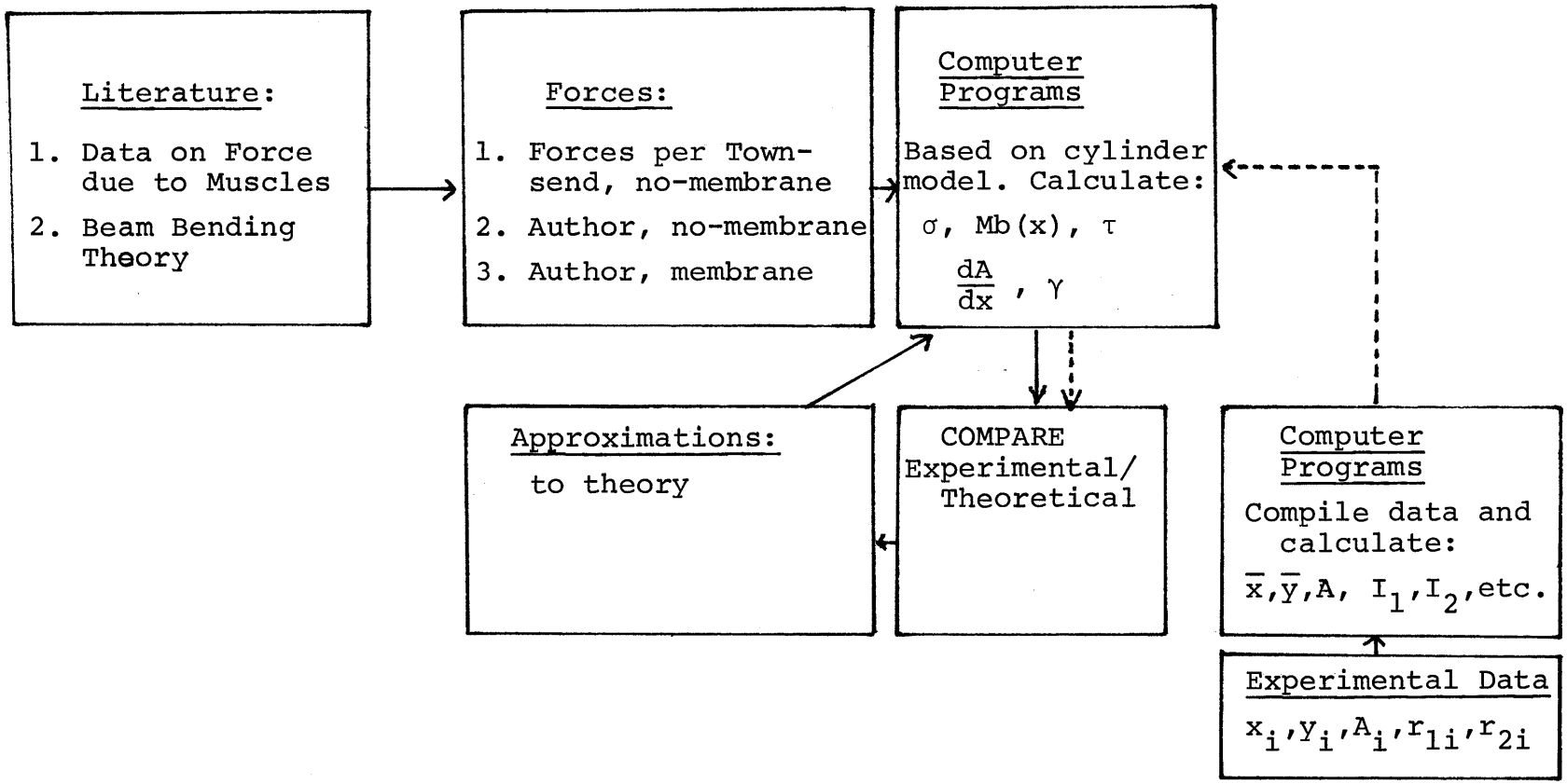

including the pivot point of the elbow;

(4) at a constant angle of supination-pronation, the annular ligament, along with the interosseous membrane, maintains the same θ for both the ulna and radius;

(5) the force due to muscles at the hand and/or resistance is shared equally by the radius and ulna at the wrist;

(6) the ulna is assumed to support the y-component of the resultant forces when separate analysis of the individual bones is undertaken;

(7) the weight of the forearm is assumed to be insignificant;

(8) a muscle's force is proportional to its cross sectional area and to the fractional change in its length.

On these bases, Townsend calculated the magnitude of the reaction force at the elbow normalized relative to the resistance at the hand. Table XIII lists the flexor muscles mentioned in Chapter II and their anatomical data.

The above assumptions are supported by experimental evidence in some cases, but rest on intuitive reasoning in others. Thus, the author used the results of the program only in preliminary investigations, and then modified the calculation to reflect the following considerations:

(a) Although the hinge motion of the ulnar articulation carries the forearm about the elbow during flexion, the insertion of the biceps brachii into the radial tuberosity of the radius and this muscle's strong participation when flexion

TABLE XIII

REFERENCED EXPERIMENTAL DATA ON MUSCLES[68]

(Attachment points are measured from the pivot point of the elbow)

Muscle	Forearm Attachment (in.) U=Ulna R=Radius	Humerus Attachment (in.)	Muscle Cross-Sectional Area (in.^{2})	[56] Lever Arm Ratio (in.) for O=90°
BRACHIALIS	1.276 (U)	4.016	1.35	.0965
BRACHIORADIALIS	8.714 (R)	3.188	.33	.2376
BICEPS BRACHII	1.777 (R)	11.403	1.04	.1393
EXTENSOR CARPI RADIALIS LONGUS	9.01 $\frac{1}{2}$(U,R)	1.306	.46	.1026
PRONATOR TERES	4.609 (R)	.562	.42	.0443
INTEROSSEOUS MEMBRANE	3.0-5.0 (U,R)	-----	.285-.475	----

is heavily resisted implies a considerable y-component of force which should be attributed to the radius, not the ulna. Therefore, assumption (6) is relaxed and the y-components of the individual forces are likewise separated into radial and ulnar. Hence, assumption (5), but not (6), the brachiolis (B), half the extensor carpi radialis longus (ECRL) and the resistance (R) are the concentrated forces under consideration in the force analysis (See Table XIII).

(b) Although the biomechanical properties of the muscles are normalized relative to each other and to the resistance, numerical data is needed to compute the desired stress equation. Yamada[69] estimated the average strength of skeletal muscle to be 47 lb./in.^{2}, while Elftmann and Ikai (as noted in Chapter II) obtained values of 47- and 70 lb./in.^{2} (3.3-4.7 kg/cm^2) for the strength of the flexor muscles. For this work, 60 lb./in^2 was chosen as the strength of the flexors. The muscle cross sectional areas are given in Table XIII, and the lever ratio, discussed in Chapter II, was used to weight the magnitude of each force relative to the angle of flexion. The resistance force was chosen arbitrarily to be 15 lbs. The forearm position was fixed at 90° to approximate the cantilever beam.

(c) Townsend did not include the interosseous membrane in his work since it is considered to act only as a stabilizer between the ulna and radius. The author initially attempted to ignore the influence of this membrane on the ulna, but examin-

ation of the bone cross sections during the experiment suggest its inclusion in force considerations. Steindler[70] (per Fessler) reports that the interosseous membrane resists tension up to 143 lbs. in the longitudinal direction and 200 lbs. in the transverse direction, yielding a resultant maximum tensile force of 246 lbs. at 54.4° to the lateral surface of the ulnar shaft. The author chose to use half of the magnitude of this force as a first approximation to express the participation of the membrane in the stress analysis of the ulna. The membrane was taken to be a uniformly distributed force acting in tension on the beam. The author also assumed that the components of the force in the plane of the cross section act only along either of the principal axes of the cross section. Figure 18 shows a free body representation of the beam model with the membrane force, as well as the concentrated loads, included.

Table XIV lists the magnitudes of the forces used in the ultimate calculations for two cases: exclusion and inclusion of the interosseous membrane. The results per Townsend were used in the former case (i.e. exclusion), while the author's results were applied to both.

To obtain these magnitudes, the cross-sectional area of each muscle was multiplied by the lever arm ratio to determine the fraction of area participating in the force for each muscle. Each fraction was then divided by the sum of the fractions and multiplied by 100 to give the percent partici-

Figure 18. Modified Beam-Bone Model

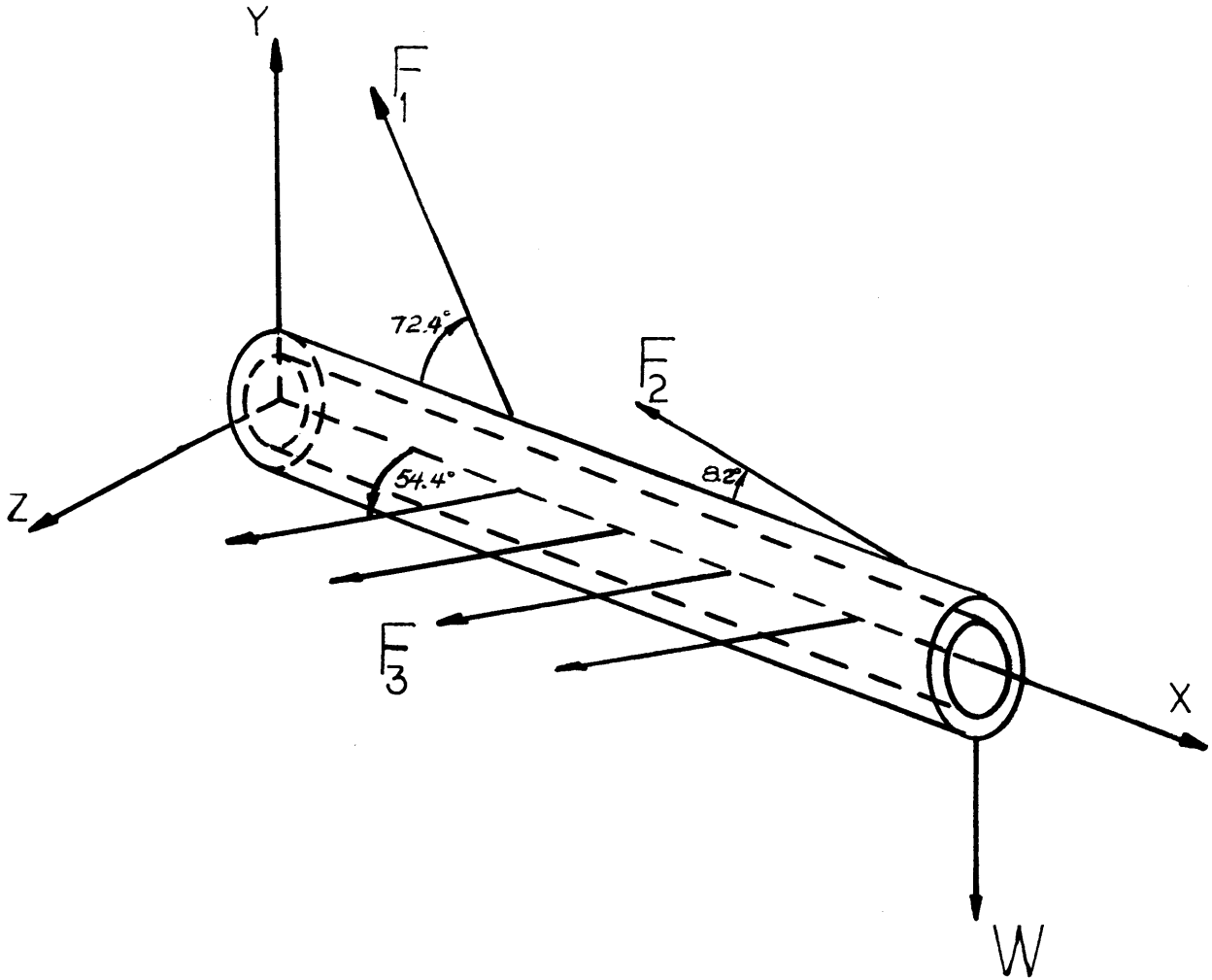
Y
F1
72.4°
F2
8.2°
54.4°
Z
F3
X
W

TABLE XIV

MAGNITUDE AND DIRECTION OF FORCES

	No Membrane		Membrane	Direction O
	I (dimensionless)	II (lbs.)	III (lbs.)	(Relative to Forearm)
Brachialis (B)	26.865	67.2	67.2	72.4°
Biceps Brachii (BB)	29.876	74.5	74.5	81.1°
Extensor Carpi (ECRL) Radialis Longus	9.850	24.4	24.4	8.2°
Brachioradialis (BR)	15.968	40.4	40.4	20.1°
Pronator Teres (PT)	3.827	9.5	9.5	6.9°
Resistance (W)	11.73	15.0	15.0	90.0°
Interosseous Membrane (IM)	------	----	123.0	54.4°

I - Townsend

II,III- Author

In case I,II, B is 63% greater than ECRL

In case III, IM is 45% greater than B

pation of each muscle. The strength chosen, 60 lb./in.^{2}, multiplied by the total cross-sectional area due to the flexor muscles represented the total force due to the muscles. Finally, the percentages were used to calculate the amount of total force attributed to each muscle. As noted in Table XIV, the (B) muscle is 63% greater than the (ECRL) muscle for both cases.

G. Modification of the Model

As noted earlier, the ulna is modeled as a cylindrical beam of variable cross section. The average inner and outer bone radii obtained experimentally are used to represent the inner and outer radii of each cross section of the beam. Modification of the beam loading to more accurately predict the actual muscle forces present changes the equations for γ and dA/dx discussed in Chapter III. The changes occur due to the addition of a bending moment about the y-axis as a result of interosseous force in the xy-plane (Figure 18) and the shear force in the z-direction. Presented below are the new equations. The derivations can be found in Appendix II and the relevant distances are noted in Figure 18.

From analysis of the modified model, the new bending moment equations are:

$$M_z = (W - F_{2y})(x-L) \qquad b<x<L \tag{4.1}$$

$$M_y' = F_{3z}\left[x-(c+\frac{d}{2})\right] \qquad b<x<c \tag{4.2}$$

$$M_y = F_{3z}\left[x-(c+\frac{d}{2})-\frac{1}{2}\,\frac{(x-c)^2}{d}\right] \qquad c<x<c+d \tag{4.3}$$

M_y' is not used in the stress equation since the sections of bone chosen for analysis do not fall in this region. The stress equation is now written

$$\sigma(x) = \pm\frac{F_{Rx}}{A} \pm \frac{M_z y}{I_z} \pm \frac{M_y z}{I_y} \quad . \tag{4.4}$$

Substituting $x' = x-L$, $P_y = W-F_{2y}$, $P_x = F_R$, and $P_z = F_{3z}$ into Eqs. (4.1)-(4.3) and using the results in (4.4), the following equations are obtained:

$$\sigma_I(x) = \frac{P_x}{A} + \frac{P_y x' y}{I_z} \qquad \begin{matrix} c+d<x<L & \text{(i)} \\ b<x<L & \text{(ii)} \end{matrix} \tag{4.5}$$

and

$$\sigma_{II}(x) = \frac{P_x}{A} + \frac{P_y x' y}{I_z} - P_z\left[x' + L-m-\frac{1}{2}\,\frac{(x-c)^2}{d}\right]\frac{z}{I_y}$$

$$c<x<c+d \tag{4.6}$$

where σ_I is the stress in the region from the end of the distributed force to the end of the beam -- case (i) -- and is equal to the stress when no membrane is present -- case (ii). (See Eq. (3.23).) σ_{II} is the stress within the membrane.

Calculation of dA/dx for constant, maximum σ_{II} at the outer fiber (i.e., $y=z=r_2(x)$) yields the following result:

$$\frac{dA}{dx'} = \frac{4A^2 I_z^2 I_y^2 \left\{\frac{\gamma_{yx}}{I_z}\left[r_2+x'\frac{dr_2}{dx'} - \frac{x' r_2 A}{2I_z}\left(\frac{r_2 dr_2}{dx'}+\frac{r_1 dr_1}{dx'}\right)\right] - \frac{\gamma_{zx}}{I_y}\left\{r_2\left[1-\left(\frac{x-c}{d}\right)\right] + \left[x'+L-m-\frac{(x-c)^2}{2d}\right]\left[\frac{dr_2}{dx'} - \frac{r_2 A}{2I_y}\left(\frac{r_2 dr_2}{dx} + \frac{r_1 dr_1}{dx}\right)\right]\right\}\right\}}{4I_z^2 I_y^2 + \left[I_y^2\gamma_{yx}x' + I_z^2\gamma_{zx}\left(x'+L-m-\frac{(x-c)^2}{2d}\right)\right] r_2 A^2 (r_1^2 + r_2^2)} \tag{4.7}$$

where $\gamma_{yx} = P_y/P_z$ and $\gamma_{zx} = P_z/P_x$. Since, for the cylinder, $I_z = I_y$, $\frac{dA}{dx'}$ reduces to

$$\frac{dA}{dx'} = \frac{4IA^2\{r_2\left[\gamma_{yx}-\gamma_{zx}(1-(\frac{x-c}{d}))\right] + \{\gamma_{yx}x'-\gamma_{zx}\left[x'+L-m-\frac{(x-c)^2}{2d}\right]\}\left[\frac{dr_2}{dx} - \frac{r_2A}{2I}(\frac{r_2dr_2}{dx} + \frac{r_1dr_1}{dx})\right]\}}{4I^2 + A^2r_2(r_1^2 + r_2^2)\{\gamma_{yx}x'-\gamma_{zx}\left[x'+L-m-\frac{(x-c)^2}{2d}\right]\}} \tag{4.8}$$

Since the ratio of $\gamma_{zx}/\gamma_{yx} = P_z/P_y$ could not be obtained (i.e., isolated on one side of the equation independent of either γ_{zx} or γ_{yx}), investigation of either term was not pursued in this region.

Variations in c(x) and z(x) are dependent upon the new bending moment and the stress, M_y and σ_{II}. The shear force in the shear stress equation (3.32) has a z-component, V_x, as well as the original y-component V_y while Q varies in both the y and z directions.

$$V_y = F_{3z}$$

and (4.9)

$$V_z = F_{3z}(1 - \frac{(x-c)}{d}) \ .$$

The shear stress becomes

$$\tau_{xy} = \frac{V_y Q_r}{I_z t} \quad \text{and} \quad \tau_{xy} = \frac{V_z Q_z}{I_y t} \quad ; \tag{4.10}$$

or for $z<r_1$ (since τ_{xy} is the same as Eq. (3.34)) we have

$$\tau_{xy} = \frac{4}{3} \frac{F_{3z}}{A} \frac{(1-\frac{(x-c)}{d})}{(r_2-r_1)(r_2^2+r_1^2)} \left[(r_2^2-z^2)^{3/2} - (r_1^2-z^2)^{3/2} \right]. \tag{4.11}$$

The programs used to analyze the equations are discussed in the next section and the results are presented in Chapter V.

H. Computer Programs

All of the computer programs written by the author for this study are listed in Appendix III. The purpose of each program will be discussed briefly. The variables are listed in Tables A and B in the Appendix and the flow chart for the major programs are presented in the Figures 19 and 20 of this section.

TABLE was developed to calculate the total area and the coordinates of the centroid for each cross section from the manually obtained x_i, y_i, A_i data. The moments of inertia relative to the centroid ($\bar{I}_{xx}$, $\bar{I}_{yy}$, $\bar{I}_{xy}$) were computed and then used to calculate the principal moments I_1 and I_2. ANGLE was written to scale the moments and calculate the direction of the maximum and minimum moments. The measured inner and outer radii were averaged in RADII. The differences between the average outer and inner radii in each section and the differences between the outer and inner radii as a function of x (i.e., $\bar{r}_{outer}$ at section i+1 - $\bar{r}_{outer}$ at section i) were also computed. TABLE, ANGLE and RADII were used to reduce the gross experimental data to useable form. In each case, the computed quantities obtained were reduced by the appropriate scale factors. The averaged radii were used to represent the variation of the cross section of the cylindrical model.

DADX and SHEAR were written to compute the x-variation of

Figure 19

FLOW CHART FOR DADX

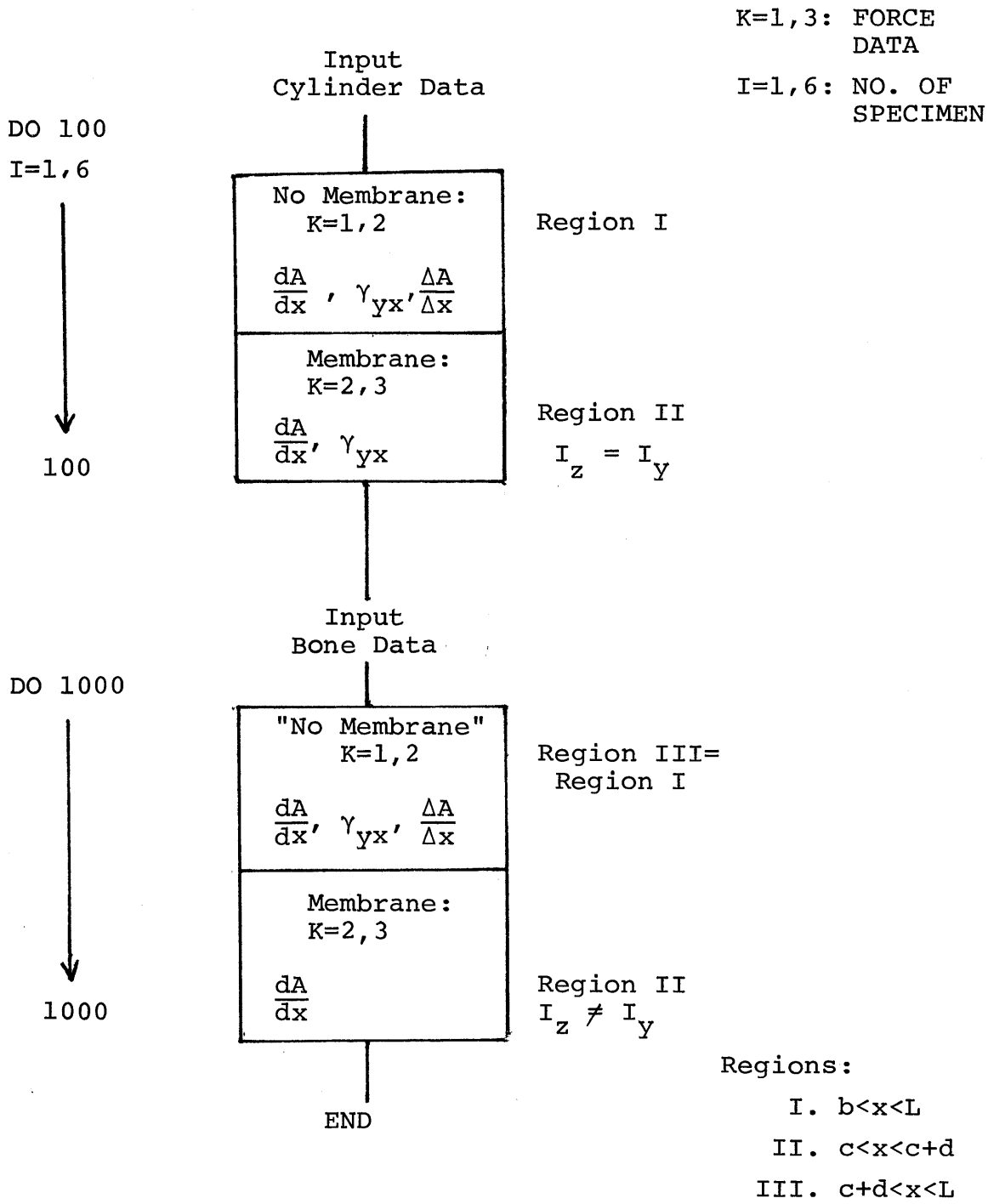

Figure 20

FLOW CHART FOR SHEAR

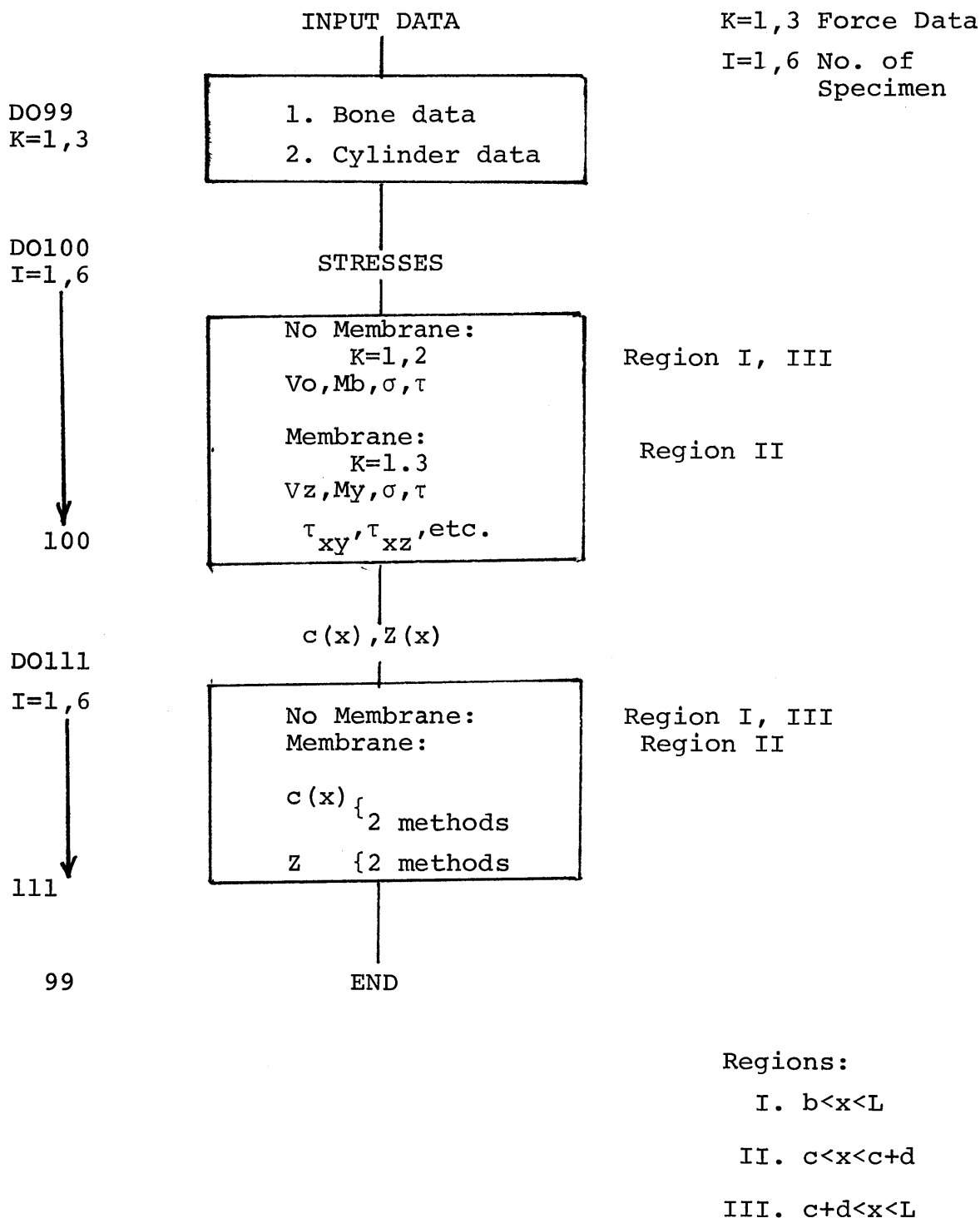

Regions:

I. $b<x<L$

II. $c<x<c+d$

III. $c+d<x<L$

equations developed on the basis of the cylindrical beam model. In both programs, the input comes from two "data sets": the set of cylinder cross-sectional areas and moments of inertia and the set of analogous quantities calculated directly from actual bone measurements. In the programs, the calculations and outputs are, correspondingly, labeled either CYLINDER or ACTUAL, depending on the data set used. Although the radial data was used in both cases, the areas and principal moments for the bone were calculated in TABLE, while the areas and the moments of inertia for the cylinder were calculated using the radial data.

The three force considerations mentioned earlier (see Figure 17) were subdivided according to the headings: no membrane and membrane. As was seen for bone, I_y does not enter into the calculations for $c+d<x<L$ (region III). Thus, the equations reduce to those used in the case where no membrane is present. The normalized forces per Townsend and the absolute forces representing the point loads per the author were employed in region I (no membrane). The absolute forces and the interosseous membrane force were employed in region II (membrane present).

In DADX, $dA/dx \approx \frac{\Delta A}{\Delta x}$, per the equations presented earlier, was computed in regions II and III using experimentally obtained data and in regions I and II using the analogous model quantities.

The SHEAR program computes the following quantities using the same subdivisions of regions and forces: M_b, V, σ_{axial}, $\sigma_{bending}$, σ_{total}, τ_{avg}, τ_{max}, τ_{r_1}, τ_{xy}, τ_{xz}, Z_1 and c. Various calculations were performed twice to determine the effect of force related terms on geometry dependent variables. For example, Z_1 was obtained from the bending moment divided by the bending stress (a "force ratio") as well as from the moment of inertia divided by c (a "geometry ratio").

The results of the computer programs and the experimental analyses are presented and discussed in Chapter V.

V. RESULTS AND DISCUSSION

A. Analysis of Experimentally Obtained Data

As mentioned previously, the experimental procedure involved graphical techniques and processing of data. Prior to sectioning, the number of cuts desired was fixed and the section positions were normalized relative to the total length of the respective forearm bone. With this approach, the relative distances of, say, the nth section from the elbow is the same for all arms and data can be readily compared. For example, consider section 8 in Figure 21. All three points do not correspond to the same absolute distance from their elbow pivot points, but rather they correspond to the same relative position along the length of their respective arms as compared to the length of the arms.

Figure 21 shows the variation in the x centroidal coordinate ($\bar{x}$) associated with sections of the left and right arms; Figure 22 shows the y variation ($\bar{y}$). Between sections 4 and 7, all plots of $\bar{x}$ appear nearly independent (uniform). $\bar{x}$ then increases (or decreases in the left arm specimens) roughly linearly before arresting near n = 13. This linear interval corresponds to the shaft region of the long bones. Whether $\bar{x}$ increases or decreases does not relate to any real increase or decrease in physical attribute, but rather is indicative only of a spatial shift of the cross sectional areas to new positions to the right or left, respectively, of their initial

Figure 21. Centroidal Coordinates ($\bar{x}$) vs. Section Number

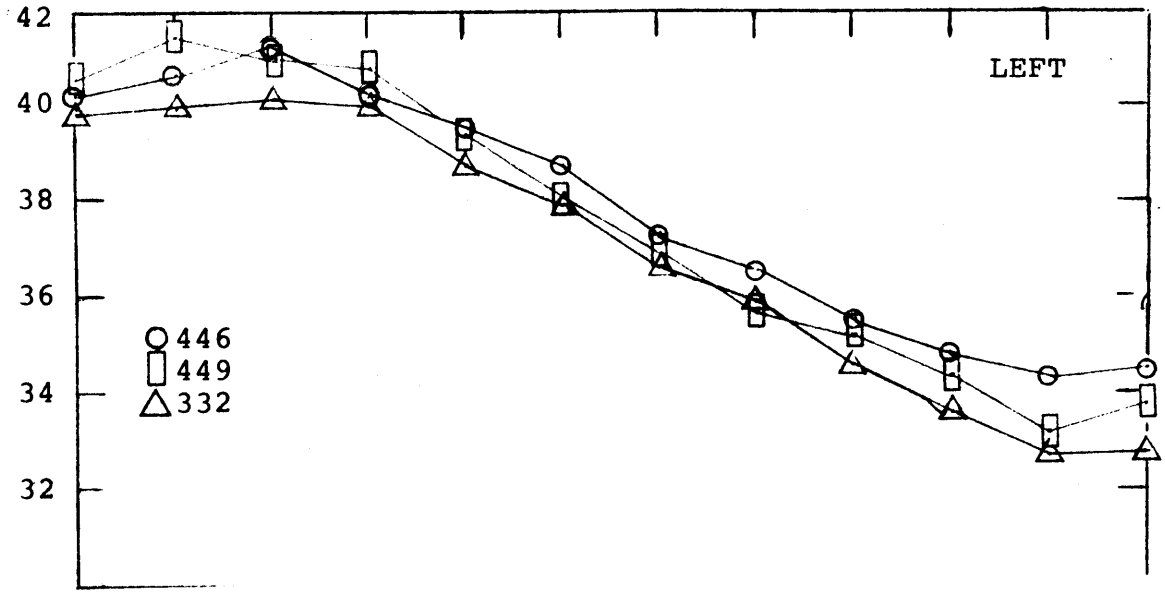
42
40
38
36
34
32
LEFT
446
449
332

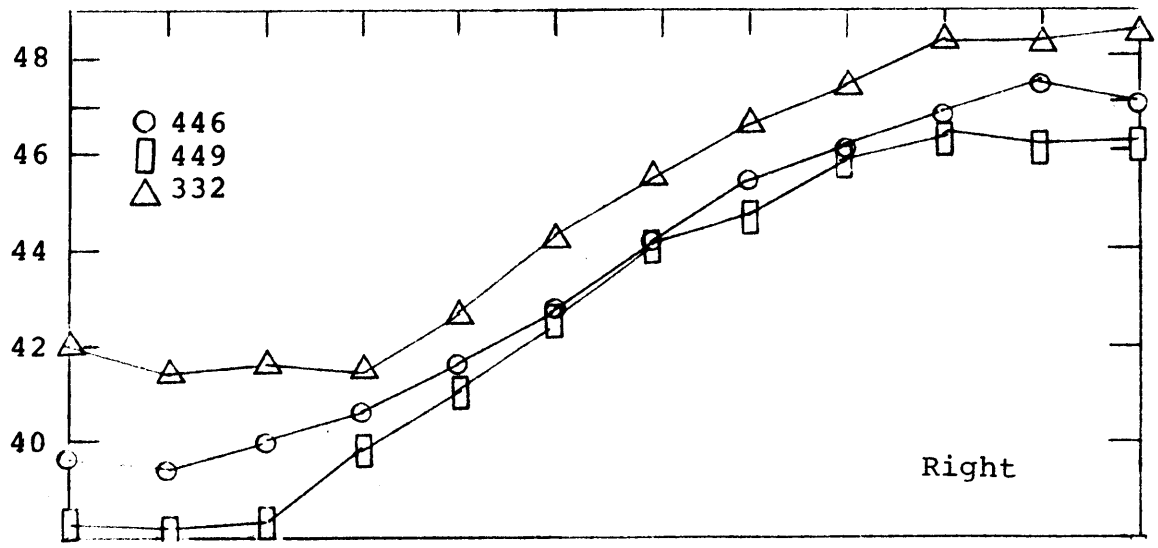
48
46
44
42
40
446
449
332
Right

position, section 4. The interosseous membrane is most pronounced in the linear region.

The curves in Figure 22, although not as uniform or smoothly varying as those in Figure 21, do rise at approximately the same rate. Thus the centroid of the cross section rose to the right (positive x) or rose to the left (negative x) as one moved along the length of the bone to increasing section numbers. The horizontal variation of $\bar{x}$ appears to be more uniform bone to bone overall, than that of $\bar{y}$. A general comment can also be made: these two figures (21 and 22) indicate the high degree of consistency with which sections were referenced one to another and the precision of specimen orientation specimen to specimen. Given the biological variables in the study, i.e. donor age, weight, height, life style, health, etc., these curves show the variation in x from specimen to specimen to be remarkably well-defined and consistent for both arms. This observation gives confidence to the author concerning the experimental procedures used.

The areas of the sections were obtained and plotted against the section numbers in Figure 23 for both the left and right arms. The curves of both arms show approximately the same rate of decrease. The left set has peaks approximately at sections 6 and 9 for specimen #446 and 332, respectively, and at number 7 for specimen #449. The right arm peaks at $n \sim 7$ and 11 for 332, while 446 and 449 decrease at about the same

Figure 22. Centroidal Coordinates ($\bar{y}$) vs. Section Number

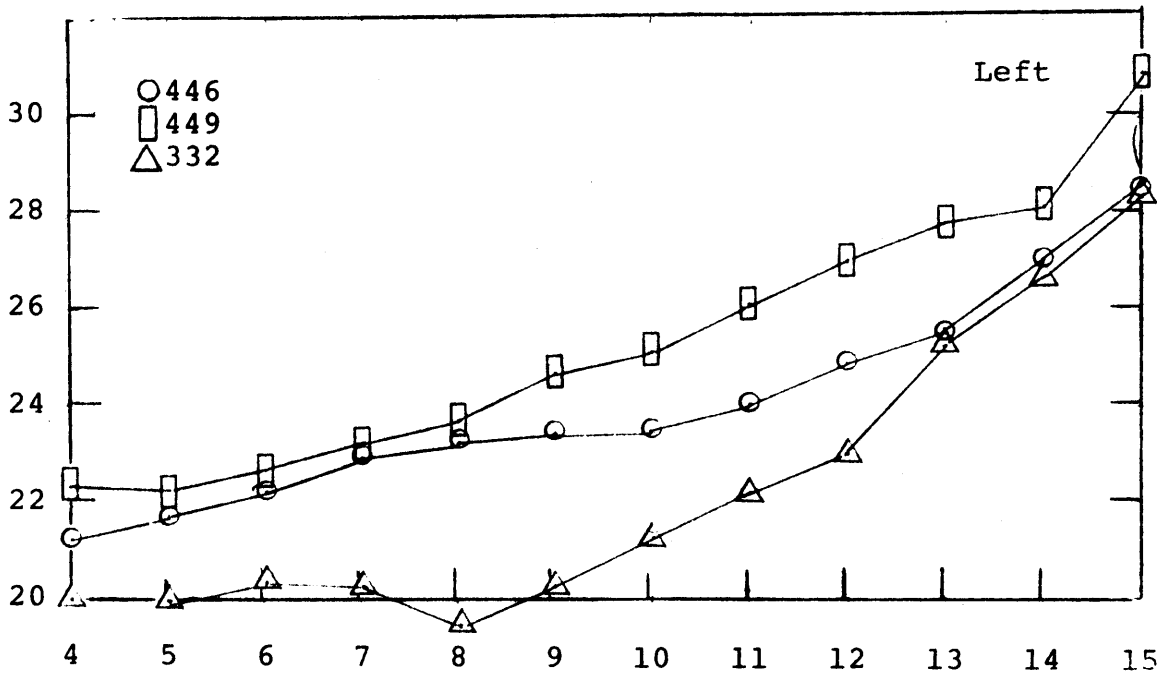
Left
446
449
332
30
28
26
24
22
20
4
5
6
7
8
9
10
11
12
13
14
15

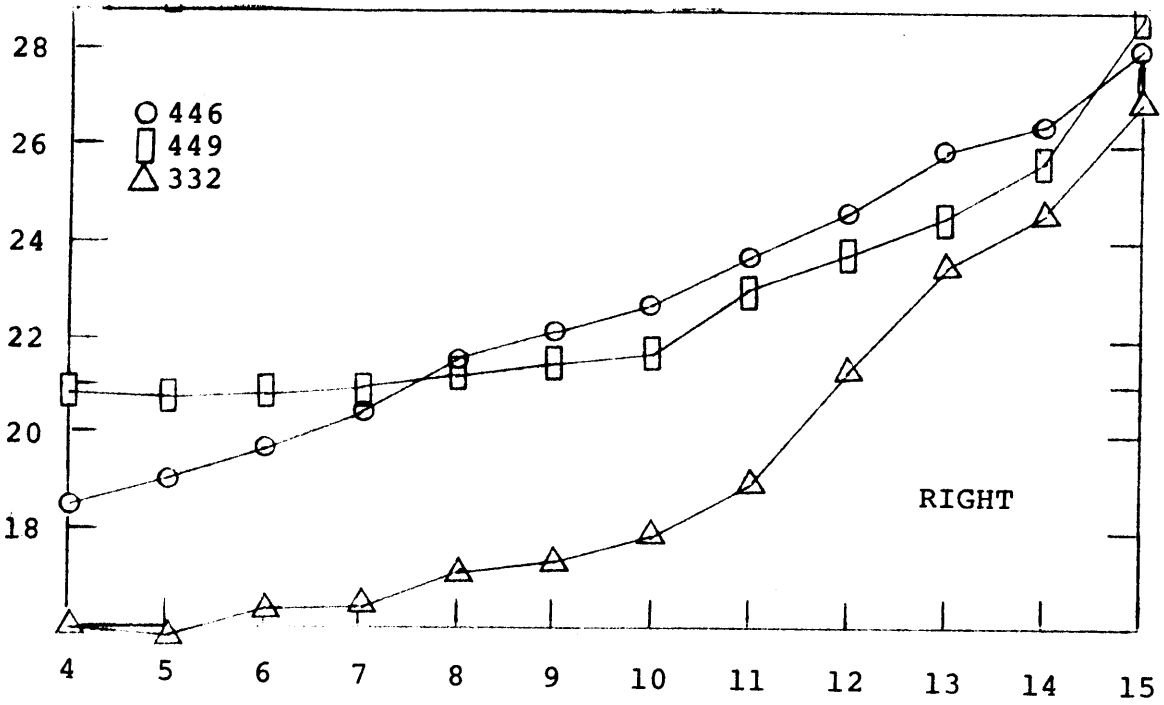
446
449
332
RIGHT
28
26
24
22
20
18
4
5
6
7
8
9
10
11
12
13
14
15

Figure 23. Experimental Cross-Sectional Areas vs. Section Number

○ 446

□ 449

△ 332

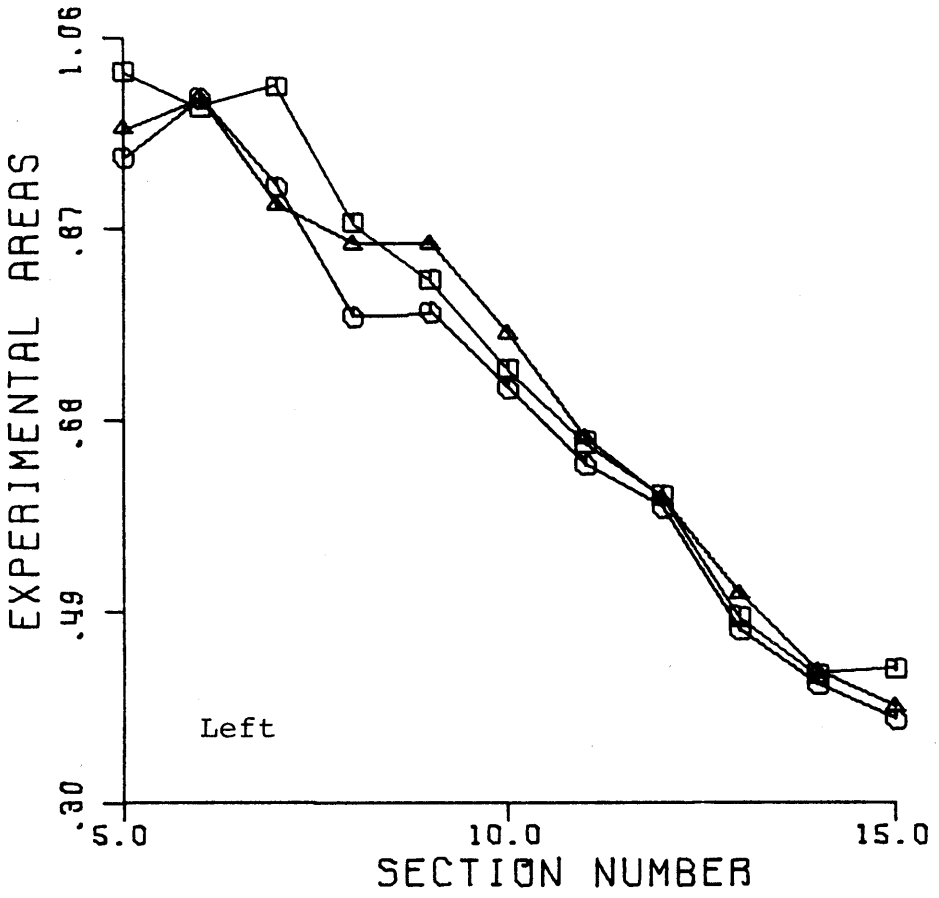
EXPERIMENTAL AREAS
1.06
.87
.68
.49
.30
5.0
10.0
15.0
SECTION NUMBER
Left

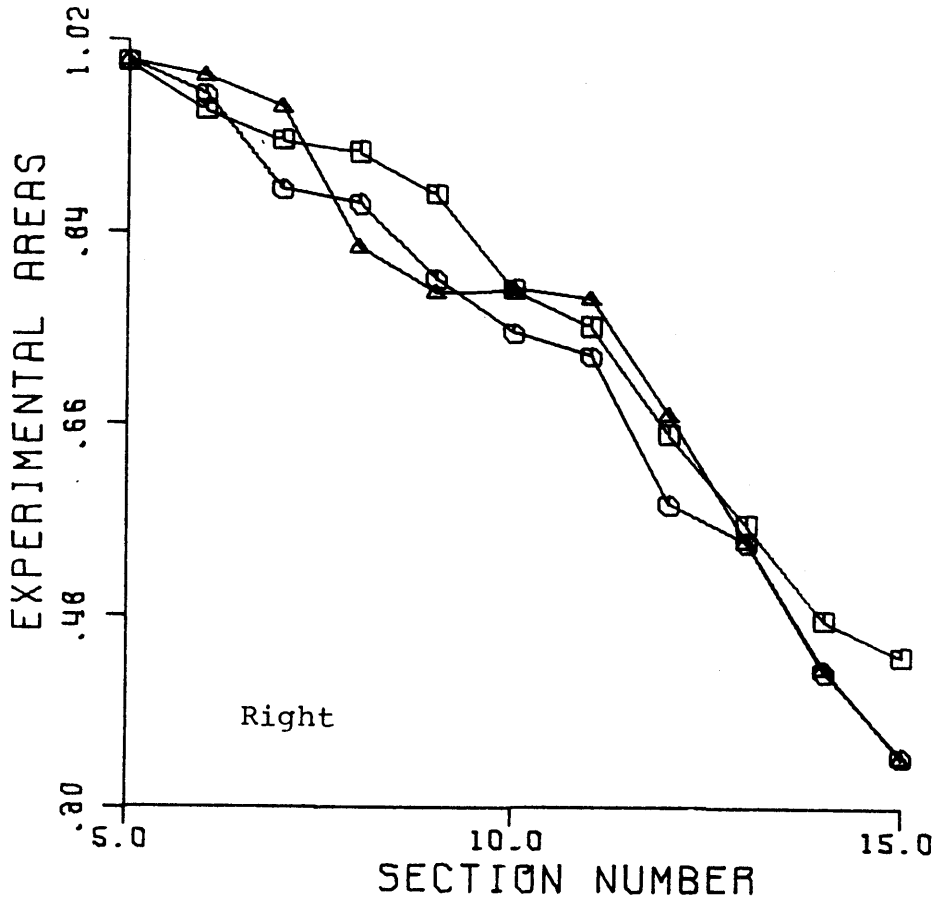
EXPERIMENTAL AREAS
1.02
.84
.66
.48
.30
5.0
10.0
15.0
SECTION NUMBER
Right

rate and with few fluctuations. Between 9 and 10 on the left arms the decrease is almost linear.

Averaged radii values are plotted in Figures 24 to 26. In Figure 24, the averaged outer radii for the right arm are plotted. The variation is fairly continuous without any abrupt transitions. The left arm variation (not plotted) was equally smooth. The averaged inner radii for both arms are presented in Figure 25. It is seen that although these tend to fluctuate a good deal, a distinct trend is still apparent. The values generally start at a maximum value, approach a minimum value in the middle portion of the shaft, and then rise to approximately the same maximum value at the distal portion of the bone. This result is consistent with the fact that inner radii define the approximate boundary of cancellous bone. Cross sections are thin-walled (cortical bone) at the elbow and composed mostly of cancellous bone (humerus and olecranon); but as one moves away from the elbow along the shaft of the bone, the amount of cortical bone increases while the amount of cancellous bone decreases. This decrease manifests itself as a decrease in the inner radii to account for the increase in cortical bone, rather than an increase in outer radii. Toward the distal end of the shaft (wrist), the amount of cancellous bone increases, the inner radii increases and the amount of cortical bone decreases. Figures 24 and 25 attest to the relatively constant and uniform behavior of the outer radii as compared with that of the inner radii.

Figure 24. Averaged Outer Radii vs. Section Number

○ 446

□ 449

△ 332

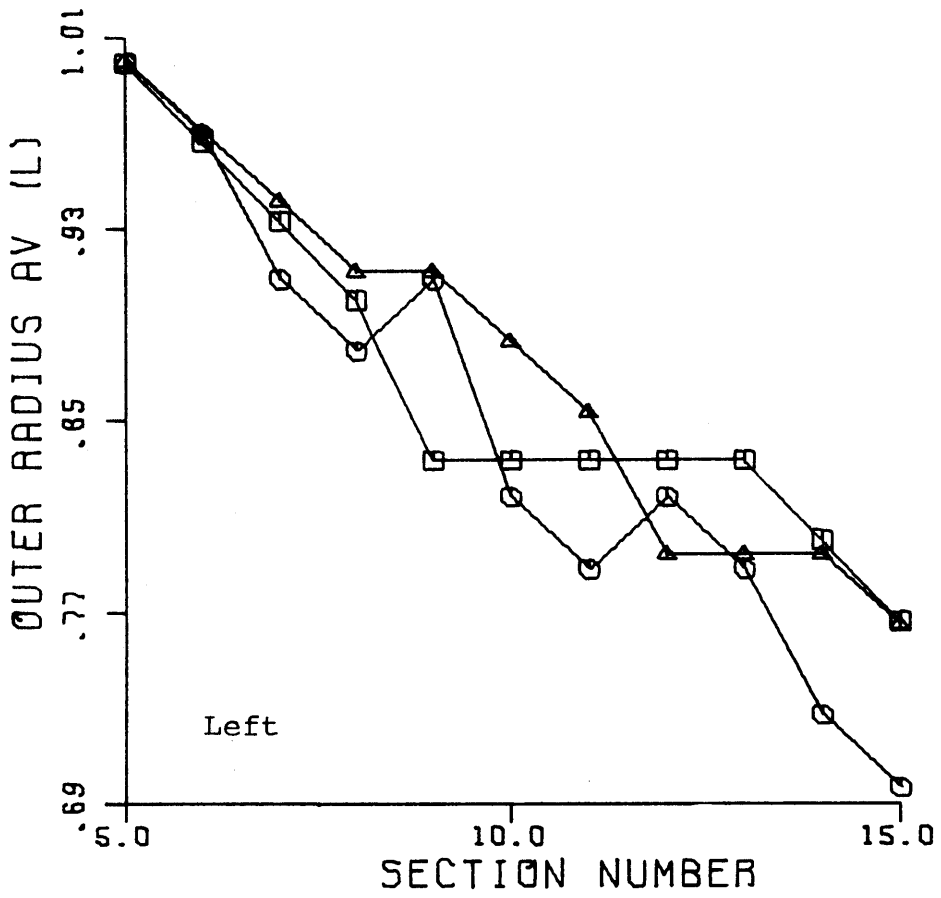
OUTER RADIUS AV (L)
1.01
.93
.85
.77
.69
5.0
10.0
15.0
SECTION NUMBER
Left

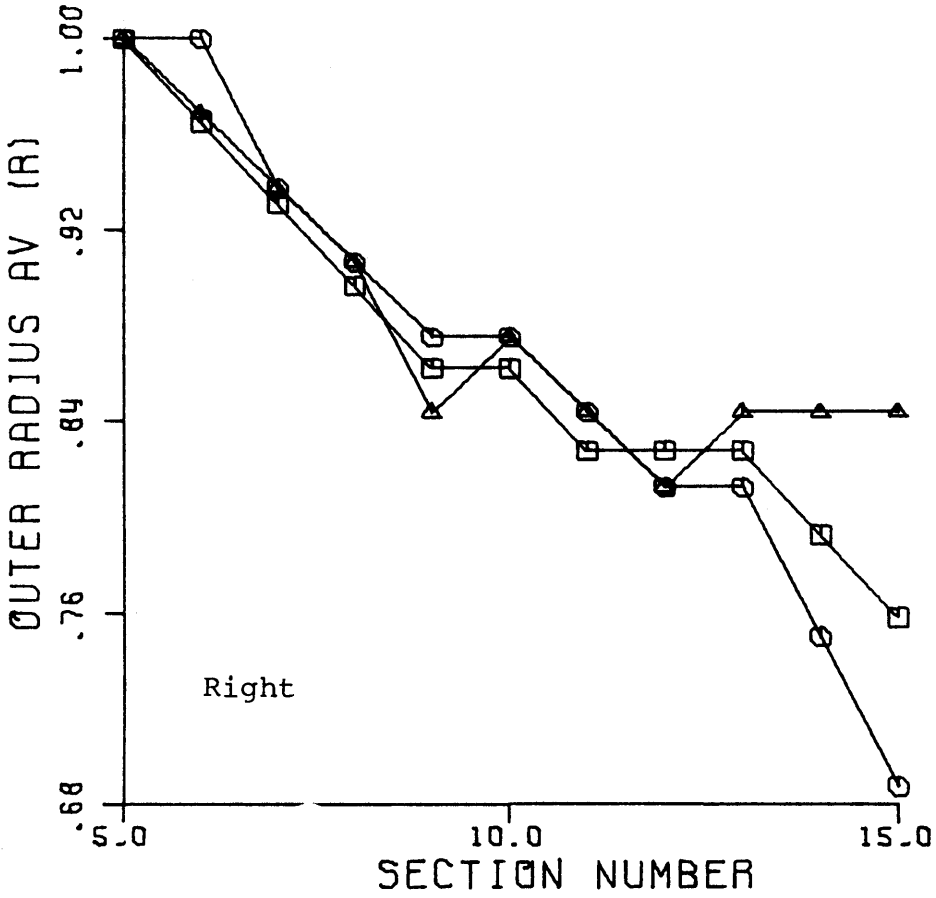
OUTER RADIUS AV (R)
1.00
.92
.84
.76
.68
5.0
10.0
15.0
SECTION NUMBER
Right

Figure 25. Averaged Inner Radii vs. Section Number

○ 446

□ 449

△ 332

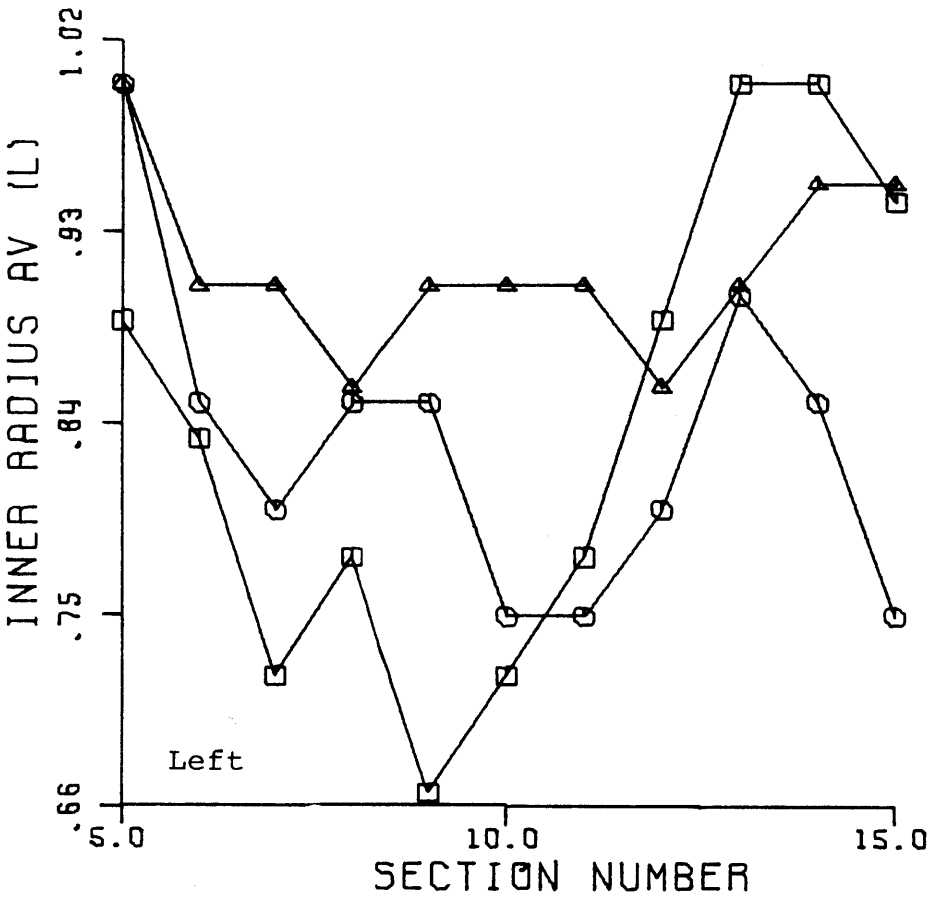
INNER RADIUS AV (L)
1.02
.93
.84
.75
.66
Left
5.0
10.0
15.0
SECTION NUMBER

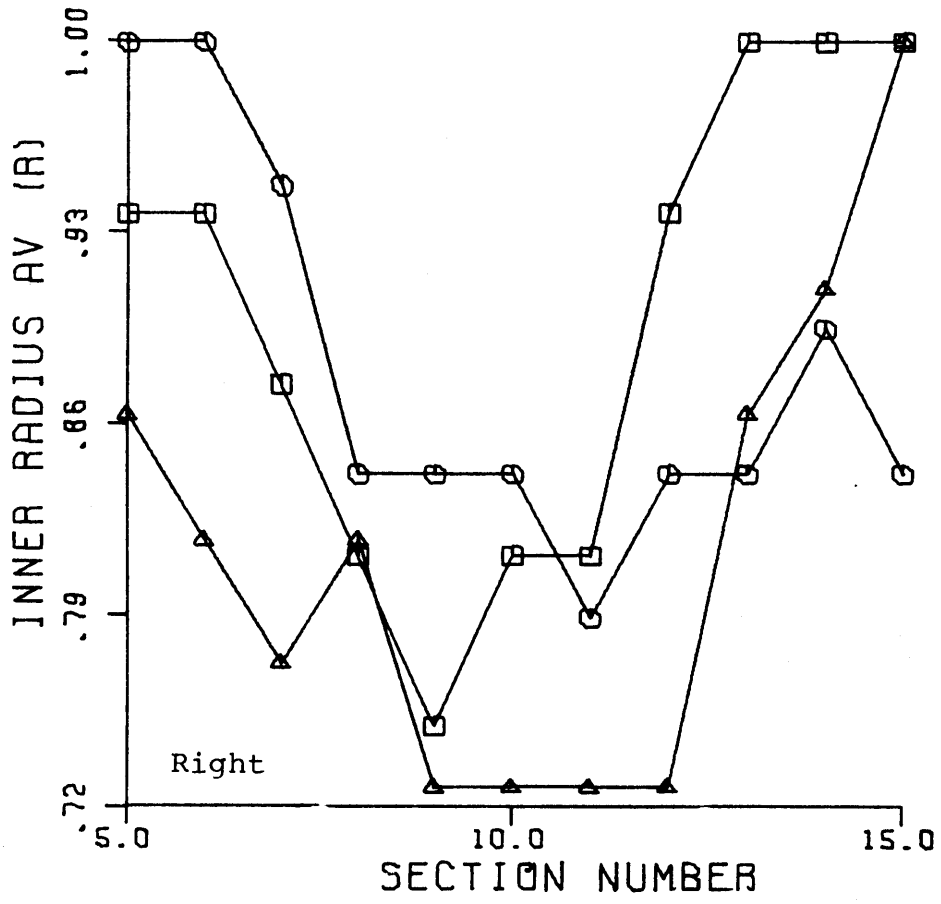
INNER RADIUS AV (R)
1.00
.93
.86
.79
.72
Right
5.0
10.0
15.0
SECTION NUMBER

Although the inner and outer radii vary differently from one another, the variation of the differences between the two, i.e., the outer averaged radii minus the inner averaged radii, is similar. As is seen in Figure 26, both the left and right arms vary in about the same manner. The small deviations of each curve represent expected biological deviations, as discussed in Chapter VI. The spread of the curves is approximately .01 inches. In the left set of curves, $\Delta\bar{r}$ appears to be roughly constant up to section 7 and then to monotonically decrease from 7 to 13. The right set shows $\Delta\bar{r}$ constant to section 9 and then decreasing to 15. The rate of decrease in both graphs is approximately the same. This difference, Δr, in averaged radii represents the amount of cortical bone (really, the thickness of cortical bone) at a given section. The amount of cortical bone, thus, appears to be a constant up to some point almost midway into the shaft of the bone before decreasing linearly.

The principal moments of inertia decreased, as expected in a uniform manner since the bone material per section decreases uniformly with bone length. The minimum principal moment varied somewhat more uniformly than did the maximum principal moment, I_1, which was dominated by the I_{xx} term. The spread in I_2 was less than that of I_1 (see Figure 27). This might be expected, however, since the minimum moment is found to occur about an approximate axis of symmetry of the

Figure 26. Averaged Radial Difference vs. Section Number

○ 446

□ 449

△ 332

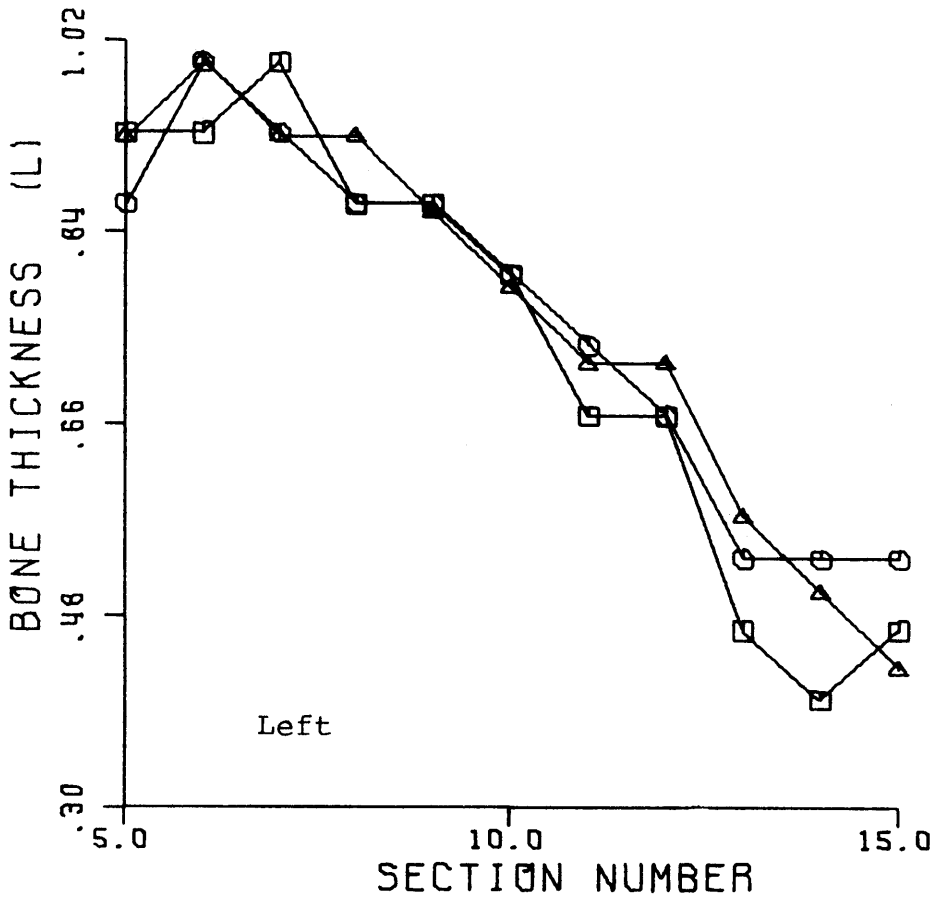
BONE THICKNESS (L)
1.02
.84
.66
.48
.30
5.0
10.0
15.0
SECTION NUMBER
Left

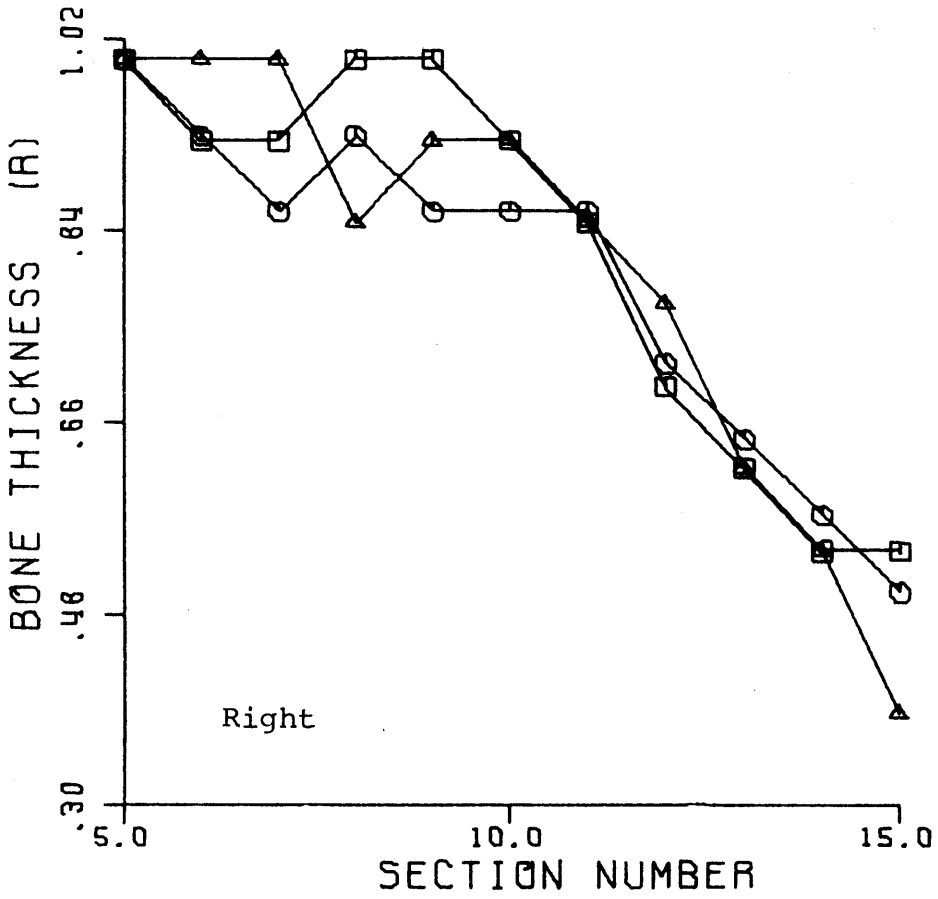
BONE THICKNESS (R)
1.02
.84
.66
.48
.30
5.0
10.0
15.0
SECTION NUMBER
Right

Figure 27. The Principal Moments of Inertia, I_1, I_2 vs. Section Number

Right Arm

$I_y = I_1$

$I_z = I_2$

○ 446

□ 449

△ 332

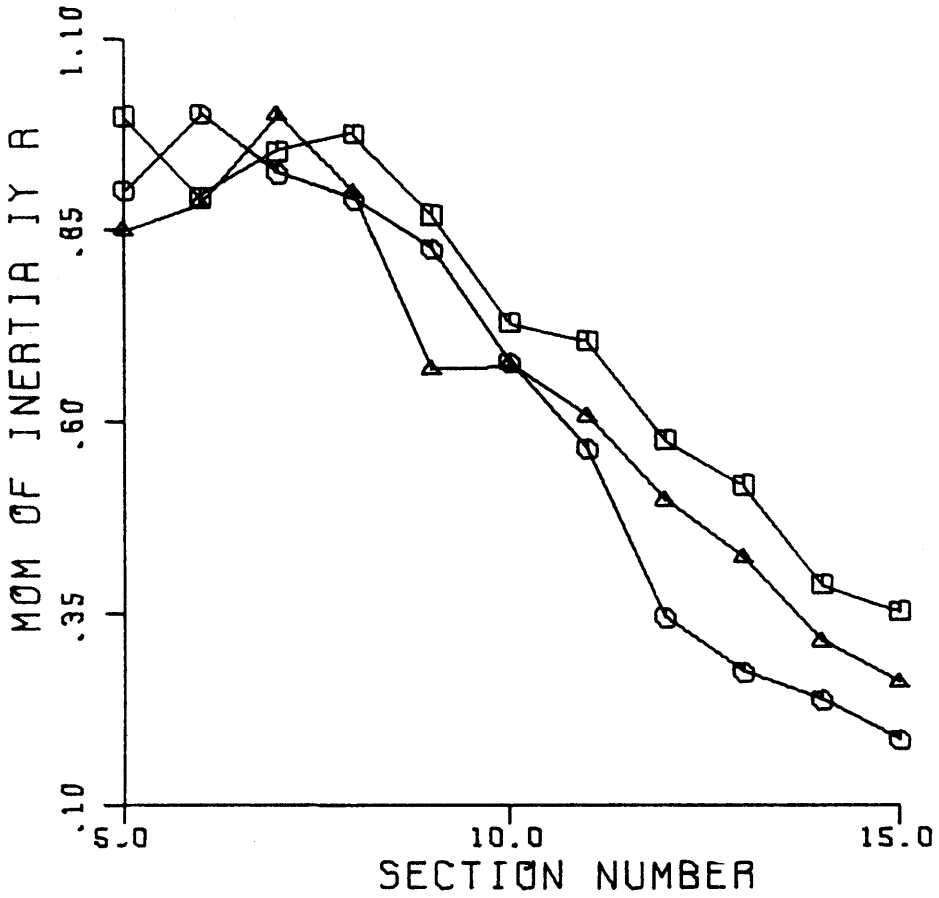
MOM OF INERTIA IY R
1.10
.85
.60
.35
.10
5.0
10.0
15.0
SECTION NUMBER

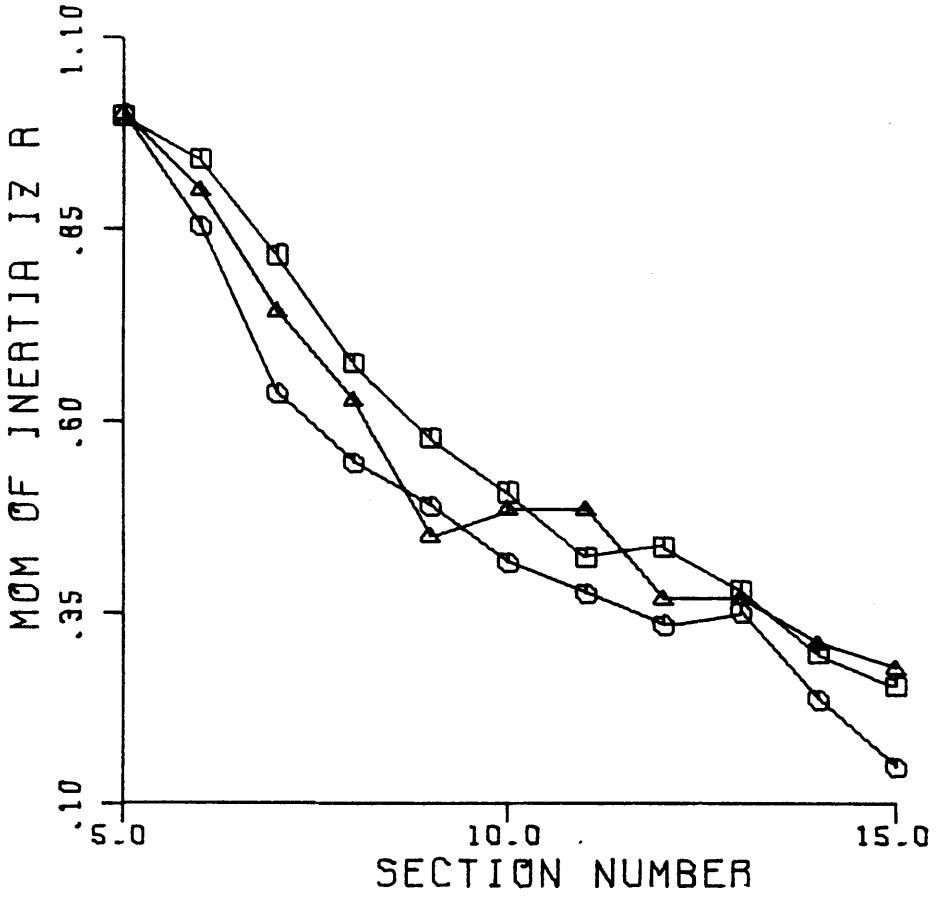
MOM OF INERTIA IZ R
1.10
.85
.60
.35
.10
5.0
10.0
15.0
SECTION NUMBER

cross section, and symmetry tends to reduce the moment of inertia. The disproportionate distribution of bone about axis 1 (I_1) implies that more bone material was needed in one direction than in another to resist the cross sectional area's tendency to bend about that axis.

The distance to the outer fiber also conveys information. For all curves above the axis associated with the maximum moment, I_1, c(x) follows an approximately smoothly peaked curve, the width of the peak extending from section 6 to sections 11 and 12 (see Figure 28)* for both the left and right arms. Below this axis, however, the curves are uniformly varying as a function of the section. Above this axis, the interosseous membrane is active while below this axis, only concentrated muscle forces are dominant. On the other hand, c(x) measured about axis 2 exhibits uniform variation about that axis, indicative of the symmetrical character of the bone structure. As can be seen, then, the experimentally determined quantity, c(x), a parameter defined within the framework of experimental centroidal axes and graphically obtained moment axes, shows behavior which is not only of likely theoretical significance but also of sensible nature in the context of the system at hand. In Figure 29, the section moduli are plotted for the

---

* All figures except Figure 28 have been scaled.

Figure 28. Distance to the Outer Fiber, c(x) vs. Section Number

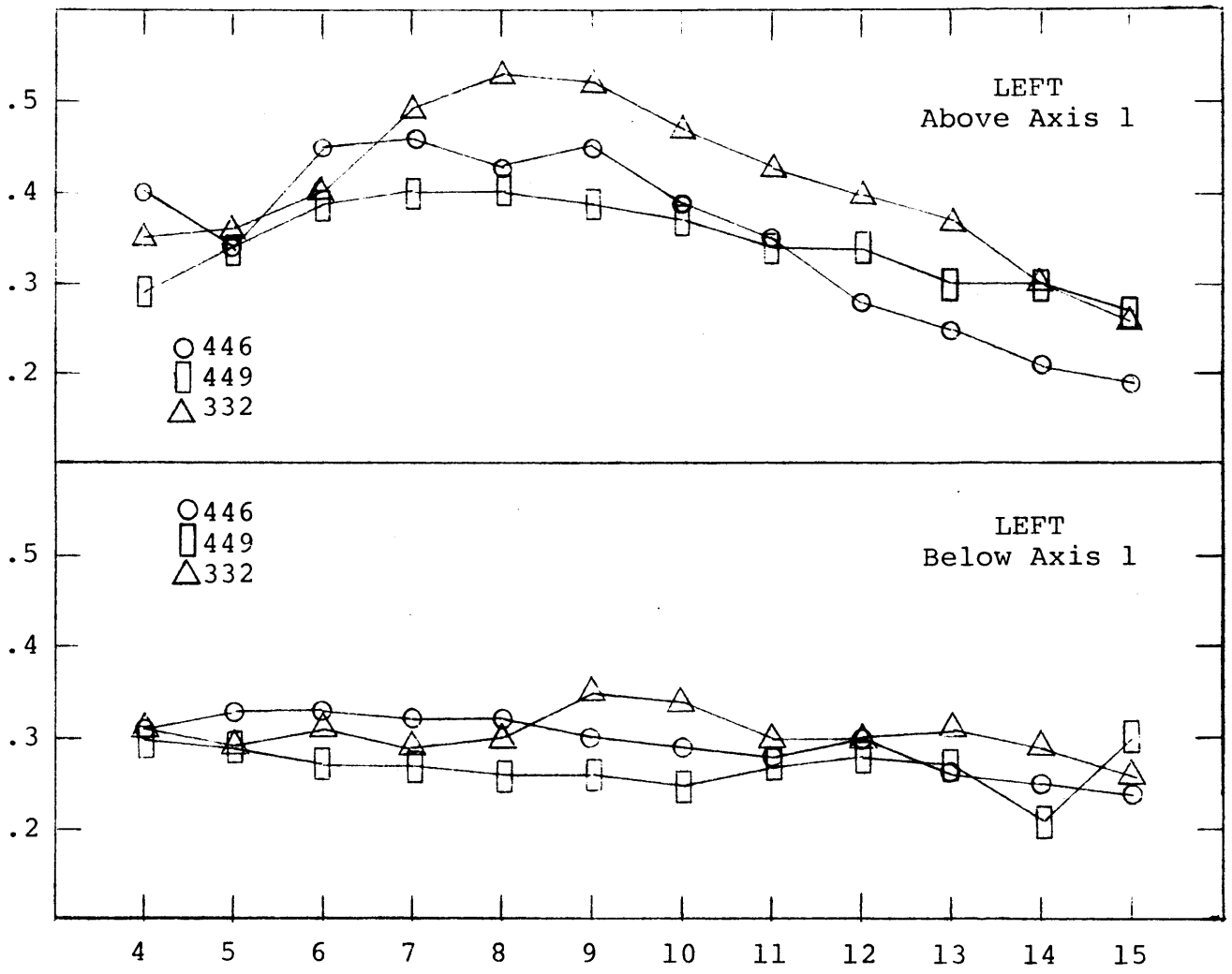
LEFT
Above Axis 1
446
449
332
LEFT
Below Axis 1
446
449
332
.5
.4
.3
.2
4
5
6
7
8
9
10
11
12
13
14
15

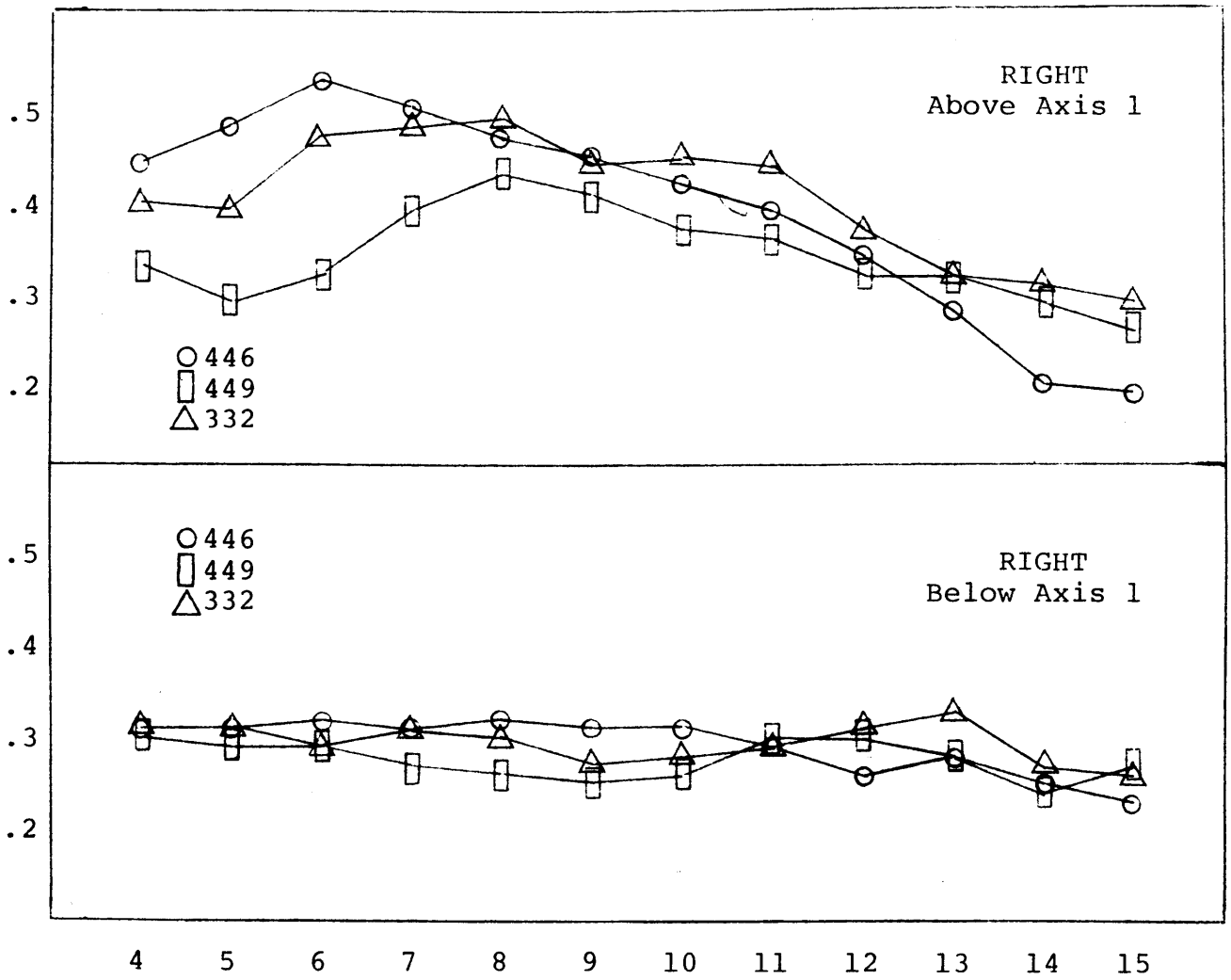
RIGHT
Above Axis 1
.5
.4
.3
.2
446
449
332
446
449
332
RIGHT
Below Axis 1
.5
.4
.3
.2
4
5
6
7
8
9
10
11
12
13
14
15

Figure 29. The Section Moduli-Left vs. Section Number

$I_y = I_1$

$I_z = I_2$

○ 446

□ 449

△ 332

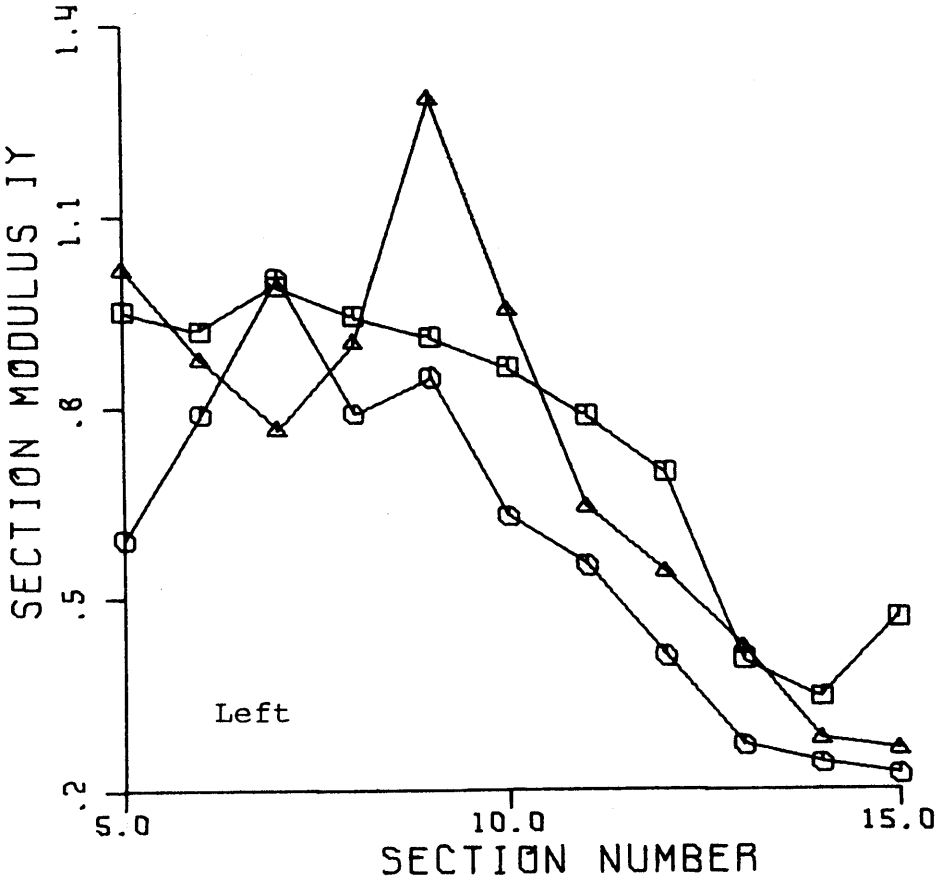
SECTION MODULUS IY
1.4
1.1
.8
.5
.2
Left
5.0
10.0
15.0
SECTION NUMBER

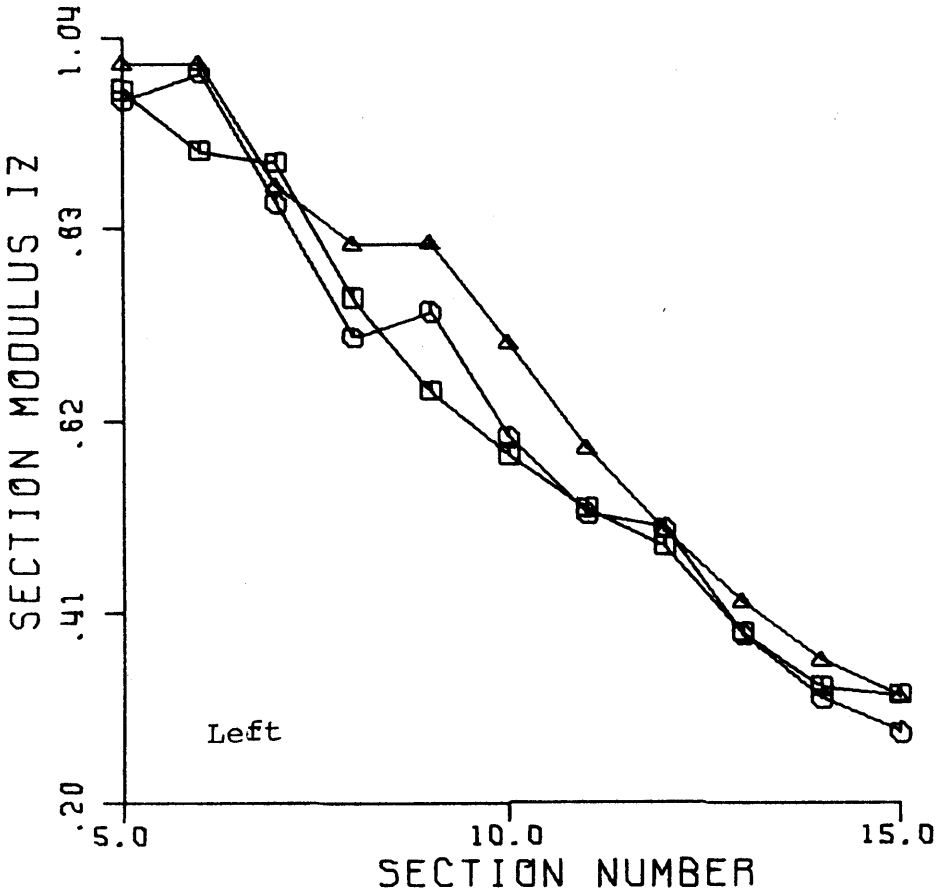
SECTION MODULUS IZ
1.04
.83
.62
.41
.20
5.0
10.0
15.0
SECTION NUMBER
Left

left arm for both $Z_1 = I_1/c(x)$ and $Z_2 = I_2 9c(x)$. Although it is not shown, the variation observed is the same in the left arm except for variations about section 9. Thus, although the principal moments, I_1 and I_2, and the c(x) vary differently from one another, their ratios, Z_1 and Z_2, respectively, tend to be the same (i.e., fall in the same range) for all the experimental data obtained. (Note that c(x) is always the maximum c(x) about either axis.)

Figure 30. Theoretical Cross-Sectional Areas vs. Section Number

○ 446

□ 449

△ 332

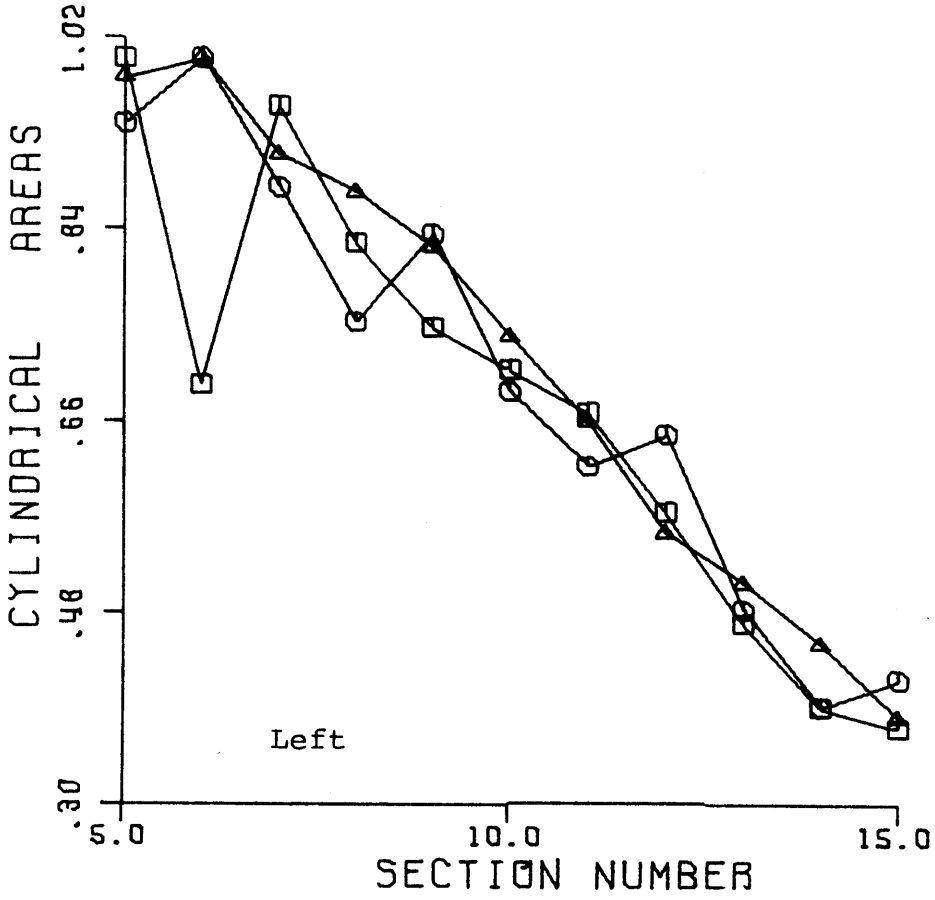
CYLINDRICAL AREAS
1.02
.84
.66
.48
.30
5.0
10.0
15.0
SECTION NUMBER
Left

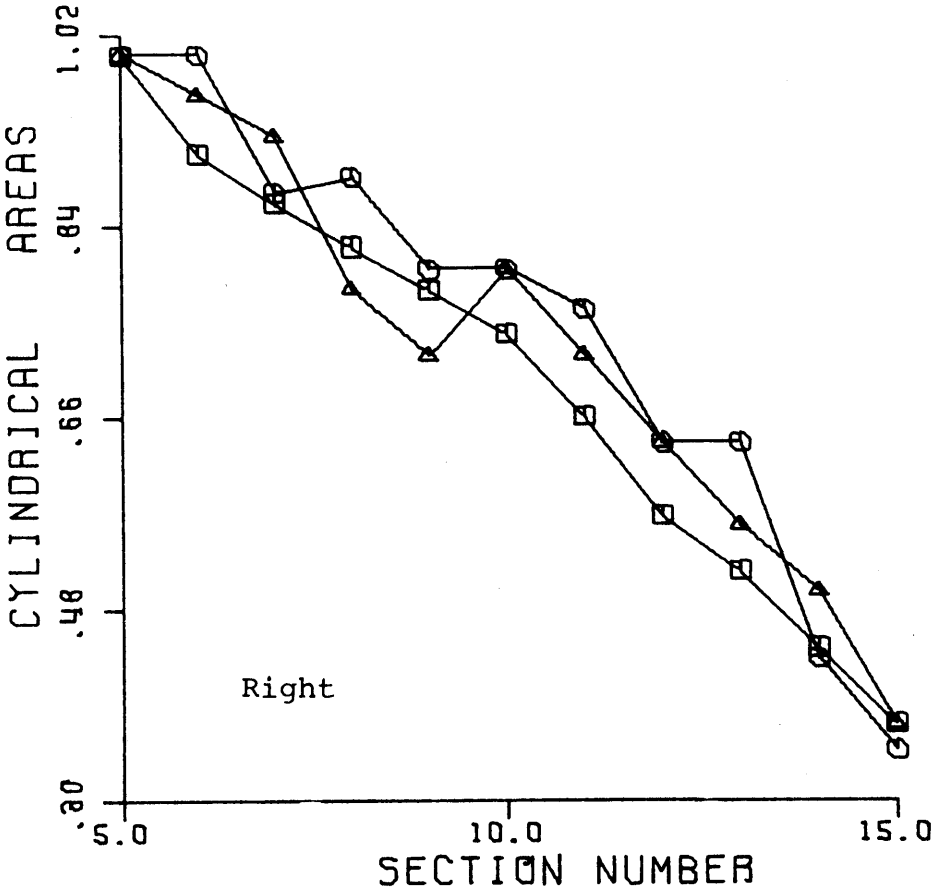
CYLINDRICAL AREAS
1.02
.84
.66
.48
.30
5.0
10.0
15.0
SECTION NUMBER
Right

B. Analysis of Theoretically Obtained Data

As discussed in Chapter IV, the experimental data is to be used to test theoretical data obtained from a hollow cylindrical loaded beam model. This comparison will give insight into the validity of the model and the extent of its usefulness. First, theoretical areas, moments of inertia, and section moduli for the beam were calculated for each specimen using for the beam's radii, the averages of the inner and outer experimental radii measured at each section position. Thus the model beam is a cylinder of variable cross-section. As can be seen in Figure 30, the theoretical area curve for 446L peaks at section numbers 6, 9, and 12 while that for 446R peaks at 6, 8, 10, and 13. The other two specimen curves vary smoothly (excepting 332R in the vicinity of section 9). The curves of Figure 30 for the right arm agree well in behavior with experimental area data obtained for the actual bone (refer Fig. 23). The theoretical left arm data also agrees well with its corresponding experimental data but with somewhat more pronounced peaking. Each of the six cylinder beam models exhibited area curves which are slightly smaller in amplitude than those of the experimental specimens. Similarly the variation of the theoretical moments of inertia for the cylinder beam behaves qualitatively the same as the variation observed for the bones. The cylinder moment agrees better in its behavior with the minimum experimental principal moment,

Figure 31. Section Moduli-Theoretical Model vs. Section Number

○ 446

□ 449

△ 332

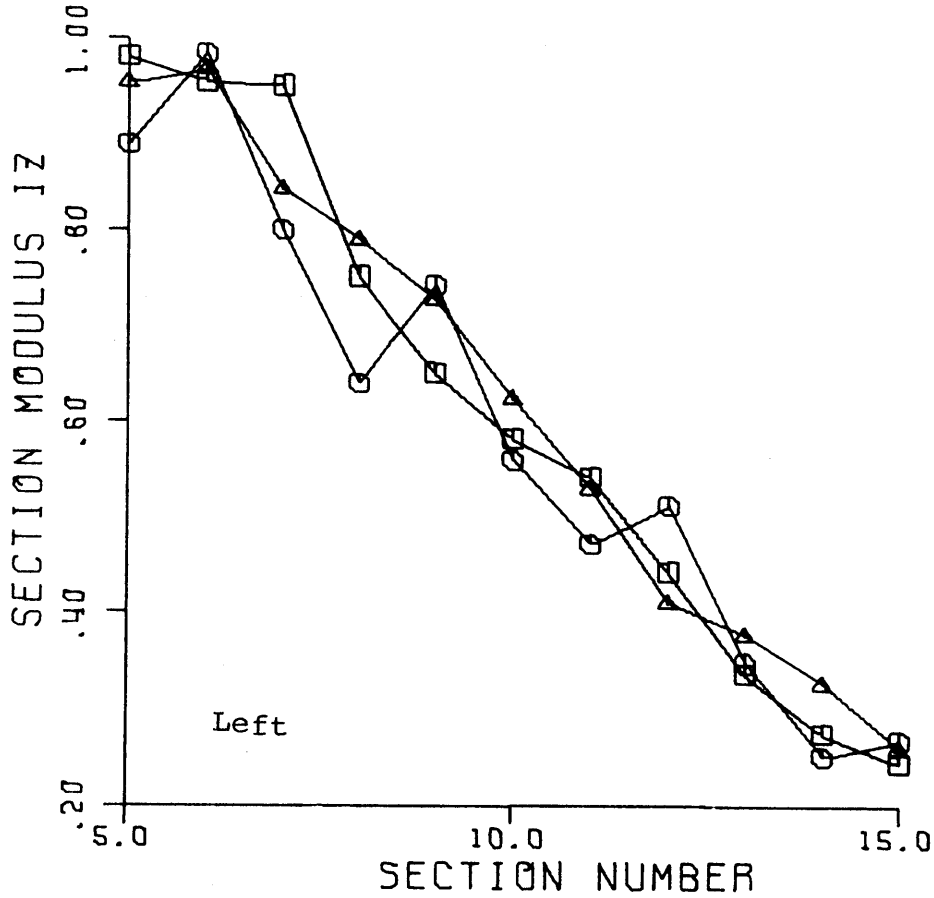
SECTION MODULUS IZ
1.00
.80
.60
.40
.20
5.0
10.0
15.0
SECTION NUMBER
Left

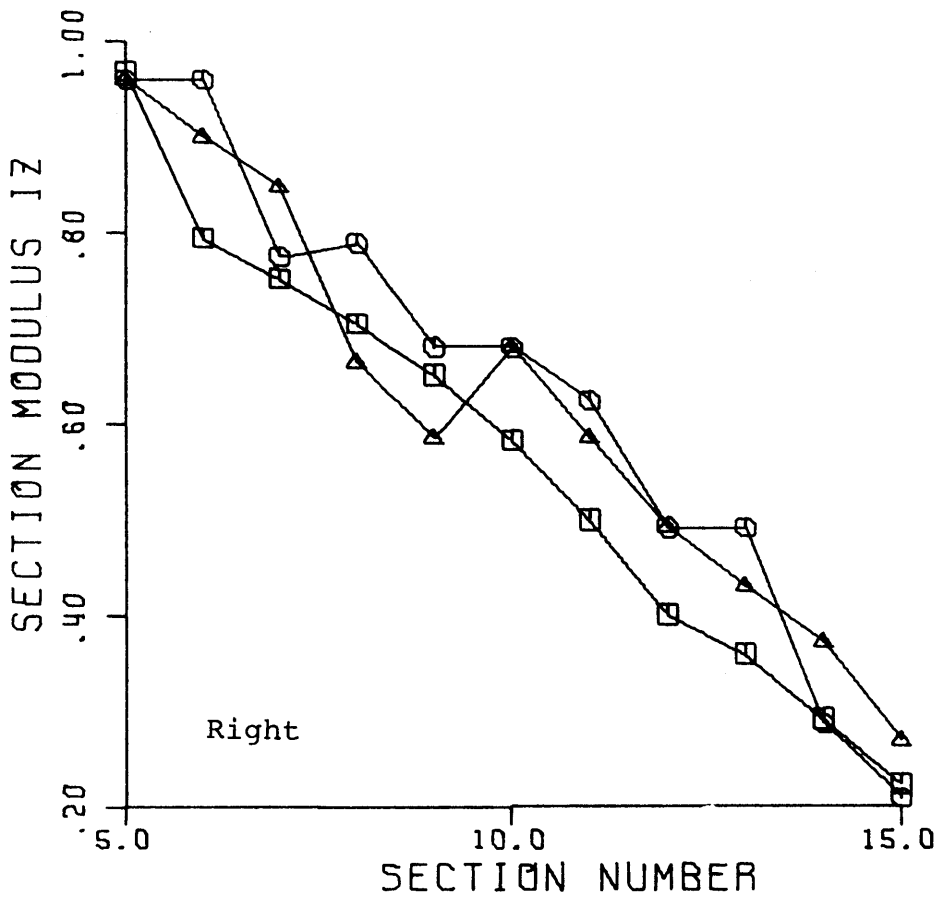
SECTION MODULUS IZ
1.00
.80
.60
.40
.20
5.0
10.0
15.0
SECTION NUMBER
Right

I_2, than with I_1. (Note that $I_y = I_z$, or $I_1 = I_2$ for the cylindrical beam cross section.) The theoretical section moduli of Figure 31 vary linearly in magnitude as a function of section number. This behavior is in qualitative agreement with the experimental data although the theoretical magnitudes are too small by a factor of 16.

The foregoing observations of the trends of the experimental data support the choice of the theoretical cylindrical beam model as a first approximation. The next test is to obtain correspondence between the "force" system used in the model and the effective experimentally suggested loading acting on the bone.

Computer programs (See Chapter IV(H)) were developed by the author to study force, stress, and geometrical relationships based on the data available. Of the three force systems to have been investigated, the third was analyzed in detail and will be discussed in this thesis because of the significant influence of the interosseous membrane.* The following discussions refer to the 5 equations plotted using experimental data.

Figures 32 to 34 show the variation in axial stress, bending stress, and the total stress as a function of the section number. The interosseous region begins just after

---

* Data were taken and partially analyzed for the first two force systems listed in Chapter IV. The uninteresting promise of these and severe time limitations precluded detailed investigations.

Figure 32. Axial Stress vs. Section Number

Left Arm

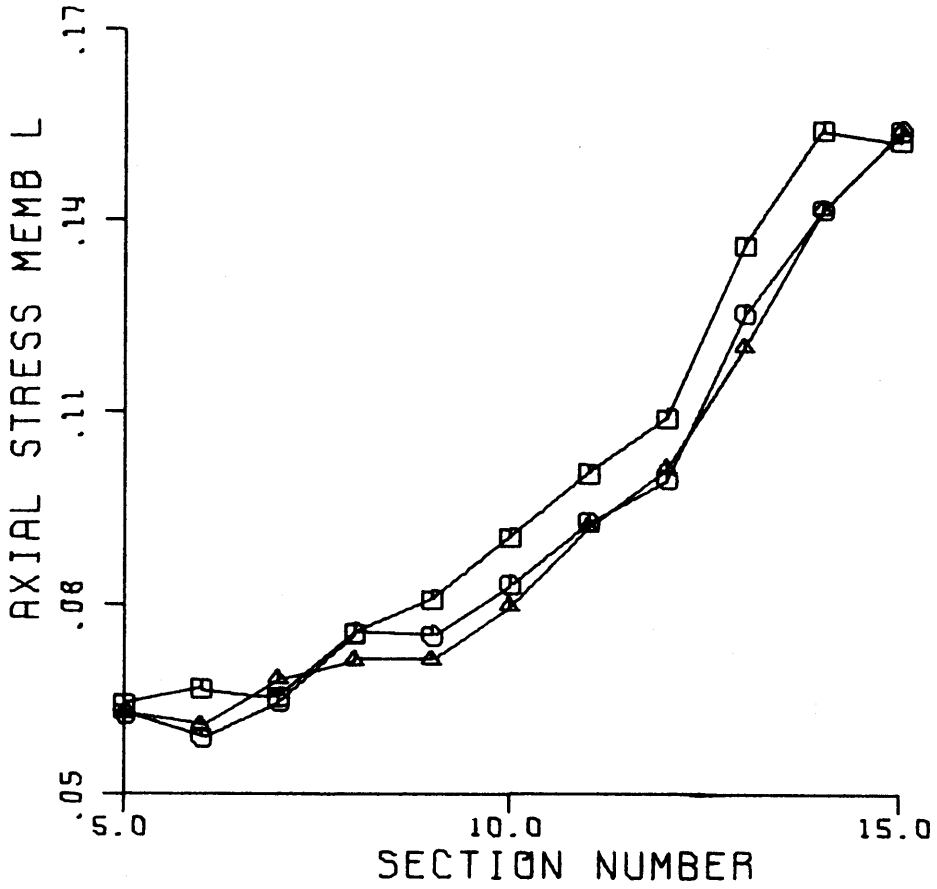
AXIAL STRESS MEMB L
.05
.08
.11
.14
.17
5.0
10.0
15.0
SECTION NUMBER

Figure 33. Bending Stress vs. Section Number

Left Arm

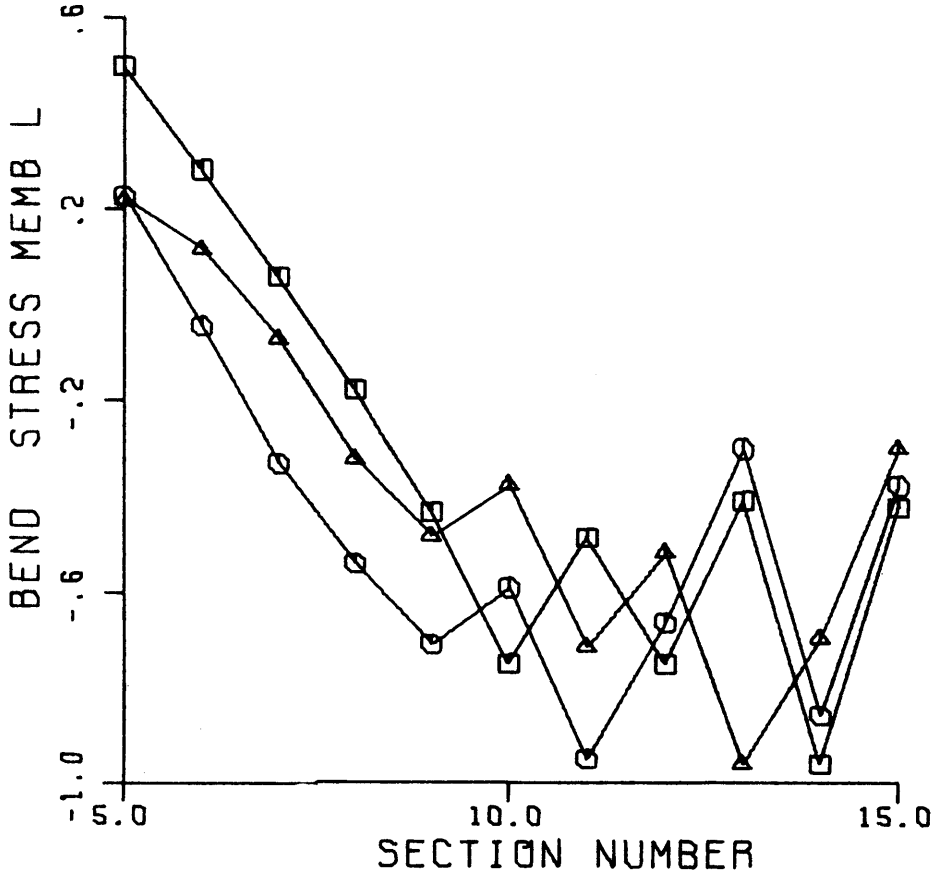
BEND STRESS MEMB L
.6
.2
-.2
-.6
-1.0
5.0
10.0
15.0
SECTION NUMBER

Figure 34. Total Stress vs. Section Number

Left Arm

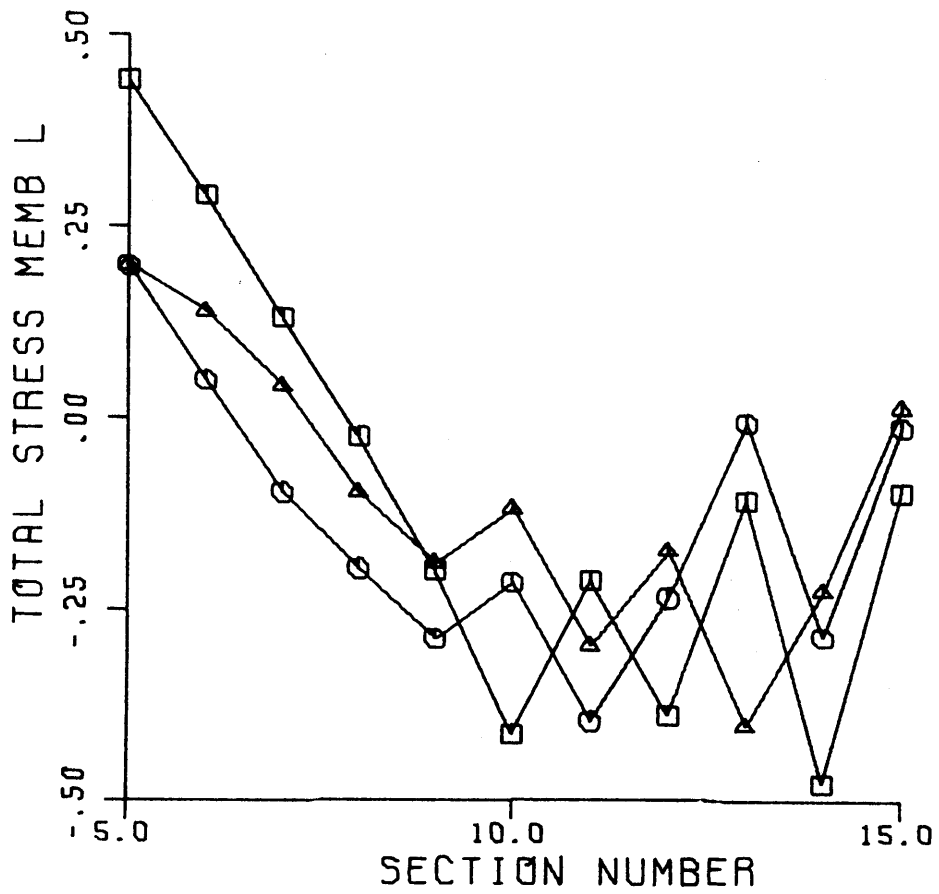
TOTAL STRESS MEMB L
.50
.25
.00
-.25
-.50
-5.0
10.0
15.0
SECTION NUMBER

section 4 and ends at 12 or 13, depending upon the specimen under consideration. The axial stress increases from 500 to approximately 1500 lb./in.^{2} but remains well below the elastic limit for bone (see Figure 8). The forces were chosen to be physically appropriate (see Chapter IV, section F). The aim was not to strain the bone to fracture. The stress due to bending decreases linearly until section 11 and then fluctuates about a constant value. The total stress (see Figure 34) initially decreases. It is influenced considerably by the stress due to bending. It appears that the stress tends to reach a minimum state and this state occurs within the membrane region. Figures 35 and 36 show the variation of the shear force and bending moment within the membrane regions. Plots of the bending moment about the y-axis due to the membrane which is oriented in the z-direction (refer to Figure 18), show a consistent linear increase in the bending moment for approximately one third of the distance into the membrane. After this point, fluctuation of the data occurs about some constant value.

The shear stress was calculated using two different approaches. The first approach utilized the shear Eq. (3.36) in terms of cross sectional area, the shear force, and geometrical quantities (i.e. the average shear stress times the structural parameters). The second approach investigated the shear stress as a function of the moment of inertia. This investigation was desirable since there are actually two components to the shear stress: one due to the vertical (y-com-

Figure 35. Shear Force-Membrane vs. Section Number

○ 446
□ 449
△ 332

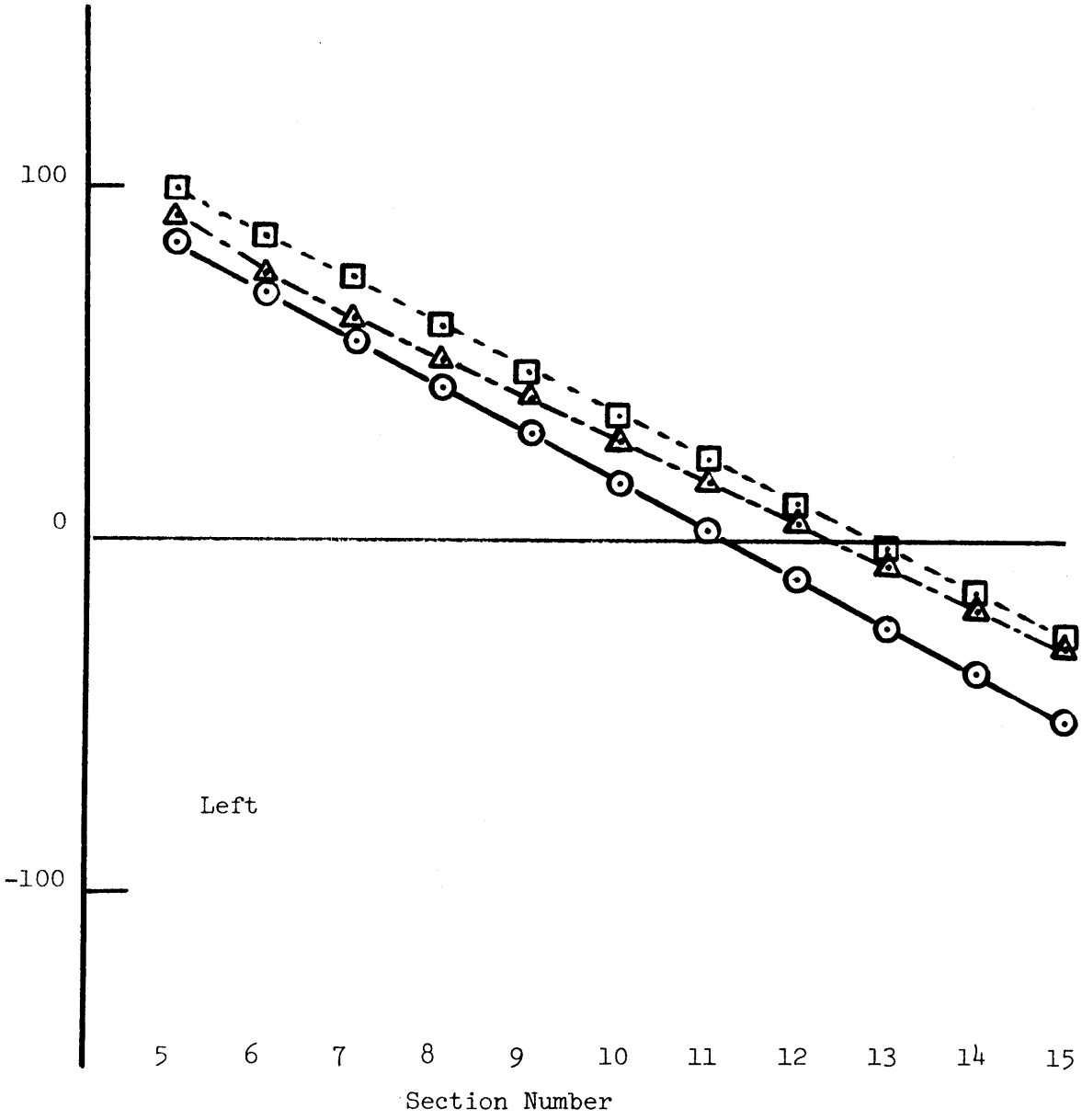
100
0
-100
Left
5
6
7
8
9
10
11
12
13
14
15
Section Number

Figure 36. Bending Moment-Membrane vs. Section Number

○ 446

□ 449

△ 332

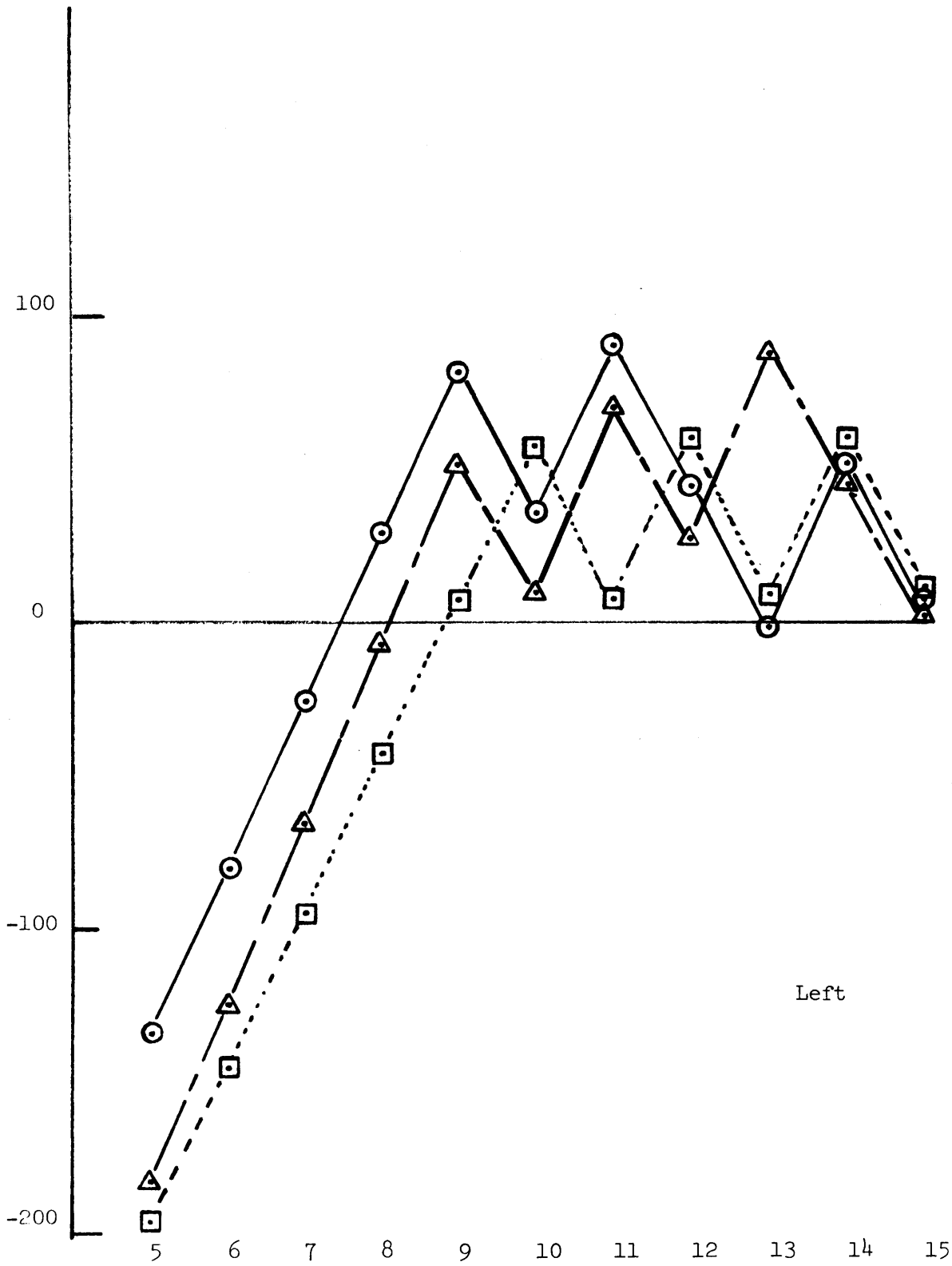
100
0
-100
-200
5
6
7
8
9
10
11
12
13
14
15
Left

ponent) shear force about the principal axis where $I = I_z$, and one due to the z-component of the membrane shear force, V_z, acting in the cross section about the principal axis where $I = I_y$. The shear stress curves vary from some asymptotic limit near section 8 (see Figure 37) and all these curves have similar behavior qualitatively. The maximum shear stress slowly decreases from a maximum of about 1000 lbs./in.^{2} to a minimum of -1000 lbs./in.^{2}.

As mentioned in Chapter III, the shear stress can also be determined using the moments of inertia. It was found that this method produces two different results. The maximum shear τ_{xy} varies uniformly. The maximum shear stress, τ_{zx} in the z-direction, however, is not as uniform, a fact which could be attributed to the asymmetric nature of the cross section in this direction. None of the graphs were studied for variation of shear across the plane of the cross section.

The section modulus was studied using both force and geometry related terms. When the ratio of the bending moment to the stress was used, the curves were linear, as was true for the case when the section modulus was calculated using I_y. For the case when I_y was used, all three plots varied randomly up to section 12 (see Figures 38 and 39).

Finally, the initial selection of dA/dx, via σ=constant, as a quantity to investigat did not meet the expectation of the theory. (See Figures 40 and 41). Attempts were made to

Figure 37. Shear Stress-Average, Maximum vs. Section Number

Left Arm

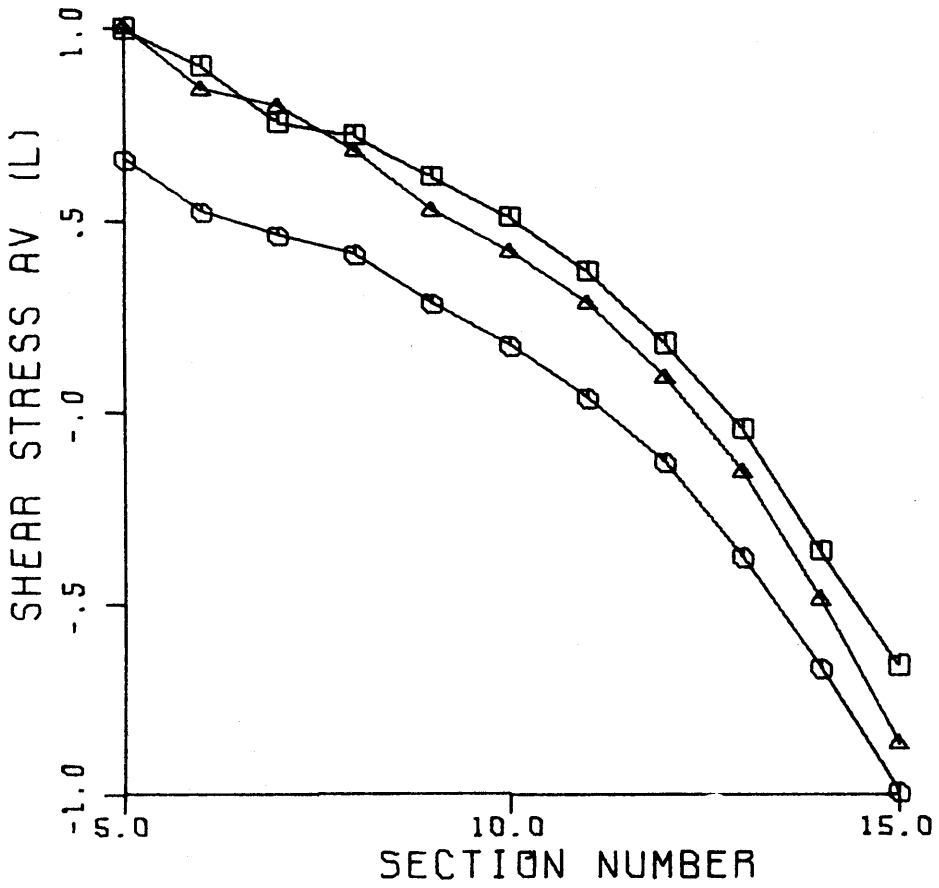
SHEAR STRESS AV (L)
1.0
.5
-.0
-.5
-1.0
5.0
10.0
15.0
SECTION NUMBER

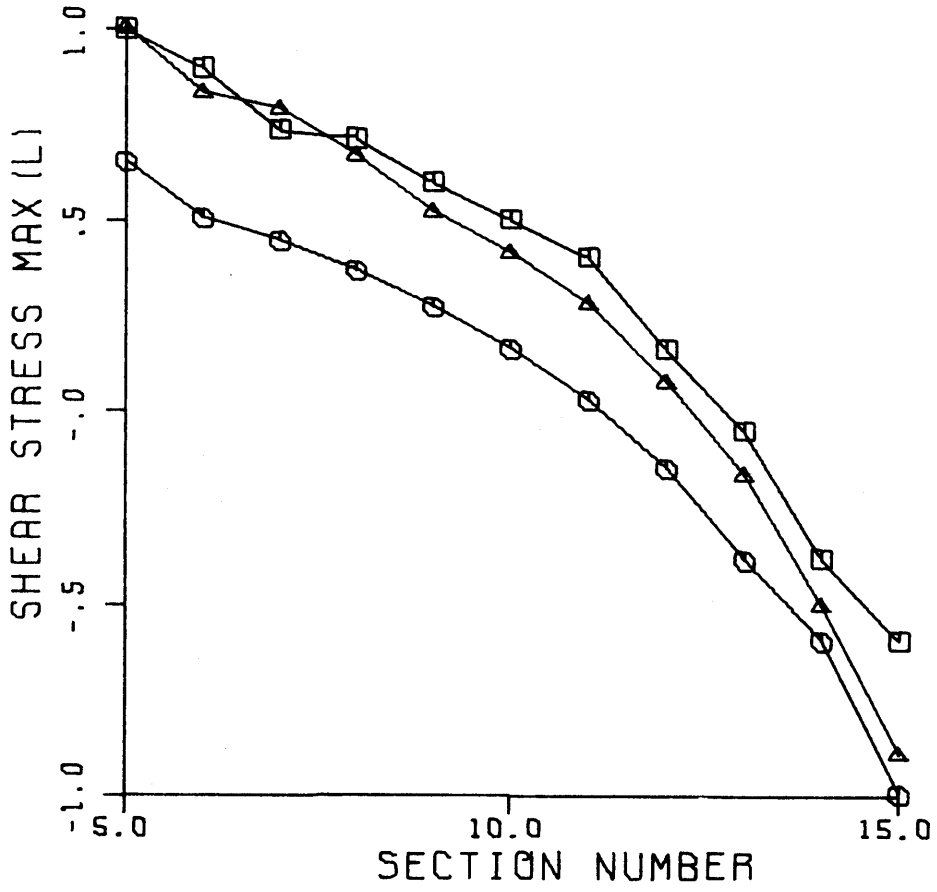
SHEAR STRESS MAX (L)
1.0
.5
-.0
-.5
-1.0
5.0
10.0
15.0
SECTION NUMBER

Figure 38. Section Moduli-M_b/σ_b vs. Section Number

○ 446

□ 449

△ 332

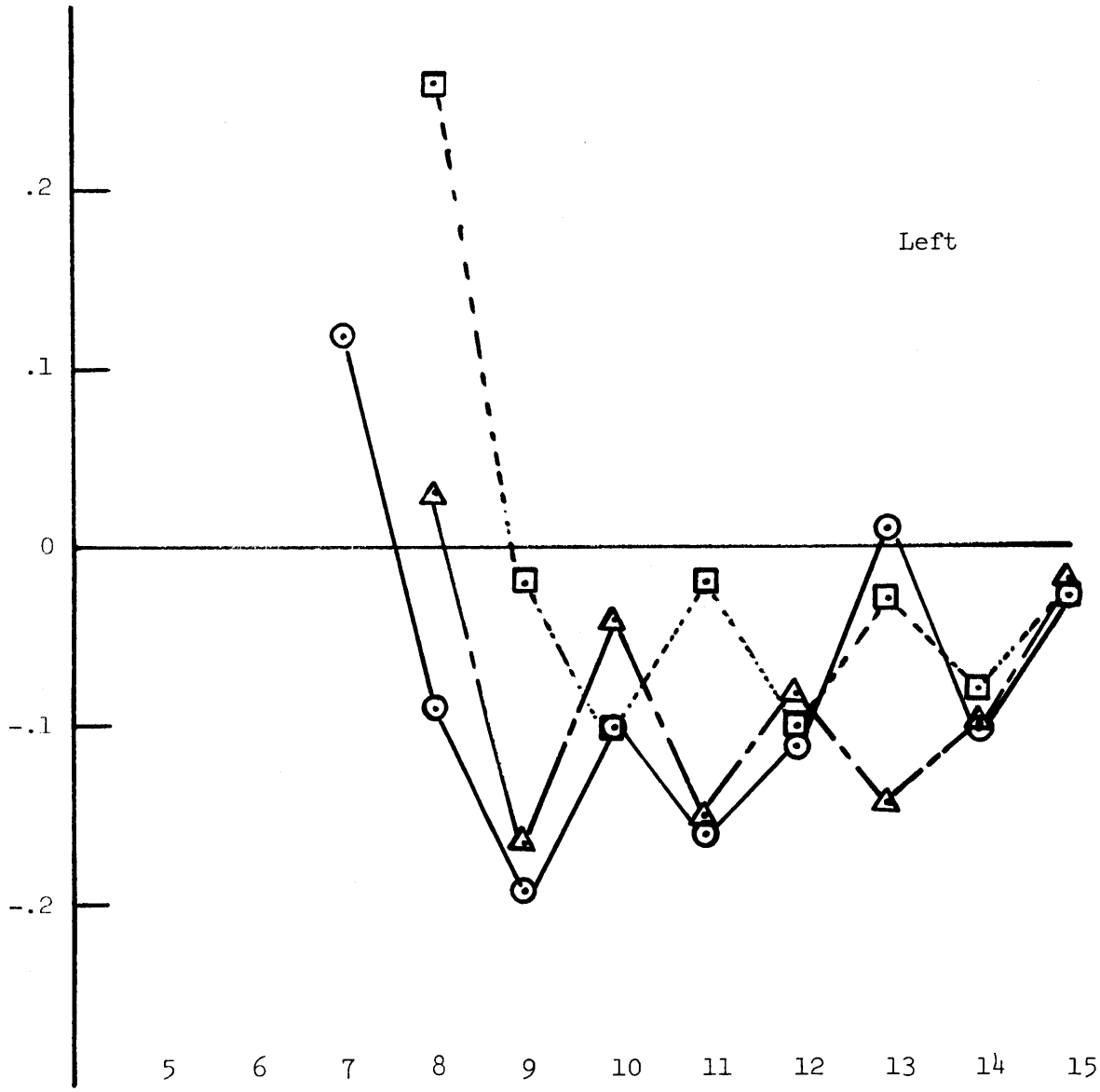
Left
.2
.1
0
-.1
-.2
5
6
7
8
9
10
11
12
13
14
15

Figure 39. Section Moduli-I_y, I_z vs. Section Number

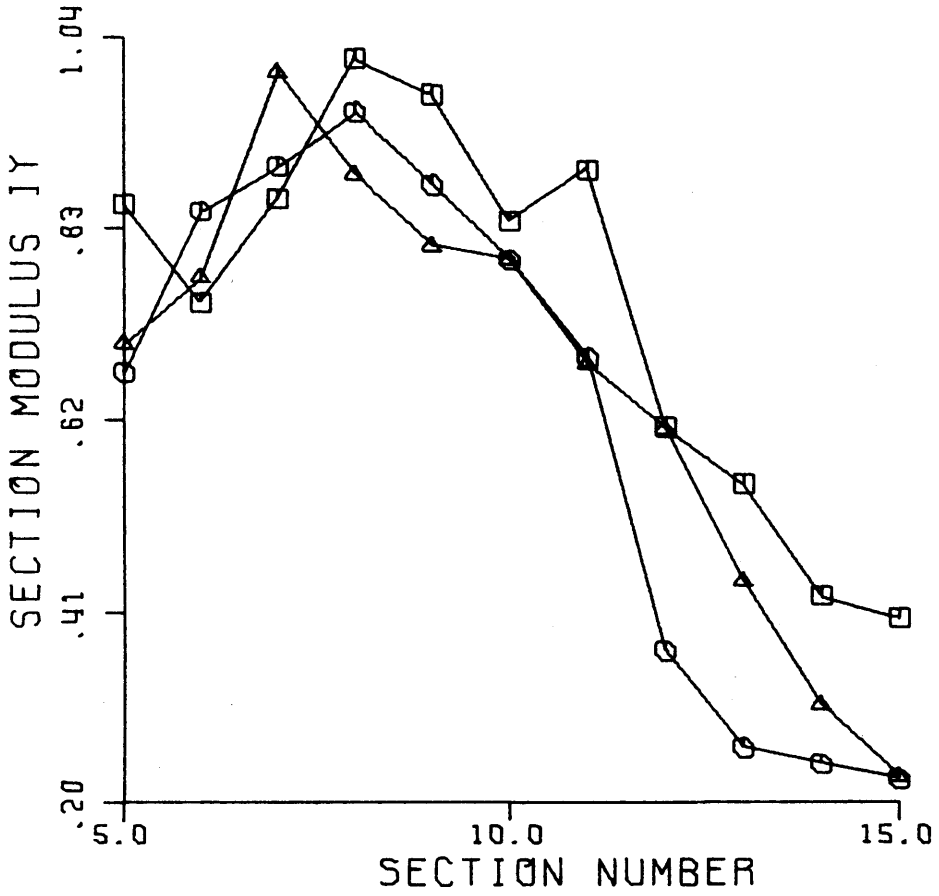
SECTION MODULUS IY
1.04
.83
.62
.41
.20
5.0
10.0
15.0
SECTION NUMBER

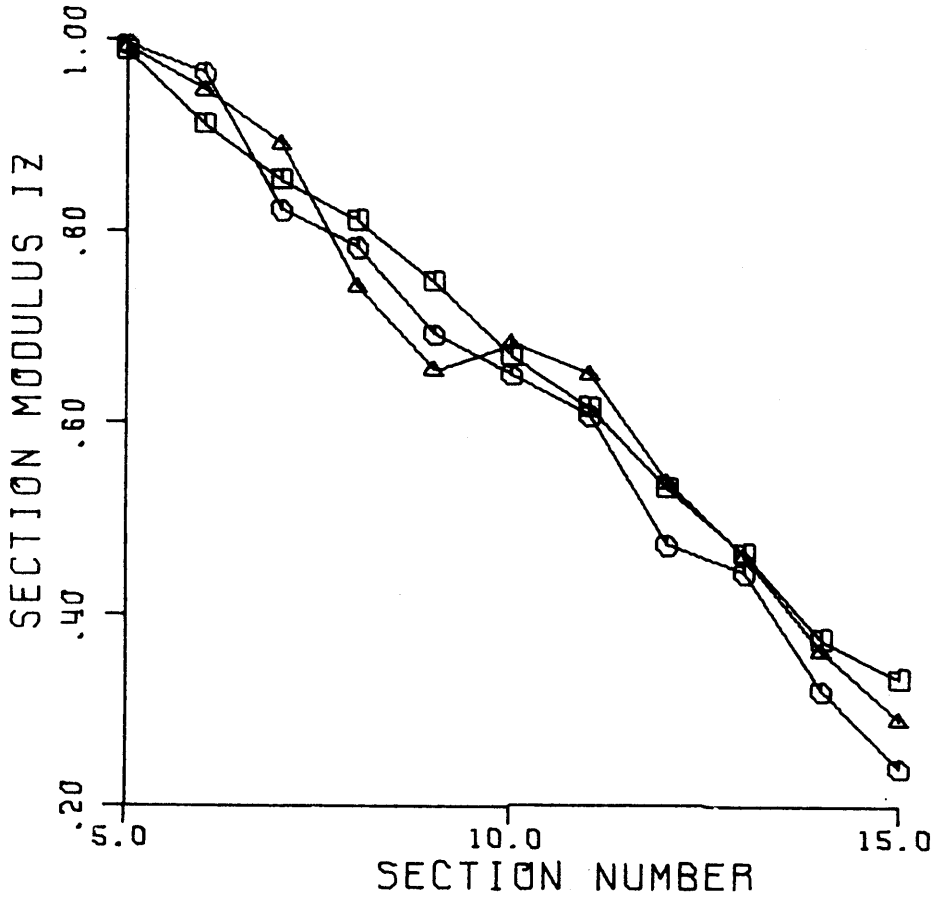
SECTION MODULUS IZ
1.00
.80
.60
.40
.20
5.0
10.0
15.0
SECTION NUMBER

Figure 40. Cylinder-$\Delta A/\Delta x$-Membrane vs. Section Number

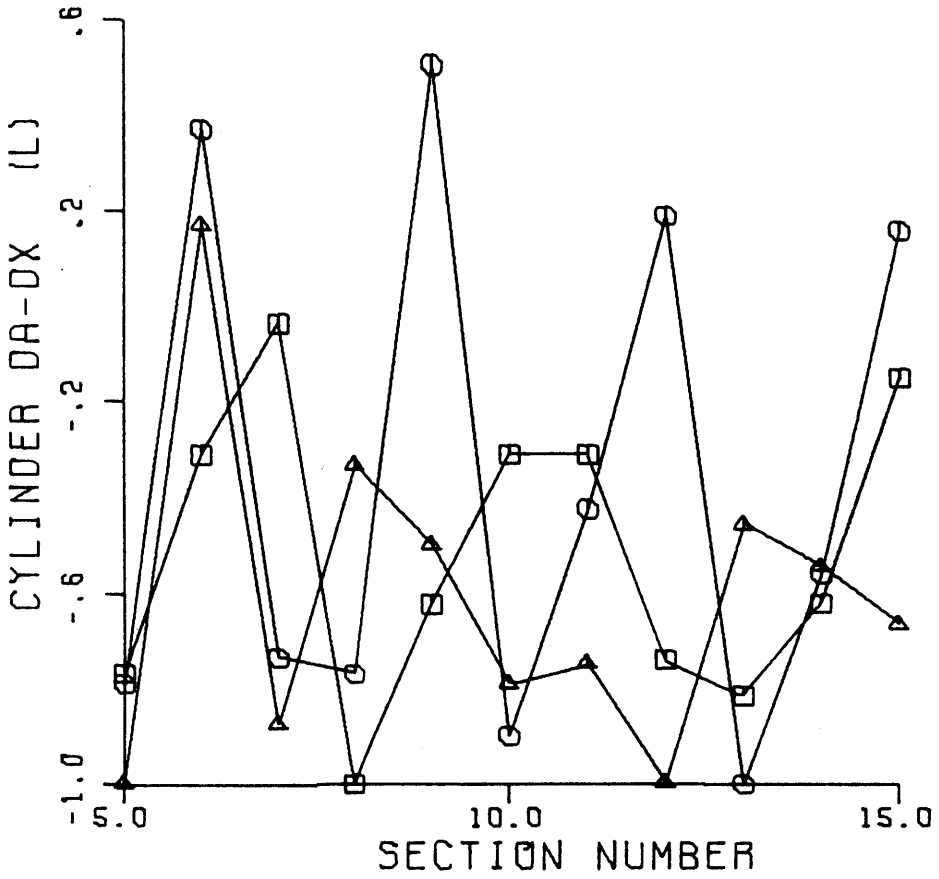
CYLINDER DA-DX (L)
.6
.2
-.2
-.6
-1.0
5.0
10.0
15.0
SECTION NUMBER

Figure 41. Experimental-$\Delta A/\Delta x$-Membrane vs. Section Number

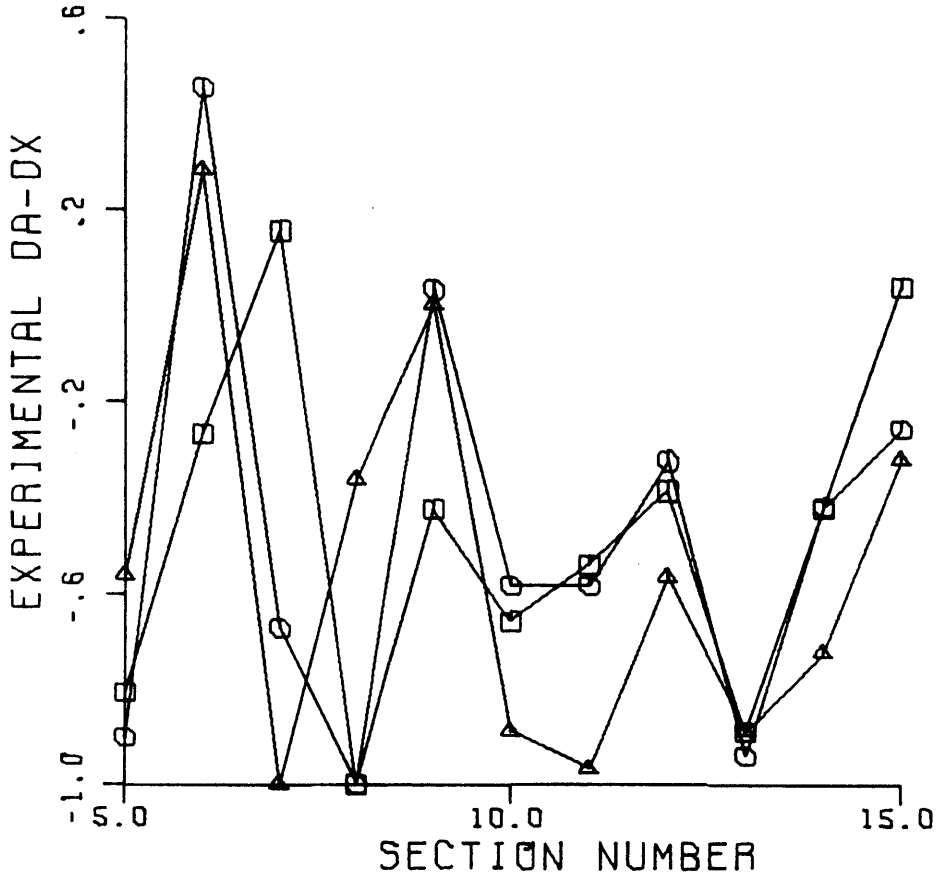
EXPERIMENTAL DA-DX
.6
.2
-.2
-.6
-1.0
5.0
10.0
15.0
SECTION NUMBER

simplify the expression by various approximations of the terms within the equation. Term by term comparison of the order of magnitudes of the component factors of the equations were performed, led to a few minor approximations, but did not satisfactorily represent the experimental data. The difficulty arises through the appearance of I(x) instead of $\frac{A(x)}{4}(r_1^2(x) + r_2^2(x))$. Because the graphs of DA/DX for the cylinder model beam appears smoother than those of the bone, the author feels that each set of cylinder model beam plots represents a superposition of the corresponding experimental plots for the bone. (See Figures 42 & 43.)

Figure 42. Cylinder - DA/DX - Membrane vs. Section Number

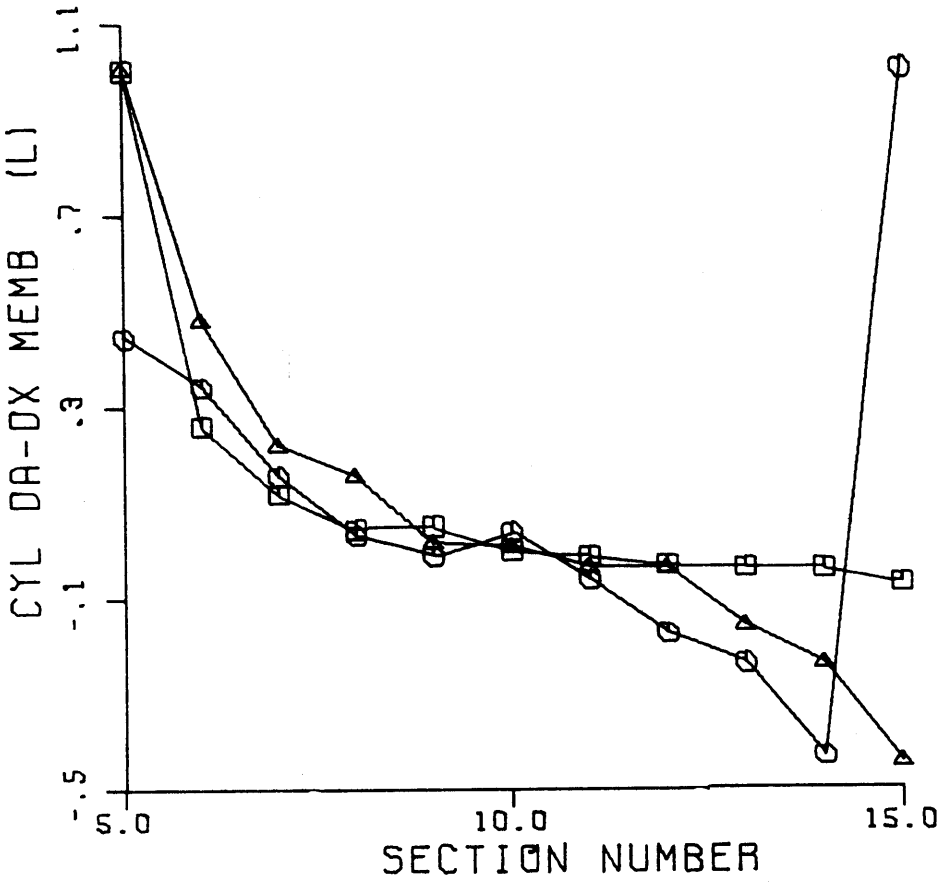
CYL DA-DX MEMB (L)
1.1
.7
.3
-.1
-.5
5.0
10.0
15.0
SECTION NUMBER

Figure 43. Experimental - DA/DX - Membrane vs. Section Number

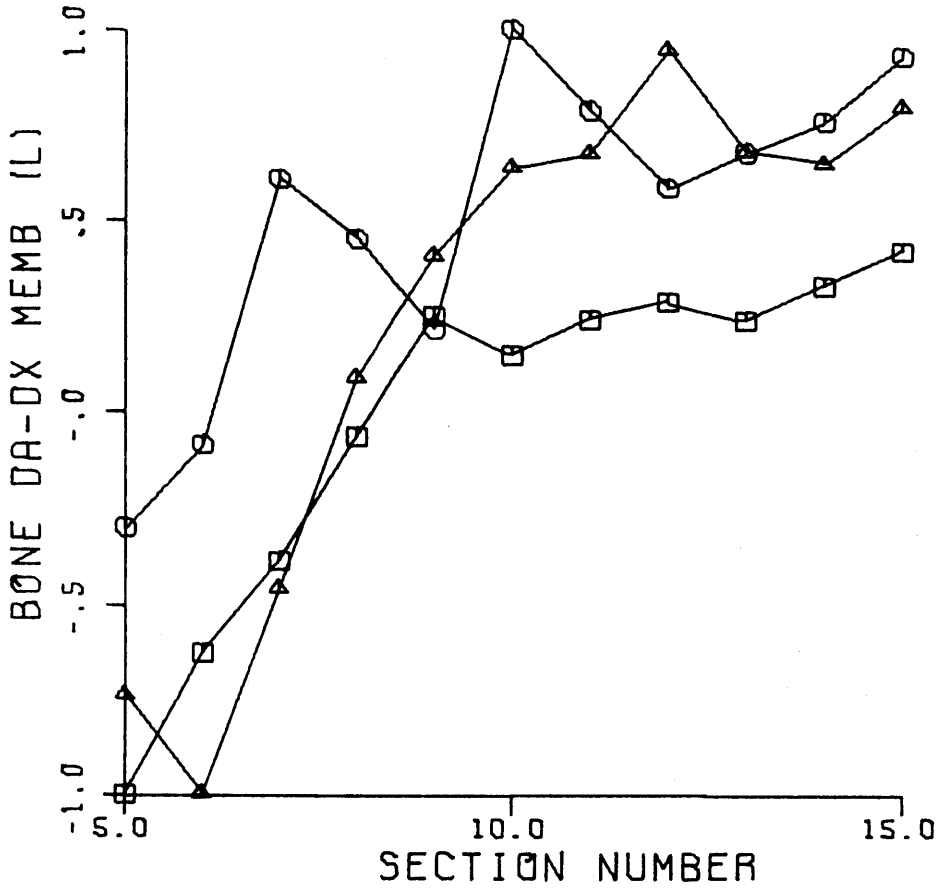
BONE DA-DX MEMB (L)
1.0
.5
-.0
-.5
-1.0
5.0
10.0
15.0
SECTION NUMBER

C. Comments

The trends in the data presented in this chapter support the author's belief that the geometrical variables A(x) and I(x) are significant as bases for an analytic relationship which can correlate force with structure. One should be cognizant, however, of the many possible sources of error in this work due to the biological variation of specimens and due to the obstacles of data definition, especially in handling of the orientation and referencing procedure and in the large volume of manual data compilations. Despite these obstacles, the author found that the actual tabulations of data sets (x_i, y_i, A_i) were experimentally accurate (or reproducible) to within 3%. The photographic enlargement procedure is straightforward, but the scale factor must be sure to be recorded accurately: The author used the circular cross section of the rod to indicate the scale. Two data points were found to go off the scale quite frequently -- 332L9 and 332R9 -- leading the author to suspect that the factor recorded in this data set is in error.

The choice of force magnitudes for the interosseous membrane may be another source of error: the ratio of the brachialis muscle force to the extensor carpi radialis longus force was approximately the same in both force situations. Instead of one choice, the author suggests that manipulation of magnitudes be done over the entire range of, but staying within, the limits reported by researchers in the field in the

hopes of obtaining better information about the interplay of muscular forces.

VI. SUGGESTIONS FOR FUTURE WORK

Several assumptions were originally postulated by the author as first approximations in the formulation of a theoretical model for cortical bone. An overview of these assumptions and their resulting conflict or agreement with the experimental analysis leads to suggestions for future work. The current status of the research problem is as follows:

1. The assumption of perfect elasticity for the bone itself, and consequently, for the theoretical model as presented in Chapter III, has been upheld and is experimentally verified in Chapter V. Therefore the applicability of beam bending theory is confirmed.

2. Areas and moments of inertia calculated by the author for the theoretical model are in good agreement with the author's experimentally obtained data. Moments of inertia differ from experimental measurements by a factor of 16 due to the initial choice of a structural model. The Law of Maximum Economy of Building Material requires a minimization of material to withstand an applied stress. It is clear from the literature that bone's structural behavior satisfies the requirements of this Law. The theoretical model's shortcoming is in the moment of inertia. The implication is that the initial model has gone beyond the minimum material requirements and is structurally too small, indicating that a different approximation should be made.

3. Stress at the outer fiber was assumed to be a constant. In Chapter V, the resulting total stress within the region of the membrane is in fact roughly a constant but approaches a minimum midway along the shaft for both the theoretical and experimental data. This result, which has been verified in the literature (see Chapter I) is physically significant since the concept of bone's remodelling to minimize the local stresses acting upon it's cross-sectional area implies that there must be some minimization criterion related to the area.

4. A limitation of the cylindrical beam model with varying cross section, is the relatively fixed nature of the varying cross section, i.e. two concentric circles of different radius. It might be better to use different geometrical constructs, although such an approach would be very entailed. The author observes that the next order approximation might be a combination of confocal ellipses or centered equilateral triangles. In choosing any internal radii an element of subjectivity is introduced into the problem because the researcher must decide what the peripheral border is between cancellous bone and cortical. The averaging of radii reduces a considerable amount of area and affects the moment of inertia. A comparison of the area of the central hole in the bone section to the area of the cross section might be significant in further analysis.

5. A first and necessary step towards an analytic muscle-force/bone-geometry correlation is to characterize an appropriate model for the force-structure system of interest. Such a characterization requires that there be established a reliable, experimental framework within which essential data may be obtained. In this thesis, the author has established such a framework and suggested a means by which data analysis may be effected. As mentioned in Chapter V, an indication of the success of the data taking process is the reproducibility of area measurements. Agreement between the old and new measurements occurred to within 4%. This is unusually good for physiological data.

Below are avenues along which future work should be directed:

1. Detailed analysis of the relationship of the calculated moment of inertia to geometries of model cross sections.

2. Application of the theory of elasticity to the solution of the theoretical stress-strain relationship for the beam to allow mathematical manipulation of the variables, to decompose terms into combinations of force and area terms, and to determine particle displacements in the plane of the cross section.

3. Inclusion in the model of the effect of twist or rotation to give a more complete description of the system's loading and its cross-sectional area response.

4. Consideration of the finite element method in stress analysis might allow better quantitative correlation of observed areas to some section characteristic parameter.

REFERENCES

1. Wolff, J., Das Gesetz der Transformation der Inneren Architektur der Knochen. Sitz. Berlin Preuss. Akad. d. Wiss. 22, Sitzg. physik. math. Kl.

2. Roux, W. (1895), Gesammelte Abhandlungen über Entwicklungsmechanik der Organismen. I u. II. Engelmann, Leipzig.

3. Pauwels, Fr. (1948b), Die Bedeutung der Bauprinzepien des Stritz und Bewegungsapparates für die Beanspruchung der Röhrenknochen. I. Beitrag zur Funktiorellen Anotonire und Kausallen Morphologie des Stutzapparates Z. Anat. 1A, p. 208.

4. Ibid., p. 208.

5. Pauwels, Ibid., p. 209.

6. Pauwels, Ibid., pp. 210-211.

7. Kummer, Benno, "Photoelastic Studies on the Functional Structure of Bone", Folia Biotheoretica, Vol. VI, Leiden, E. J. Brill, (1966) p. 31.

8. Hopkins, R. Bruce, Design Analysis of Shafts and Beams, McGraw-Hill, New York, 1970, p. 151.

9. Kummer, B., Ibid., p. 31.

10. Townsend, Paul, "Biomechanics of Elbow Joint", 1975 unpublished.

11. Ibid.

12. Wells, Katherine, Kinesiology, W. B. Saunders Co., Philadelphia, Pa. (1971), pp. 9-14.

13. King, Barry G. and Showers, Mary Jane, Human Anatomy and Physiology (6th ed.), W.B. Saunders Co., Philadelphia, Pa. (1969), p. 8.

14. King and Showers, ibid., pp. 179-180.

15. Hollingshead, W.H., Anatomy for Surgeons: Volume 3, Back and Limbs, p. 382, Hoeber Medical Division, Harper & Row Publishers, New York (1969).

16. Grant, J.C.B., An Atlas of Anatomy (6th ed.) No. 51, The Williams & Wilkins Co., Baltimore, (1972).

17. Kelley, David L., Kinesiology: Fundamentals of Motion Description, Prentice-Hall, Inc., Eaglewood Cliffs, New Jersey (1971) pp. 306-307.

18. Kelley, ibid., p. 145.

19. Basmajian, J.V., Muscles Alive: Their Functions Revealed by Electromyography, Williams & Wilkins Co., Baltimore, Md., (1962) p. 124.

20. Ibid., p. 124.

21. King and Showers, ibid., pp. 202-203.

22. Wells, ibid., pp. 39-43.

23. Hollingshead, W.H., Anatomy for Surgeons: Volume 3, Back and Limbs, p. 382, Hoeber Medical Division, Harper 7 Row Publishers, New York (1969).

24. Kelley, ibid., pp. 298-299.

25. Kelley, ibid., pp. 300-301.

26. Kelley, ibid., pp. 302-303.

27. Steindler, Human Anatomy & Physiology Under Normal and Pathological Conditions, Springfield, Ill., Charles C. Thomas, Publishers, p. 490.

28. Ibid., p. 490.

29. Steindler, ibid., pp. 292, 296.

30. Kelley, ibid., p. 293.

31. Hill, A.V., "The Abrupt Transition from Rest to Activity in Muscle", Proc. Roy. Soc. B., Vol. 136, pp. 399-402.

32. Wilkie, D.R., "The Relation Between Force and Velocity in Human Muscle", J. Physiol., Vol. 110 (1950) p. 249.

33. Pertuzon, E. and Bouisset, S., "Instantaneous Force-Velocity Relationship in Human Muscle", Medicine and Sport, Vol. 8: Biomechanics III, Karger, Basel, (1973) p. 233.

34. de Duca, Carlo and Forrest, W. J., "Force Analysis of Individual Muscles Acting Simultaneously on the Shoulder Joint During Isometric Abduction", J. Biomechanics (1973), Vol. 6, p. 389.

35. Ibid., p. 389.

36. Morris, Carrie, "The Measurement of the Strength of Muscle Relative to the Cross Section", Res. Quarterly (1948), p. 295.

37. Ibid., pp. 301-302.

38. Ibid., p. 295.

39. deDuca, Carlo and Forrest, W.J., p. 389.

40. deDuca, Carlo and Forrest, W.J., p. 393.

41. Steindler, p. 502.

42. Singh, M. and Kaysovich, P., "Isotonic and Isometric Forces of Forearm flexors and Extensors", J. Appl. Physiol., Vol. 4 (1966) p. 1435.

43. Wilkie, pp. 250, 267.

44. Jorgensen, K. and Bankov, S., "Maximum Strength of Elbow Flexors with Pronated and Supinated Forearm", Medicine & Sport, Vol. 6; Biomechanics II (Karger, Basel 1971), p.178.

45. Singh, M. and Karpovich, P., p. 1435.

46. Pertuzon, p. 231.

47. Komi, P.V., "Measurement of the Force-Velocity Relationship in Human Muscle under Concentric and Eccentric Contraction" , Medicine & Sport, Vol. 8; Biomechanics III, p. 226.

48. Basmajian, Muscles Alive: Their Function Revealed by Electromyography, Baltimore, Md. (1967).

49. Kelley, p. 301.

50. Basmajian, p. 65.

51. Steindler, ibid., p. 502.

52. Kelley, ibid., p. 301.

53. Wilkie, ibid., p. 267.

54. Basmajian, p. 114.

55. Timoshenko, S. and MacCullough, G., Elements of Strengths of Materials, New York, D. Van Nostrand Co., Inc. (1949).

56. Hopkins, R.B., Design Analysis of Shafts and Beams, New York, McGraw-Hill Book Co., (1970).

57. Timoshenko, S. and MacCullough, G., p. 94.

58. Ibid., p. 119.

59. Byars, E. and Snyder, R., Engineering Mechanics of Deformable Bodies, New York, Intext Educational Publishers, (1975).

60. Boley, B.A., "On the Accuracy of the Bernoulli-Euler Theory for Beams of Variable Section", Journal of Applied Mechanics, TRANS. ASME, Vol. 30 (1963), pp. 373-378.

61. Yamada, H., Strength of Biological Materials, The Williams and Wilkins Co., Publishers, Baltimore, (1970).

62. Evans, F. G., Mechanical Properties of Bone, Springfield, Ill., Charles C. Thomas, Publisher, (1973).

63. Kummer, B., "Biomechanics of Bone: Mechanical Properties, Functional Structure, Functional Adaptation", Biomechanics-Its Foundations and Objectives, edited by Fung, Y.C., Perrone, N. and Anliker, M., (1972), Prentice-Hall, Inc., Englewood Cliffs, N.J.

64. Kummer, B., pp. 239-242.

65. Evans, F.G.

66. Yamada

67. Ibid.

68. Wilkie, p. 267.

69. Yamada, p. 94.

70. Steindler, p. 498.

APPENDIX I

DERIVATIONS FOR INITIAL MODEL

Useful Relationships: $A = \pi(r_2^{\,2} - r_1^{\,2})$

$$I = \frac{\pi}{4}(r_2^{\,4} - r_1^{\,4}) = \frac{A}{4}(r_2^{\,2} + r_1^{\,2})$$

$$\frac{d}{dx}\left(\frac{1}{A}\right) = \frac{-dA/dx}{A} \qquad \frac{dI}{dx} = \frac{1}{4}\frac{dA}{dx}(r_1^{\,2}+r_2^{\,2}) + \frac{A}{2}\left(r_1\frac{dr_1}{dx} + r_2\frac{dr_2}{dx}\right)$$

Case 1: σ_x = Maximum and Constant at r_2.
Solve for γ. $r_2 = r_2(x)$, $r_1 = r_1(x)$

$$\sigma_x = \pm\frac{P_x}{A} \pm \frac{P_y x r_2(x)}{I}$$

Taking the derivative

$$\frac{d\sigma_x}{dx} = 0 = \pm\frac{P_x}{A^2}\left(-\frac{dA}{dx}\right) \pm \left[\frac{P_y x r_2(x)}{I^2}\left(\frac{-dI}{dx}\right) + \frac{P_y x}{I}\frac{dr_1}{dx} + \frac{P_y r_2}{I}\right] \quad (A.1)$$

Assume that both signs are positive; factor out P_y/I and divide through by P_x:

$$0 = \frac{1}{A^2}\left(\frac{-dA}{dx}\right) + \frac{P_y/P_x}{I}\left[-\frac{xr_2}{I}\left(\frac{-dI}{dx}\right) + \frac{xdr_2}{dx} + r_2\right] \quad (A.2)$$

Expanding Eq. (A.2) and rewriting yields:

$$\left(\frac{I}{A^2}\ \frac{dA}{dx^2}\right) = \gamma \left[\frac{xr_2 \cdot 4}{A(r_1{}^2+r_2{}^2)} \left[-\frac{1}{4}\frac{dA}{dx}(r_1{}^2+r_2{}^2) - \frac{A}{2}\left(\frac{r_1 dr_1}{dx}+\frac{r_2 dr_2}{dx}\right)\right]\right.$$

$$\left. + \frac{xdr_2}{dx} + r^2 \right] \tag{A.3}$$

where $\gamma = P_y/P_x$.

Finally, factoring and recombination of terms yields

$$\gamma = \frac{\frac{I}{A^2}\ \frac{dA}{dx}}{r_2 + \frac{xdr_2}{dx} - \frac{xr_2 A}{2I}\left(r_2\frac{dr_2}{dx} + r_1\frac{dr_1}{dx}\right) - \frac{xr_2}{A}\ \frac{dA}{dx}} \tag{A.4}$$

<u>Case 1</u>: σ_x = Maximum and Constant at r_2

$r_2 = r_2(x)$, $r_1 = r_1(x)$

Solve for $\frac{dA}{dx}$.

Referring to Eq. (A.2) and expanding $\frac{dI}{dx}$ gives

$$0 = -\frac{1}{A^2}\frac{dA}{dx} + \gamma\left[\frac{r_2}{I} + \frac{x}{I}\frac{dr_2}{dx} - \frac{xr_2}{I^2}\left(\frac{A}{4}\frac{d}{dx}(r_2{}^2+r_1{}^2) + \frac{(r_1{}^2+r_2{}^2)}{4}\ \frac{dA}{dx}\right)\right] \tag{A.5}$$

$$0 = -\frac{1}{A^2}\frac{dA}{dx} - \frac{\gamma xr_2}{4I^2}\frac{dA}{dx}(r_1{}^2+r_2{}^2) + \frac{\gamma r_2}{I}\ \frac{\gamma x}{I}\ \frac{dr_2}{dx} - \frac{\gamma xr_2 A}{4I^2}\ \frac{d}{dx}(r_1{}^2+r_2{}^2)$$

or regrouping,

$$0 = -\frac{dA}{dx}\left[\frac{1}{A^2} + \frac{\gamma x r_2}{4I^2}\,(r_1{}^2+r_2{}^2)\right] + \frac{\gamma}{I}\left[r_2 + \frac{x dr_2}{dx} - \frac{x r_2 A}{4I}\left(r_1\frac{dr_1}{dx} + \frac{r_2 dr_2}{dx}\right)\right] \tag{A.6}$$

Finally, transposing $\frac{dA}{dx}\left[\quad\right]$ and dividing gives

$$\frac{dA}{dx} = \frac{\frac{\gamma}{I}\left[r_2 + \frac{x dr_2}{dx} - \frac{x r_2 A}{4I}\frac{d}{dx}(r_2{}^2+r_1{}^2)\right]}{\frac{I}{A^2} + \frac{\gamma x r_2}{4I^2}(r_1{}^2 + r_2{}^2)}\ , \tag{A.7}$$

or

$$\frac{dA}{dx} = \frac{4I\gamma A^2\left[r_2 + \frac{x dr_2}{dx} - \frac{x r_2 A}{2I}\left(r_2\frac{dr_2}{dx} + r_1\frac{dr_1}{dx}\right)\right]}{4I^2 + \gamma A^2 x r_2 (r_1{}^2+r_2{}^2)}\ . \tag{A.8}$$

<u>Case 2</u>: σ_x = Maximum and Constant at r_2

r_2 = constant, $r_1 = r_1(x)$

Solve for γ_1.

In Eq. (A.4), $dr_2/dx = 0$ and dA/dx is not expanded. Thus,

$$\gamma_1 = \frac{\frac{I}{A^2}\ \frac{dA}{dx}}{r_2 - \frac{x r_2 A}{2I}\ \frac{r_1 dr_1}{dx} - \frac{x r_2}{A}\ \frac{dA}{dx}} \tag{A.9}$$

or

$$\gamma_1 = \frac{\frac{r_1{}^2+r_2{}^2}{4A}\left(\frac{dA}{dx}\right)}{r_2 - \frac{x r_2 r_1}{r_1{}^2+r_1{}^2}\ \frac{dr_1}{dx} - \frac{x r_2}{A}\ \frac{dA}{dx}} \tag{A.10}$$

and finally,

$$\gamma_1 = \left(\frac{r_1^{\,2}+r_2^{\,2}}{4Ar_2}\right) \frac{dA}{dx} \left[1 - \frac{xr_1}{r_1^{\,2}+r_2^{\,2}} \frac{dr_1}{dx} - \frac{x}{A} \frac{dA}{dx} \right]^{-1} \tag{A.11}$$

Solve for γ_2. Setting $\frac{dr_2}{dx} = 0$ and expanding $\frac{dA}{dx}$ in Eq. (A.4) gives

$$\gamma_2 = \frac{\frac{I}{A^2} \left(-2\pi r_1 \frac{dr_1}{dx}\right)}{r_2 - \frac{xr_2A}{2I} \frac{r_1dr_1}{dx} + \frac{2\pi xr_2}{A} \frac{r_1dr_1}{dx}}$$

or

$$\gamma_2 = \frac{2\pi I}{A^2} \frac{r_1dr_1}{dx} \left[r_2 - \frac{xr_1dr_1}{dx}\left(\frac{r_2A}{2I} - \frac{2\pi r_2}{A}\right) \right]^{-1} \tag{A.12}$$

<u>Case 2</u>: σ_x = Maximum and Constant at r_2

r_2 = constant, $r_1 = r_1(x)$

Solve for $\frac{dA}{dx}$.

Setting $\frac{dr_2}{dx} = 0$ and expanding I gives

$$\frac{dA}{dx} = \frac{A(r_1^{\,2}+r_2^{\,2})\gamma A^2 \left[r_2 - \frac{xr_2Ar_1{}^4}{2A(r_1^{\,2}+r_2^{\,2})} \frac{dr_1}{dx} \right]}{\frac{A^2(r_1^{\,2}+r_2^{\,2})^2}{4} + xA^2r_2\gamma(r_1^{\,2}+r_2^{\,2})} \quad . \tag{A.13}$$

Factoring and recombining terms gives

$$\frac{dA}{dx} = \frac{4Ar_2\gamma \left[1 - \frac{2xr_1}{(r_1^2+r_2^2)} \frac{dr_1}{dx}\right]}{r_1^2 + r_2^2 + 4xr_2\gamma} \quad . \tag{A.14}$$

APPENDIX II

DERIVATIONS - MEMBRANE

The relations presented at the outset of Appendix I will be used here. The stress in the region of the membrane is given by

$$\sigma_{II} = \frac{P_x}{A} + \frac{yP_y x'}{I_z} - \frac{zP_z}{I_y}\left[x' + L-m-\frac{(x-c)^2}{2d}\right] . \qquad \text{(A2.1)}$$

For the case of a cylinder, $I_y = I_z$. Using this fact and taking the derivative of σ_{II}, assumed to be constant and a maximum at $z = y = r_2$ yields,

$$\frac{d\sigma_{II}}{dx} = 0 = \frac{r_2}{I}\left\{P_y - P_z\left(1-\frac{x-c}{d}\right)\right\} + \left\{P_y x' - P_z\left[x'+L-m-\frac{(x-c)^2}{2d}\right]\right\} \text{ (times)}$$

$$\left[\frac{\frac{Idr_2}{dx'} - \frac{r_2 dI}{dx'}}{I^2}\right] - \frac{P_x}{A^2}\frac{dA}{dx} \qquad \text{(A2.2)}$$

Expanding $\frac{dI}{dx}$, and multiplying by I/P_x gives

$$0 = r_2\left[\gamma_{yx} - \gamma_{zx}\left(1-\frac{x-c}{d}\right)\right] + \left\{\gamma_{yx}x' - \gamma_{zx}\left[x'+L-m-\frac{(x-c)^2}{2d}\right]\right\}\left[\frac{dr_2}{dx} - \frac{r_2}{I}\left\{\frac{A}{4}\frac{d}{dx'}(r_2^2+r_1^2) + \frac{r_1^2+r_2^2}{4}\frac{dA}{dx'}\right\}\right] \cdot$$

$$- \frac{I}{A^2}\frac{dA}{dx'} \qquad \text{(A2.3)}$$

where $\gamma_{yx} = P_y/P_x$, $\gamma_{zx} = P_z/P_x$.

Regrouping terms:

$$0 = \frac{dA}{dx'}\left[\frac{I}{A^2} + \{\gamma_{yx}x'-\gamma_{zx}\left[x'+L-m-\frac{(x-c)^2}{2d}\right]\}\frac{r_2}{I}\cdot\frac{r_1^2+r_2^2}{4}\right] + r_2\left[\gamma_{yx}-\gamma_{zx}(1-\frac{x-c}{d})\right]+\{\gamma_{yx}x'-\gamma_{zx}\left[x'+L-m-\frac{(x-c)^2}{2d}\right]\}\left[\frac{dr_2}{dx'} - \frac{r_2A}{2I}(\frac{r_2dr_2}{dx'} + \frac{r_1dr_1}{dx'})\right] \tag{A2.4}$$

Finally,

$$\frac{dA}{dx'} = \frac{4IA^2\{r_2\left[\gamma_{yx}- \gamma_{zx}(1-\frac{x-c}{d})\right]+\{\gamma_{yx}x'-\gamma_{zx}\left[x'+L-m-\frac{(x-c)^2}{2d}\right]\}\left[\frac{dr_2}{dx'} - \frac{r_2A}{2I}(\frac{r_2dr_2}{dx'}+\frac{r_1dr_1}{dx'})\right]\}}{4I^2 + A^2r\ (r_1{}^2+ r_2^2)\{\gamma_{yx}x' - \gamma_{zx}\left[x'+L-m-\frac{(x-c)^2}{2d}\right]\}} . \tag{A2.5}$$

The derivation for $\frac{dA}{dx'}$ in the case when bone is investigated, i.e. $I_z \neq I_y$, will not be presented here. The calculation is straightforward and similar to the one above for $I_z=I_y$. It can be seen that Eq. (4.7) does reduce to Eq. (4.8) when the substitution $I_z = I_y = I$ is made.

APPENDIX III

Computer Programs

TABLE A

VARIABLES IN DADX PROGRAM

(Regions I, II - Cylinder; Regions II, III=1 - Bone)

Unless explicitly specified, i.e., DIM=, the dimension of all variables listed below is (6.11). The six refers to the specimen and the eleven refers to the sections. Terms, intermediate in the calculation of dA/dx which are of interest are expanded at the end of this Table.

SPEC(6)	section identification number	
C, DL, D, B - DIM=6	distances; c, L, d, b	
W, F2Y, FRX, - DIM=3	components of the forces	
F3Z	z-component of IM force	
G - DIM=3	three force cases	
A, DA, YI, ZI, DX, R1, R2, DR1, DR2, X, XL	A, dA, Iy, Iz, dx r_1, r_2, dr_1, dr_2, x, x'	input data for cylinder, bone
W1, W2, W3, W4, W5, W6, W7 W45, W21	the terms computed in calculations of dA/dx	I, III
ANS1	$dA/dx = \frac{W7 \cdot W4}{W6+W5}$	I, III
CYL, EXPTL	$DA/DX = \Delta A/\Delta x$	Cylinder, Bone
W8, W9	add'l terms used in calculation of γ_{yx}	
GYX	$\gamma_{yx} = \frac{W8}{(W3-W2-W9)}$	I, III
M, M1 DIM=6	distances; $m=c+{}^{d}/_{2}$, m1=c+d	
P1, P2, P7, Q1, Q2, Q3 P6, P9	terms computed in calculation of dA/dx	II, cylinder
ANS4	$dA/dx = \frac{(Q3+Q2 \cdot P2) \cdot P7}{W6+P9}$	
P3, Q4, Q5, Q6, Q7, Q8 Q9, Q10	terms computed in calculation of dA/dx	II, Bone
ANS5	$\frac{dA}{dx} = \frac{(Q7-Q6) \cdot Q4}{(Q9+Q10)}$	

TABLE B

VARIABLES IN SHEAR PROGRAM

(Regions I, II - Cylinder; Regions II, III=1 - Bone)

Unless explicitly specified, i.e., DIM=, the dimension of all variables listed below is (6.11). The six refers to the specimen and the eleven refers to the sections. Terms, intermediate in the calculation of dA/dx which are of interest are expanded at the end of this Table.

SPEC(6)	section identification number
C, DL, D, B	distances; c, L, d, b
W, F2Y, FRX DIM=3	components of the forces
F3Z	z-component of IM force
G DIM=3	three force cases
A, DR, ZI, YI, R1, R2, X, XL	A, dr, Iz, Iy, r_1, r_2, x, x' input data for cylinder bone
VO, MBO	shear force, bending moment I, III
SAO, SBO, STO TAV	σ_{axial}, $\sigma_{bending}$, σ_{total} axial, bending total stress. τ_{avg}=VO/A
G1, G2, G3, G4, G5, G8, G9	terms computed in calculation of τ_{max}, τ_{r_1} I, III
TMX	τ_{max} = TAV·G5/G9 I,III
TR1	τ_{r_1} = TAV·G8/G9 I,III
M, M1 DIM=6	distances, M=c+d/2, M1=c+d
M2	$M2 = \frac{1}{2}\frac{(x-c)^2}{d}$ II
MBZ	Mz = MBO Bone/Cylinder
MBY2	My = P3Z(x-M-M2) Bone/Cylinder
VZ2	$Vz = F3Z(1-\frac{x-c}{d})$

Table B (continued)

SA2, SB2, ST2	σ_a axial, σ_b bending, σ_t total stress Bone/Cylinder
TZAV	τ_{avg} = VZ2/A Bone/Cylinder
TZMX	τ_{max} = TZAV·G5/G9 Bone/Cylinder
TZR1	τ_{r_1} = TZAV·G8/G9 Bone/Cylinder
G6, G7	terms computed in calculation of shear using, using Iz, Iy
TXYX	$\tau_{xy_{max}}$ = VO·G5/G6 I,III
TXYR	$\tau_{xy_{r_1}}$ = VO·G8/G6 I,III
TXZX	$\tau_{xz_{max}}$ = VZ2·G5/G7 II
TXZR	$\tau_{xz_{r_1}}$ = VZ2·G8/G7 II
TMAX	$\tau_{max} = \sqrt{\tau_{xy_{max}}^2 + \tau_{xz_{max}}^2}$
TMAR	$\tau_{r_{1_{max}}} = \sqrt{\tau_{xy_{r_1}}^2 + \tau_{xz_{r_1}}^2}$
K1, K2, KM1, KM2	terms computed in calculation of c(x) I, III, II
CX1, CX2, CM1, CM2	$C_{I,III}$ = K1±K2 or, C_{II}=KM1±KM2
CY1, CZ1, CYIM, CZ1M	terms computed in calculation of c(x) I, III, II using Iz, Iy
Z1, Z2	section moduli I, III using $\frac{Mb}{\sigma}$
ZZ2, ZY2	section moduli in II, bone, $I_z \neq I_y$ using $\frac{I}{c}$

```
      REAL*8 K1,K2,KM1,KM2
      REAL*8 SPEC,M,M1,MB0,MBY2,MBZ
      DIMENSION FM(66),AXI(15),ARM(12),YES(12),CAN(12),E(6,11)
      DIMENSION V0(3),MB0(6,11),SA0(6,11),SB0(6,11),ST0(6,11),TAV(6,11)
      DIMENSION G9(6,11)
      DIMENSION K1(6,11),K2(6,11),CX1(6,11),CX2(6,11),KM2(6,11
     C)
      DIMENSION CYI(6,11),CZI(6,11),CYIM(6,11),CZIM(6,11)
      DIMENSION Z1(6,11),Z2(6,11),ZZ2(6,11),ZY2(6,11),KM1(6,11
     C)
      DIMENSION CM1(6,11),CM2(6,11)
      DIMENSION SPEC(6),M(6),M1(6),C(6),DL(6),D(6),B(6),W(3),G
     C(3),F2Y(3)
      DIMENSION A(6,11),DR(6,11),ZI(6,11),YI(6,11)
      DIMENSION X(6,11),R1(6,11),R2(6,11),M2(6,11),FRX(3),XL(6
     C,11)
      DIMENSION G1(6,11),G2(6,11),G3(6,11),G4(6,11),G5(6,11),G
     C8(6,11)
      DIMENSION MBZ(6,11),VZ2(6,11),SA2(6,11),SB2(6,11),G6(6,1
     C1)
      DIMENSION TMX(6,11),TR1(6,11),ST2(6,11),MBY2(6,11),G7(6,
     C11)
      DIMENSION TZAV(6,11),TZMX(6,11),TZR1(6,11),TXYX(6,11),TX
     CZX(6,11)
      DIMENSION TXZR(6,11),TXYR(6,11),TMAX(6,11),TMAR(6,11)
C
C
      DATA W(1),W(2),W(3)/11.73,15.0,15.0/
      DATA F2Y(1),F2Y(2),F2Y(3)/1.405,3.48,3.48/
      DATA FRX(1),FRX(2),FRX(3)/17.87,44.47,116.07/
      F3Z=100.01
      G(1)=(W(1)-F2Y(1))/FRX(1)
      G(2)=(W(2)-F2Y(2))/FRX(2)
      G(3)=F3Z/FRX(3)
      CALL PLOTS(IDUM,IDUM,04)
C
```

```
C
C CALCULATION OF AXIAL AND BENDING AND SHEAR STRESS
C
C
C         C    Y    L    I    N    D    E    R
C
C
      READ(5,5000) MOST
 5000 FORMAT(I2)
      READ(5,5010) (FM(I),I=1,MOST)
 5010 FORMAT( 6F12.4)
      DO 1700 I=5,15
      J=I-4
 1700 AXI(J)=I
      WRITE(6,6225)
 6225 FORMAT(/,1X,'C',3X,'Y',3X,'L',3X,'I',3X,'N',3X,'D',3X,'E
     C',3X,'R')
      DO 11 I=1,6
      READ(5,505) SPEC(I),DL(I),C(I),D(I),B(I)
 505  FORMAT(A8,4F6.2)
  11  CONTINUE
      WRITE(6,6230)
 6230 FORMAT(/,1X,'A',3X,'C',3X,'T',3X,'U',3X,'A',3X,'L')
      READ(5,500) ((A(I,J),J=1,11),I=1,6),((DR(I,J),J=1,11),I=
     C1,6),
     C((ZI(I,J),J=1,11),I=1,6),((YI(I,J),J=1,11),I=1,6)
      READ(5,500) ((P1(I,J),J=1,11),I=1,6),((R2(I,J),J=1,11),I
     C=1,6),
     C((X(I,J),J=1,11),I=1,6)
 500  FORMAT(11F6.4,14X)
      DO 99 K=1,3
      DO 100 I=1,6
      WRITE(6,601) SPEC(I)
 601  FORMAT(10X,'******',2X,A8,2X,'******',/)
      WRITE(6,6203) G(K)
 6203 FORMAT(/,' GAMMA YX=', F6.2)
```

```
      WRITE(6,600)  (A(I,J),J=1,11),(ZI(I,J),J=1,11),(YI(I,J),J
     C=1,11)
 600  FORMAT(/,' DATA CHECK',/,3(11F6.3,/),/)
      WRITE(6,610)  (R1(I,J),J=1,11),(R2(I,J),J=1,11),(DR(I,J),
     CJ=1,11)
 610  FORMAT(/,' DATA CHECK',/,4(11F6.3,/),/)
C
C     ****** NO MEMBRANE ******   V0,MB0
C
      WRITE(6,6201)
 6201 FORMAT(/,' STRESS - NO MEMBRANE - SA0,SB0',/)
      DO 120 J=1,11
      XL(I,J)=X(I,J)-DL(I)
      V0(K)=F2Y(K)-W(K)
      MB0(I,J)=-V0(K)*XL(I,J)
      IF(K.EQ.3) GO TO 350
C
C AXIAL AND BENDING STRESS
C
      SA0(I,J)=FRX(K)/A(I,J)
      SB0(I,J)=MB0(I,J)*R2(I,J)/ZI(I,J)
      ST0(I,J)=SA0(I,J)+SB0(I,J)
      IF((SA0(I,J).GT.0.).AND.(SB0(I,J).GT.0.))GO TO 300
      IF((SA0(I,J).LT.0.).AND.(SB0(I,J).LT.0.))GO TO 300
      WRITE(6,620) SA0(I,J),SB0(I,J),ST0(I,J)
 620  FORMAT(/,' THE STRESS IS NOT A MAX :',3F10.3,/)
      GO TO 120
 300  WRITE(6,625) SA0(I,J),SB0(I,J),ST0(I,J),SPEC(I),J
 625  FORMAT(/,' THE STRESS IS A MAX :',3F10.3,'FOR',A8,I3,/)
 120  CONTINUE
      WRITE(6,616) (MB0(I,J),J=1,11),V0(K)
 616  FORMAT(/,' BENDING MOMENT- NO MEMB  - SHEAR',/,1X,12F10.
     C3)
C
C  SHEAR STRESS
C
```

```
      DO 130 J=1,11
      TAV(I,J)=V0(K)/A(I,J)
      G1(I,J)=(R1(I,J)**2.+R2(I,J)**2.)
      G2(I,J)=R2(I,J)**3.-R1(I,J)**3.
      G3(I,J)=(R2(I,J)**2.-R1(I,J)**2.)**1.5
      G4(I,J)=8./(3.*G1(I,J))
      G5(I,J)=G4(I,J)*G2(I,J)
      G8(I,J)=G4(I,J)*G3(I,J)
      G9(I,J)=2.*DR(I,J)
      TMX(I,J)=TAV(I,J)*G5(I,J)/G9(I,J)
      TR1(I,J)=TAV(I,J)*G8(I,J)/G9(I,J)
 130  CONTINUE
      WRITE(6,630)  (G1(I,J),G2(I,J),G3(I,J),G4(I,J),G5(I,J),G8
     C(I,J),
     1TAV(I,J),TMX(I,J),TR1(I,J),J=1,11)
 630  FORMAT(/,' THE COMPONENTS OF THE SHEAR--NO MEMBRANE:
     1    AVG,MX,R1:',//,11(9F10.3,/1X),/)
C
C     ****** MEMBRANE ****** VZ2,MBZ,MBY2
C
      WRITE(6,6200)
 6200 FORMAT(/,' STRESS - MEMBRANE - SA2,SB2',/)
 350  DO 140 J=1,11
      M(I)=C(I)+D(I)/2.
      M1(I)=C(I)+D(I)
      M2(I,J)=(.5*(X(I,J)-C(I))**2.)/D(I)
      MBZ(I,J)=MB0(I,J)
      MBY2(I,J)=F3Z*(X(I,J)-M(I)-M2(I,J))
      VZ2(I,J)=F3Z*(1-(X(I,J)-C(I))/D(I))
C
C AXIAL AND BENDING STRESS
C
      SA2(I,J)=FRX(K)/A(I,J)
      SB2(I,J)=MBZ(I,J)*R2(I,J)/ZI(I,J)-MBY2(I,J)*R2(I,J)/YI(I
     C,J)
      ST2(I,J)=SA2(I,J)+SB2(I,J)
```

```
      IF((SA2(I,J).GT.0.).AND.(SB2(I,J).GT.0.))GO TO 333
      IF((SA2(I,J).LT.0.).AND.(SB2(I,J).LT.0.))GO TO 333
      WRITE(6,621) SA2(I,J),SB2(I,J),ST2(I,J)
 621  FORMAT(/,' THE STRESS IS NOT A MAX :',3F10.3,/)
      GO TO 140
 333  WRITE(6,626) SA2(I,J),SB2(I,J),ST2(I,J),SPEC(I),J
 626  FORMAT(/,' THE STRESS IS A MAX :',3F10.3,'FOR',A8,I3,/)
 140  CONTINUE
      WRITE(6,629) (MBY2(I,J),J=1,11),(VZ2(I,J),J=1,11)
 629  FORMAT(/,' BENDG MOMT, SHEAR-FORCE - MEMB',/,2(1X,11F10.
     C3,/,1X))
C
C SHEAR STRESS
C
C
C   FOR VY= V0 = SHEAR FORCE: TAV,TMX,TR1 ARE THE SAME
C
C  THE FOLLOWING CALCULATION IS FOR VZ2 =SHEAR FORCE
C
C
      WRITE(6,6202)
 6202 FORMAT(/,' SHEAR FORCE = VZ2,VY=V0',/)
      DO 150 J=1,11
      P1=G5(I,J)/G9(I,J)
      P2=G8(I,J)/G9(I,J)
      WRITE (6,96) P1,P2
  96  FORMAT(/,'P1,P2:', 2F10.3)
      TZAV(I,J)=VZ2(I,J)/A(I,J)
      TZMX(I,J)=TZAV(I,J)*G5(I,J)/G9(I,J)
      TZR1(I,J)=TZAV(I,J)*G8(I,J)/G9(I,J)
 150  CONTINUE
      WRITE(6,628) (TZAV(I,J),J=1,11),(TZMX(I,J),J=1,11),(TZR1(
     CI,J),
     1J=1,11)
 628  FORMAT(/,' THE COMPONENTS OF SHEAR -MEMBRANE: TZAV,TZMX,TZR1',
     1//,1X,3(11F10.3,/,1X))
```

```
C
C
C  COMPARISON OF THE SHEAR WITH I  VS  A  :
C
C  CHANGES OCCUR FOR  MEMBRANE AND ACTUAL BONE CASES
C     TXY     VS    TXZ
C
C
      WRITE(6,640)
 640  FORMAT(/,1X,'TEST OF SQRT FACTORS: TXY-TXZ MAX; TXY-TXZ
     C R1')
      DO 166 J=1,11
      G6(I,J)=ZI(I,J)*2.*DR(I,J)
      G7(I,J)=YI(I,J)*2.*DR(I,J)
      TXYX(I,J)=V0(K)*G5(I,J)/G6(I,J)
      TXYR(I,J)=V0(K)*G8(I,J)/G6(I,J)
      TXZX(I,J)=VZ2(I,J)*G5(I,J)/G7(I,J)
      TXZR(I,J)=VZ2(I,J)*G8(I,J)/G7(I,J)
      WRITE(6,642)TXYX(I,J),TXZX(I,J),TXYR(I,J),TXZR(I,J)
 642  FORMAT(/,1X,4F10.3)
      TMAX(I,J)=SQRT(TXYX(I,J)**2+TXZX(I,J)**2)
      TMAR(I,J)=SQRT(TXYR(I,J)**2+TXZR(I,J)**2)
 166  CONTINUE
      WRITE(6,678)
 678  FORMAT(/,1X,' SHEAR  W/ I  VS. SHEAR W/ A : G6,G7,TXY,TX
     CZ,TYR,TZR,
     1TMAX,TMAR:',/)
      DO 177 J=1,11
      WRITE(6,677) G6(I,J),G7(I,J),TXYX(I,J),TXZX(I,J),TXYR(I,
     CJ),TXZR(I,
     1J),TMAX(I,J),TMAR(I,J)
 677  FORMAT(/,11(1X,8F10.3))
 177  CONTINUE
 100  CONTINUE
      DO 1825  I=1,6
      DO 1825  J=1,11
```

```
      E(I,J)=SA2(I,J)
 1825 CONTINUE
      DO 1703 I=1,6,2
      DO 1703 J=1,11
      L=I
      E(I,J)=E(I,J)/FM(L)
      IF(I.EQ.1) ARM(J)=E(I,J)
      IF(I.EQ.1) GO TO  1703
      IF(I.EQ.3) YES(J)=E(I,J)
      IF(I.EQ.3) GO TO  1703
      CAN(J)=E(I,J)
 1703 CONTINUE
      CALL PLOT(13.0,3.0,-3)
      CALL PICTUR(4.0,4.0,'   SECTION NUMBER  ',19,
     1'AXIAL STRESS MEMB L',
     C19,AXI,ARM,11,.1,1,AXI,YES,11,.1,0,AXI,CAN,11,.1,2)
      DO 1702 I=2,6,2
      DO 1702 J=1,11
      L=I
      E(I,J)=E(I,J)/FM(L)
      IF(I.EQ.2) ARM(J)=E(I,J)
      IF(I.EQ.2) GO TO  1702
      IF(I.EQ.4) YES(J)=E(I,J)
      IF(I.EQ.4) GO TO  1702
      CAN(J)=E(I,J)
 1702 CONTINUE
      CALL PLOT(13.0,0.0,-3)
      CALL PICTUR(4.0,4.0,'   SECTION NUMBER  ',19,
     1'AXIAL STRESS MEMB R',
     C19,AXI,ARM,11,.1,1,AXI,YES,11,.1,0,AXI,CAN,11,.1,2)
      DO 1800 I=1,6
      DO 1800 J=1,11
      E(I,J)=SB2(I,J)
 1800 CONTINUE
      DO 1705 I=1,6,2
      DO 1705 J=1,11
```

```
      L=I+6
      E(I,J)=E(I,J)/FM(L)
      IF(I.EQ.1) ARM(J)=E(I,J)
      IF(I.EQ.1) GO TO  1705
      IF(I.EQ.3) YES(J)=E(I,J)
      IF(I.EQ.3) GO TO  1705
      CAN(J)=E(I,J)
 1705 CONTINUE
      CALL PLOT(13.0,0.0,-3)
      CALL PICTUR(4.0,4.0,'   SECTION NUMBER  ',19,
     1'BEND  STRESS MEMB L',
     C19,AXI,ARM,11,.1,1,AXI,YES,11,.1,0,AXI,CAN,11,.1,2)
      DO 1706 I=2,6,2
      DO 1706 J=1,11
      L=I+6
      E(I,J)=E(I,J)/FM(L)
      IF(I.EQ.2) ARM(J)=E(I,J)
      IF(I.EQ.2) GO TO  1706
      IF(I.EQ.4) YES(J)=E(I,J)
      IF(I.EQ.4) GO TO  1706
      CAN(J)=E(I,J)
 1706 CONTINUE
      CALL PLOT(13.0,0.0,-3)
      CALL PICTUR(4.0,4.0,'   SECTION NUMBER  ',19,
     1'BEND  STRESS MEMB R',
     C19,AXI,ARM,11,.1,1,AXI,YES,11,.1,0,AXI,CAN,11,.1,2)
      DO 1805 I=1,6
      DO 1805 J=1,11
      E(I,J)=ST2(I,J)
 1805 CONTINUE
      DO 1709 I=1,6,2
      DO 1709 J=1,11
      L=I+12
      E(I,J)=E(I,J)/FM(L)
      IF(I.EQ.1) ARM(J)=E(I,J)
      IF(I.EQ.1) GO TO  1709
```

```
      IF(I.EQ.3) YES(J)=E(I,J)
      IF(I.EQ.3) GO TO  1709
      CAN(J)=E(I,J)
 1709 CONTINUE
      CALL PLOT(13.0,0.0,-3)
      CALL PICTUR(4.0,4.0,'   SECTION NUMBER  ',19,
     1'TOTAL STRESS MEMB L',
     C19,AXI,ARM,11,.1,1,AXI,YES,11,.1,0,AXI,CAN,11,.1,2)
      DO 1710 I=2,6,2
      DO 1710 J=1,11
      L=I+12
      E(I,J)=E(I,J)/FM(L)
      IF(I.EQ.2) ARM(J)=E(I,J)
      IF(I.EQ.2) GO TO  1710
      IF(I.EQ.4) YES(J)=E(I,J)
      IF(I.EQ.4) GO TO  1710
      CAN(J)=E(I,J)
 1710 CONTINUE
      CALL PLOT(13.0,0.0,-3)
      CALL PICTUR(4.0,4.0,'   SECTION NUMBER  ',19,
     1'TOTAL STRESS MEMB R',
     C19,AXI,ARM,11,.1,1,AXI,YES,11,.1,0,AXI,CAN,11,.1,2)
      DO 1810 I=1,6
      DC 1810 J=1,11
      E(I,J)=DR(I,J)
 1810 CONTINUE
      DO 1715 I=1,6,2
      DO 1715 J=1,11
      L=I+18
      E(I,J)=E(I,J)/FM(L)
      IF(I.EQ.1) ARM(J)=E(I,J)
      IF(I.EQ.1) GO TO  1715
      IF(I.EQ.3) YES(J)=E(I,J)
      IF(I.EQ.3) GO TO  1715
      CAN(J)=E(I,J)
 1715 CONTINUE
```

```
      CALL PLOT(13.0,0.0,-3)
      CALL PICTUR(4.0,4.0,'   SECTION NUMBER  ',19,
     1'BONE THICKNESS  (L)',
     C19,AXI,ARM,11,.1,1,AXI,YES,11,.1,0,AXI,CAN,11,.1,2)
      DO 1716 I=2,6,2
      DO 1716 J=1,11
      L=I+18
      E(I,J)=E(I,J)/FM(L)
      IF(I.EQ.2) ARM(J)=E(I,J)
      IF(I.EQ.2) GO TO  1716
      IF(I.EQ.4) YES(J)=E(I,J)
      IF(I.EQ.4) GO TO  1716
      CAN(J)=E(I,J)
 1716 CONTINUE
      CALL PLOT(13.0,0.0,-3)
      CALL PICTUR(4.0,4.0,'   SECTION NUMBER  ',19,
     1'BONE THICKNESS  (R)',
     C19,AXI,ARM,11,.1,1,AXI,YES,11,.1,0,AXI,CAN,11,.1,2)
      DO 1815 I=1,6
      DO 1815 J=1,11
      E(I,J)=TZAV(I,J)
 1815 CONTINUE
      DO 1719 I=1,6,2
      DO 1719 J=1,11
      L=I+24
      E(I,J)=E(I,J)/FM(L)
      IF(I.EQ.1) ARM(J)=E(I,J)
      IF(I.EQ.1) GO TO  1719
      IF(I.EQ.3) YES(J)=E(I,J)
      IF(I.EQ.3) GO TO  1719
      CAN(J)=E(I,J)
 1719 CONTINUE
      CALL PLOT(13.0,0.0,-3)
      CALL PICTUR(4.0,4.0,'   SECTION NUMBER  ',19,
     1'SHEAR STRESS AV (L)',
     C19,AXI,ARM,11,.1,1,AXI,YES,11,.1,0,AXI,CAN,11,.1,2)
```

```
      DO 1720 I=2,6,2
      DO 1720 J=1,11
      L=I+24
      E(I,J)=E(I,J)/FM(L)
      IF(I.EQ.2) ARM(J)=E(I,J)
      IF(I.EQ.2) GO TO  1720
      IF(I.EQ.4) YES(J)=E(I,J)
      IF(I.EQ.4) GO TO  1720
      CAN(J)=E(I,J)
 1720 CONTINUE
      CALL PLOT(13.0,0.0,-3)
      CALL PICTUR(4.0,4.0,'   SECTION NUMBER  ',19,
     1'SHEAR STRESS AV (R)',
     C19,AXI,ARM,11,.1,1,AXI,YES,11,.1,0,AXI,CAN,11,.1,2)
      DO 1820 I=1,6
      DO 1820 J=1,11
      E(I,J)=TZMX(I,J)
 1820 CONTINUE
      DO 1725 I=1,6,2
      DO 1725 J=1,11
      L=I+30
      E(I,J)=E(I,J)/FM(L)
      IF(I.EQ.1) ARM(J)=E(I,J)
      IF(I.EQ.1) GO TO  1725
      IF(I.EQ.3) YES(J)=E(I,J)
      IF(I.EQ.3) GO TO  1725
      CAN(J)=E(I,J)
 1725 CONTINUE
      CALL PLOT(13.0,0.0,-3)
      CALL PICTUR(4.0,4.0,'   SECTION NUMBER  ',19,
     1'SHEAR STRESS MAX(L)',
     C19,AXI,ARM,11,.1,1,AXI,YES,11,.1,0,AXI,CAN,11,.1,2)
      DO 1726 I=2,6,2
      DO 1726 J=1,11
      L=I+30
      E(I,J)=E(I,J)/FM(L)
```

```
      IF(I.EQ.2) ARM(J)=E(I,J)
      IF(I.EQ.2) GO TO  1726
      IF(I.EQ.4) YES(J)=E(I,J)
      IF(I.EQ.4) GO TO  1726
      CAN(J)=E(I,J)
 1726 CONTINUE
      CALL PLOT(13.0,0.0,-3)
      CALL PICTUR(4.0,4.0,'   SECTION NUMBER  ',19,
     1'SHEAR STRESS MAX(R)',
     C19,AXI,ARM,11,.1,1,AXI,YES,11,.1,0,AXI,CAN,11,.1,2)
C
C ALL CALCULATIONS FOR S,MB,T HAVE BEEN DONE
C
C
C     ******C(X) NO MEMBRANE******
C
C C(X) USING CYL APPROX. VIA I-SQRT
C
      DO 111 I=1,6
      WRITE(6,679)
 679  FORMAT(/,'C(X) FOR SQRT APPROX--NO MEMBRANE--FACTORS ARE:K1,K2,C
     C1(X),C2(X):')
      DO 170 J=1,11
      K1(I,J)=2.*MB0(I,J)/(SB0(I,J)*A(I,J))
C
      E1=(2.*K1(I,J))**2
      E2=(4.*R1(I,J))**2
      F=E1-E2
      IF(F.GE.0.)GO TO 366
      E3=ABS(F)
      WRITE(6,639)E1,E2,E3
 639  FORMAT(2X,'***',3F10.3)
      K2(I,J)=.5*SQRT(E3)
      GO TO 368
 366  K2(I,J)=.5*SQRT(F)
 368  BETA=0
```

```
      CX1(I,J)=K1(I,J)+K2(I,J)
      CX2(I,J)=K1(I,J)-K2(I,J)
      WRITE(6,680) K1(I,J),K2(I,J),CX1(I,J),CX2(I,J)
 680  FORMAT(/,1X,4F10.3)
 170  CONTINUE
C
C  C(X) USING STRESS/MOMENT APPROX.--IY.NE.IZ
C
      WRITE(6,683)
 683  FORMAT(/,1X,'COMPARISON OF C(X):',/,1X,'CYI(X)',4X,'CZ
     CI(X)',4X,
     C'CX1(X)',4X,'CX2(X)',/)
      DO 172 J=1,11
      CYI(I,J)=SB0(I,J)*YI(I,J)/MB0(I,J)
      CZI(I,J)=SB0(I,J)*ZI(I,J)/MB0(I,J)
      WRITE(6,684)CYI(I,J),CZI(I,J),CX1(I,J),CX2(I,J)
 684  FORMAT(/,1X,4F10.3)
 172  CONTINUE
C      ******C(X)      MEMBRANE******
C
      WRITE(6,686)
  686  FORMAT(/,1X,'C(X)-SQRT APPROX-MEMB-ANE:KM1,KM2,CM1,CM2'
     C,/)
      DO 174 J=1,11
      KM1(I,J)=2.*MBY2(I,J)/(SB2(I,J)*A(I,J))
      F1=(2.*KM1(I,J))**2
      F2=4.*B1(I,J)**2
      F=F1-F2
      IF(F.GE.0.)GO TO 399
      F3=ABS(F)
      WRITE(6,637)F1,F2,F3
 637  FORMAT(2X,'***',3F10.3)
      KM2(I,J)=.5*SQRT(F3)
      GO TO 398
 399  KM2(I,J)=.5*SQRT(F)
 398  BETA=0.0
```

```
      CM1(I,J)=KM1(I,J)+KM2(I,J)
      CM2(I,J)=KM1(I,J)-KM2(I,J)
      WRITE(6,685)KM1(I,J),KM2(I,J),CM1(I,J),CM2(I,J)
 685  FORMAT(/,1X,4F10.3)
 174  CONTINUE
      WRITE(6,687)
 687  FORMAT(/,'COMPARISON OF C(X)-MEMBRANE:',/,1X,'CYI(X)',4X
     C,
     C'CZI(X)',4X,'CX1(X)',4X,'CX2(X)',/)
      DO 176 J=1,11
      IF(MBY2(I,J).LE.0.000001) GO TO 33
      CYIM(I,J)=SB2(I,J)*YI(I,J)/MBY2(I,J)
      CZIM(I,J)=SB2(I,J)*ZI(I,J)/MBY2(I,J)
      GO TO 38
   33  CYIM(I,J)=999.9
      CZIM(I,J)=999.9
  38  WRITE(6,688)CYIM(I,J),CZIM(I,J),CM1(I,J),CM2(I,J)
 688  FORMAT(/,1X,4F10.3)
 176  CONTINUE
C
C SECTION MODULUS USING 2 METHODS:  MB/SB AND I/C
C
      WRITE(6,689)
  689 FORMAT(/,1X,'THE SECTION MODULUS--NO MEMBRANE/MEMBRANE--
     C2 METHODS:  MB-SB, AND I-C:  Z1,Z2,ZZ2,ZY2')
      DO 178 J=1,11
      Z1(I,J)=MB0(I,J)/SB0(I,J)
      Z2(I,J)=MBY2(I,J)/SB2(I,J)
      IF(ABS(CX1(I,J)).GT.ABS(CX2(I,J)))GO TO 360
      ZZ2(I,J)=ZI(I,J)/CX2(I,J)
      ZY2(I,J)=YI(I,J)/CX2(I,J)
      GO TO 178
 360  ZZ2(I,J)=ZI(I,J)/CX1(I,J)
      ZY2(I,J)=YI(I,J)/CX1(I,J)
 178  CONTINUE
      DO 179 J=1,11
```

```
      WRITE(6,692)Z1(I,J),Z2(I,J),ZZ2(I,J),ZY2(I,J)
692   FORMAT(/,1X,2F10.3,5X,2F10.3)
179   CONTINUE
111   CONTINUE
      DO 1830 I=1,6
      DO 1830 J=1,11
      E(I,J)=ZZ2(I,J)
1830  CONTINUE
      DO 1729 I=1,6,2
      DO 1729 J=1,11
      L=I+36
      E(I,J)=E(I,J)/FM(L)
      IF(I.EQ.1) ARM(J)=E(I,J)
      IF(I.EQ.1) GO TO  1729
      IF(I.EQ.3) YES(J)=E(I,J)
      IF(I.EQ.3) GO TO  1729
      CAN(J)=E(I,J)
1729  CONTINUE
      CALL PLOT(13.0,0.0,-3)
      CALL PICTUR(4.0,4.0,'   SECTION NUMBER  ',19,
     1'SECTION MODULUS IZ ',
     C19,AXI,ARM,11,.1,1,AXI,YES,11,.1,0,AXI,CAN,11,.1,2)
      DO 1730 I=2,6,2
      DO 1730 J=1,11
      L=I+36
      E(I,J)=E(I,J)/FM(L)
      IF(I.EQ.2) ARM(J)=E(I,J)
      IF(I.EQ.2) GO TO  1730
      IF(I.EQ.4) YES(J)=E(I,J)
      IF(I.EQ.4) GO TO  1730
      CAN(J)=E(I,J)
1730  CONTINUE
      CALL PLOT(13.0,0.0,-3)
      CALL PICTUR(4.0,4.0,'   SECTION NUMBER  ',19,
     1'SECTION MODULUS IZ ',
     C19,AXI,ARM,11,.1,1,AXI,YES,11,.1,0,AXI,CAN,11,.1,2)
```

```
      DO 1835 I=1,6
      DO 1835 J=1,11
      E(I,J)=ZY2(I,J)
 1835 CONTINUE
      DO 1735 I=1,6,2
      DO 1735 J=1,11
      L=I+42
      E(I,J)=E(I,J)/FM(L)
      IF(I.EQ.1) ARM(J)=E(I,J)
      IF(I.EQ.1) GO TO  1735
      IF(I.EQ.3) YES(J)=E(I,J)
      IF(I.EQ.3) GO TO  1735
      CAN(J)=E(I,J)
 1735 CONTINUE
      CALL PLOT(13.0,0.0,-3)
      CALL PICTUR(4.0,4.0,'   SECTION NUMBER  ',19,
     1'SECTION MODULUS IY ',
     C19,AXI,ARM,11,.1,1,AXI,YES,11,.1,0,AXI,CAN,11,.1,2)
      DO 1736 I=2,6,2
      DO 1736 J=1,11
      L=I+42
      E(I,J)=E(I,J)/FM(L)
      IF(I.EQ.2) ARM(J)=E(I,J)
      IF(I.EQ.2) GO TO  1736
      IF(I.EQ.4) YES(J)=E(I,J)
      IF(I.EQ.4) GO TO  1736
      CAN(J)=E(I,J)
 1736 CONTINUE
      CALL PLOT(13.0,0.0,-3)
      CALL PICTUR(4.0,4.0,'   SECTION NUMBER  ',19,
     1'SECTION MODULUS IY ',
     C19,AXI,ARM,11,.1,1,AXI,YES,11,.1,0,AXI,CAN,11,.1,2)
      DO 1840 I=1,6
      DO 1840 J=1,11
      E(I,J)=TMAX(I,J)
 1840 CONTINUE
```

```
      DO 1739 I=1,6,2
      DO 1739 J=1,11
      L=I+48
      E(I,J)=E(I,J)/FM(L)
      IF(I.EQ.1) ARM(J)=E(I,J)
      IF(I.EQ.1) GO TO  1739
      IF(I.EQ.3) YES(J)=E(I,J)
      IF(I.EQ.3) GO TO  1739
      CAN(J)=E(I,J)
 1739 CONTINUE
      CALL PLOT(13.0,0.0,-3)
      CALL PICTUR(4.0,4.0,'   SECTION NUMBER  ',19,
     1'SHEAR-TXY,TXZ-MAX L',
     C19,AXI,ARM,11,.1,1,AXI,YES,11,.1,0,AXI,CAN,11,.1,2)
      DO 1740 I=2,6,2
      DO 1740 J=1,11
      L=I+48
      E(I,J)=E(I,J)/FM(L)
      IF(I.EQ.2) ARM(J)=E(I,J)
      IF(I.EQ.2) GO TO  1740
      IF(I.EQ.4) YES(J)=E(I,J)
      IF(I.EQ.4) GO TO  1740
      CAN(J)=E(I,J)
 1740 CONTINUE
      CALL PLOT(13.0,0.0,-3)
      CALL PICTUR(4.0,4.0,'   SECTION NUMBER  ',19,
     1'SHEAR-TXY,TXZ-MAX R',
     C19,AXI,ARM,11,.1,1,AXI,YES,11,.1,0,AXI,CAN,11,.1,2)
      DO 1806 I=1,6
      DO 1806 J=1,11
      E(I,J)=TXYX(I,J)
 1806 CONTINUE
      DO 1713 I=1,6,2
      DO 1713 J=1,11
      L=I+54
      E(I,J)=E(I,J)/FM(I)
```

```
      IF(I.EQ.1) ARM(J)=E(I,J)
      IF(I.EQ.1) GO TO  1713
      IF(I.EQ.3) YES(J)=E(I,J)
      IF(I.EQ.3) GO TO  1713
      CAN(J)=E(I,J)
1713  CONTINUE
      CALL PLOT(13.0,0.0,-3)
      CALL PICTUR(4.0,4.0,'   SECTION NUMBER  ',19,
     1'SHEAR STRESS TXY  L',
     C19,AXI,ARM,11,.1,1,AXI,YES,11,.1,0,AXI,CAN,11,.1,2)
      DO 1712 I=2,6,2
      DO 1712 J=1,11
      L=I+54
      E(I,J)=E(I,J)/FM(L)
      IF(I.EQ.2) ARM(J)=E(I,J)
      IF(I.EQ.2) GO TO  1712
      IF(I.EQ.4) YES(J)=E(I,J)
      IF(I.EQ.4) GO TO  1712
      CAN(J)=E(I,J)
1712  CONTINUE
      CALL PLOT(13.0,0.0,-3)
      CALL PICTUR(4.0,4.0,'   SECTION NUMBER  ',19,
     1'SHEAR STRESS TXY  R',
     C19,AXI,ARM,11,.1,1,AXI,YES,11,.1,0,AXI,CAN,11,.1,2)
      DO 1821 I=1,6
      DO 1821 J=1,11
      E(I,J)=TXZX(I,J)
1821  CONTINUE
      DO 1717 I=1,6,2
      DO 1717 J=1,11
      L=I+60
      E(I,J)=E(I,J)/FM(L)
      IF(I.EQ.1) ARM(J)=E(I,J)
      IF(I.EQ.1) GO TO  1717
      IF(I.EQ.3) YES(J)=E(I,J)
      IF(I.EQ.3) GO TO  1717
```

```
      CAN(J)=E(I,J)
1717  CONTINUE
      CALL PLOT(13.0,0.0,-3)
      CALL PICTUR(4.0,4.0,'   SECTION NUMBER  ',19,
     1'SHEAR STRESS TXZ  L',
     C19,AXI,ARM,11,.1,1,AXI,YES,11,.1,0,AXI,CAN,11,.1,2)
      DO 1718 I=2,6,2
      DO 1718 J=1,11
      L=I+60
      E(I,J)=E(I,J)/FM(L)
      IF(I.EQ.2) ARM(J)=E(I,J)
      IF(I.EQ.2) GO TO  1718
      IF(I.EQ.4) YES(J)=E(I,J)
      IF(I.EQ.4) GO TO  1718
      CAN(J)=E(I,J)
1718  CONTINUE
      CALL PLOT(13.0,0.0,-3)
      CALL PICTUR(4.0,4.0,'   SECTION NUMBER  ',19,
     1'SHEAR STRESS TXZ  R',
     C19,AXI,ARM,11,.1,1,AXI,YES,11,.1,0,AXI,CAN,11,.1,2)
 99   CONTINUE
      WRITE(6,6000)
 6000 FORMAT(//,' THE   END  ',//)
      CALL ENDPLT(16.0,5.0,999)
      STOP
      END
```

```
      REAL*8 SPEC,M,M1
      DIMENSION FM(66),AXI(15),ARM(12),YES(12),CAN(12),E(6,11)
      DIMENSION SPEC(6),M(6),M1(6),C(6),DL(6),D(6),B(6),W(3),G
     C(3),F2Y(3)
      DIMENSION A(6,11),DA(6,11),ZI(6,11),YI(6,11),DX(6,11),XL
     C(6,11)
      DIMENSION X(6,11),R1(6,11),R2(6,11),Q1(6,11),Q2(6,11),Q3
     C(6,11)
      DIMENSION Q4(6,11),Q5(6,11),Q6(6,11),Q7(6,11),Q8(6,11),Q
     C9(6,11)
      DIMENSION DR1(6,11),DR2(6,11),FRX(3),W45(6,11),GYX(6,11)
     C,W9(6,11)
      DIMENSION P1(6,11),P2(6,11),P6(6,11),P7(6,11),W7(6,11),W
     C8(6,11)
      DIMENSION ANS1(6,11),ANS2(6,11),ANS3(6,11),ANS4(6,11),AN
     CS5(6,11)
      DIMENSION Q10(6,11),P3(6,11),P9(6,11)
      DIMENSION W21(6,11),CYL(6,11),EXPTL(6,11)
      DIMENSION W1(6,11),W2(6,11),W3(6,11),W4(6,11),W5(6,11),W
     C6(6,11)
C
C
      DATA W(1),W(2),W(3)/11.73,15.0,15.0/
      DATA F2Y(1),F2Y(2),F2Y(3)/1.405,3.48,3.48/
      DATA FRX(1),FRX(2),FRX(3)/17.87,44.47,116.07/
      F3Z=100.01
      G(1)=(W(1)-F2Y(1))/FRX(1)
      G(2)=(W(2)-F2Y(2))/FRX(2)
      G(3)=F3Z/FRX(3)
      CALL PLOTS(IDUM,IDUM,04)
C
C
C  THE PURPOSE OF THIS  PROGRAM IS TO CALCULATE THE QUANTITY
C  DA/DX AND TO COMPARE THE COMPONENTS OF THE CALCULATION,
C SPECIFICALLY
C  RELATIVE MAGNITUDES AND SIGNIFICANT VS INSIGNFINANT NUMBERS
```

```
C  WITH THE AID OF THESE NUMBERS MEANINGFUL APPROXIMATIONS
C  WILL BE MADE
C  TWO CASES ARE INVOLVED:  THE FIRST W/ A CYLINDER, THE
C  SECOND W/ BONE
C
C
C        C    Y    L    I    N    D    E    R
C
C
C
C CALCULATION OF DA/DX FOR CASE W/OUT MEMBRANE, SO=SIII
C           AND TERMWISE COMPARISON  :
C
C
C INPUT DATA
      READ(5,5000) MOST
 5000 FORMAT(I2)
      READ(5,5010) (FM(I),I=1,MOST)
 5010 FORMAT( 6F12.4)
      DO 1700 I=5,15
      J=I-4
 1700 AXI(J)=I
      DO 11 I=1,6
      READ(5,505) SPEC(I),DL(I),C(I),D(I),B(I)
 505  FORMAT(A8,4F6.2)
  11  CONTINUE
      READ(5,500) ((A(I,J),J=1,11),I=1,6),((DA(I,J),J=1,11),I=
     C1,6),
     C((ZI(I,J),J=1,11),I=1,6),((YI(I,J),J=1,11),I=1,6),
     C((DX(I,J),J=1,11),I=1,6)
 500  FORMAT(11F6.4,14X)
      DO 1825  I=1,6
      DO 1825  J=1,11
      E(I,J)=ZI(I,J)
 1825 CONTINUE
      DO 1703 I=1,6,2
```

```
      DO 1703 J=1,11
      L=I
      E(I,J)=E(I,J)/FM(L)
      IF(I.EQ.1) ARM(J)=E(I,J)
      IF(I.EQ.1) GO TO  1703
      IF(I.EQ.3) YES(J)=E(I,J)
      IF(I.EQ.3) GO TO  1703
      CAN(J)=E(I,J)
1703  CONTINUE
      CALL PLOT(13.0,3.0,-3)
      CALL PICTUR(4.0,4.0,'   SECTION NUMBER  ',19,
     1'MOM OF INERTIA CYL ',
     C19,AXI,ARM,11,.1,1,AXI,YES,11,.1,0,AXI,CAN,11,.1,2)
      DO 1702 I=2,6,2
      DO 1702 J=1,11
      L=I
      E(I,J)=E(I,J)/FM(L)
      IF(I.EQ.2) ARM(J)=E(I,J)
      IF(I.EQ.2) GO TO  1702
      IF(I.EQ.4) YES(J)=E(I,J)
      IF(I.EQ.4) GO TO  1702
      CAN(J)=E(I,J)
 1702 CONTINUE
      CALL PLOT(13.0,0.0,-3)
      CALL PICTUR(4.0,4.0,'   SECTION NUMBER  ',19,
     1'MOM OF INERTIA CYL ',
     C19,AXI,ARM,11,.1,1,AXI,YES,11,.1,0,AXI,CAN,11,.1,2)
      READ(5,510)  ((R1(I,J),J=1,11),I=1,6),((R2(I,J),J=1,11),I
     C=1,6),
     1((DR1(I,J),J=1,11),I=1,6),((DR2(I,J),J=1,11),I=1,6),
     2((X(I,J),J=1,11),I=1,6)
 510  FORMAT(11F6.2,14X)
      DO 1800 I=1,6
      DO 1800 J=1,11
      E(I,J)=A(I,J)
 1800 CONTINUE
```

```
      DO 1705 I=1,6,2
      DO 1705 J=1,11
      L=I+6
      E(I,J)=E(I,J)/FM(L)
      IF(I.EQ.1) ARM(J)=E(I,J)
      IF(I.EQ.1) GO TO  1705
      IF(I.EQ.3) YES(J)=E(I,J)
      IF(I.EQ.3) GO TO  1705
      CAN(J)=E(I,J)
 1705 CONTINUE
      CALL PLOT(13.0,0.0,-3)
      CALL PICTUR(4.0,4.0,'   SECTION NUMBER  ',19,
     1'CYLINDRICAL   AREAS',
     C19,AXI,ARM,11,.1,1,AXI,YES,11,.1,0,AXI,CAN,11,.1,2)
      DO 1706 I=2,6,2
      DO 1706 J=1,11
      L=I+6
      E(I,J)=E(I,J)/FM(L)
      IF(I.EQ.2) ARM(J)=E(I,J)
      IF(I.EQ.2) GO TO  1706
      IF(I.EQ.4) YES(J)=E(I,J)
      IF(I.EQ.4) GO TO  1706
      CAN(J)=E(I,J)
 1706 CONTINUE
      CALL PLOT(13.0,0.0,-3)
      CALL PICTUR(4.0,4.0,'   SECTION NUMBER  ',19,
     1'CYLINDRICAL   AREAS',
     C19,AXI,ARM,11,.1,1,AXI,YES,11,.1,0,AXI,CAN,11,.1,2)
      DO 100 I=1,6
      DO 99 K=1,2
      WRITE(6,642)G(K)
 642  FORMAT(1X,'GAMMA-YX =',2X,F6.3)
      WRITE(6,6)
 6    FORMAT(//,3X,'C',3X,'Y',3X,'L',3X,'I',3X,'N',3X,'D',3X,'
     CE',3X,'R'
     1,//)
```

```
      WRITE(6,601) SPEC(I)
 601  FORMAT(10X,'******',2X,A8,2X,'******',/)
      WRITE(6,600) (A(I,J),J=1,11),(DA(I,J),J=1,11),(ZI(I,J),J
     C=1,11),
     1(YI(I,J),J=1,11),(DX(I,J),J=1,11)
 600  FORMAT(/,' DATA CHECK',/,5(11F6.3,/),/)
      WRITE(6,600) (R1(I,J),J=1,11),(R2(I,J),J=1,11),(DR1(I,J)
     C,J=1,11),
     1(DR2(I,J),J=1,11),(X(I,J),J=1,11)
C
C CALCULATION OF TERMS
C
      DO 110 J=1,11
      XL(I,J)=X(I,J)-DL(I)
      W1(I,J)=R2(I,J)*DR2(I,J)/DX(I,J)+R1(I,J)*DR1(I,J)/DX(I,J
     C)
      W2(I,J)=(XL(I,J)*R2(I,J)*A(I,J)/(2.0*ZI(I,J)))*W1(I,J)
      W3(I,J)=(R2(I,J)+XL(I,J)*DR2(I,J)/DX(I,J))
      W4(I,J)=W3(I,J)-W2(I,J)
      W45(I,J)=(R1(I,J)**2.+R2(I,J)**2.)
      W5(I,J)=(A(I,J)**2.)*XL(I,J)*R2(I,J)*W45(I,J)*G(K)
      W6(I,J)=4.*ZI(I,J)**2.
      W7(I,J)=4.*ZI(I,J)*G(K)*(A(I,J)**2.)
      W21(I,J)=XL(I,J)*R2(I,J)*A(I,J)/(2.0*ZI(I,J))
      ANS1(I,J)=W7(I,J)*W4(I,J)/(W6(I,J)+W5(I,J))
      CYL(I,J)=DA(I,J)/DX(I,J)
 110  CONTINUE
      WRITE(6,606) SPEC(I),B(I),DL(I)
 606  FORMAT(/,' RESULTS FOR DA/DX COMPONENTS-NO MEMBRANE:',A8
     C,2F6.2,/)
      WRITE(6,646)
 646  FORMAT(/,'  THE COLUMN HEADINGS ARE: X,W1,W2,W3,W4,W5,W6
     C,W7,
     CW45,ANS')
      DO 120 J=1,11
      WRITE(6,605) X(I,J),W1(I,J),W2(I,J),W3(I,J),W4(I,J),W5(I
```

```
     C,J),
     1W6(I,J),W7(I,J),W45(I,J),ANS1(I,J)
 605  FORMAT (/,1X,9F10.6,10X,F10.6,/)
 120  CONTINUE
      WRITE(6,644) (CYL(I,J),J=1,11)
 644  FORMAT(/,1X,'CYL= ',11F10.6)
C
C APPROXIMATIONS   W2=W5=0 ;  AR2 DOMINANT - NO MEMBRANE
C
      DO 130 J=1,11
      ANS2(I,J)=(4.*A(I,J)*W3(I,J)/W45(I,J))*G(K)
      ANS3(I,J)=20.*A(I,J)*R2(I,J)*G(K)
 130  CONTINUE
      WRITE(6,610) (ANS2(I,J),J=1,11),(ANS3(I,J),J=1,11)
 610  FORMAT(/,' APPROXIMATIONS: W2=0 , AR2 DOMT',/,2(11F10.6,
     C/,1X))
C
C GAMMA-YX FOR NO MEMBRANE : S0=SIII
C
      DO 140 J=1,11
      W8(I,J)=(ZI(I,J)/A(I,J)**2.)*DA(I,J)/DX(I,J)
      W9(I,J)=(XL(I,J)*R2(I,J)/A(I,J))*DA(I,J)/DX(I,J)
      GYX(I,J)=W8(I,J)/(W3(I,J)-W2(I,J)-W9(I,J))
 140  CONTINUE
      WRITE(6,620) (W8(I,J),J=1,11),(W9(I,J),J=1,11),(GYX(I,J)
     C,J=1,11)
 620  FORMAT(' GAMMA-YX AND FACTORS',/,1X,'W8',2X,11F9.6,/,1X,
     C'W9',2X,
     111F9.6,/,1X,'GYX',1X,11F9.6,/)
 99   CONTINUE
C
C
C
C
C CALCULATION OF DA/DX FOR CASE WITHIN MEMBRANE, S0=SIII
C            AND TERMWISE COMPARISON  :
```

```
C     REGION II OMITTED , X ALWAYS>C>B        C<X<C+D
C
C
      M(I)=C(I)+D(I)/2.
      M1(I)=C(I)+D(I)
C
C CALCULATION OF TERMS
C
      DO 150 J=1,11
      P1(I,J)=W2(I,J)/XL(I,J)
      P2(I,J)=DR2(I,J)/DX(I,J)-P1(I,J)
      P7(I,J)=4.*ZI(I,J)*A(I,J)**2.
      Q1(I,J)=(XL(I,J)+DL(I)-M(I)-(X(I,J)-C(I))**2./(2.*D(I)))
     C*G(3)
      Q2(I,J)=XL(I,J)*G(2)-Q1(I,J)
      Q3(I,J)= (G(2)-G(3)*(1-(X(I,J)-C(I))/D(I)))*R2(I,J)
      P6(I,J)=(A(I,J)**2.)*W45(I,J)*R2(I,J)
      P9(I,J)=Q2(I,J)*P6(I,J)
      ANS4(I,J)=(Q3(I,J)+Q2(I,J)*P2(I,J))*P7(I,J)/(W6(I,J)+P9(
     CI,J))
 150  CONTINUE
      WRITE(6,625) SPEC(I),M1(I),DL(I)
 625  FORMAT(/,'RESULTS FOR DA/DX COMPONENTS FOR CASE WITHIN M
     CEMBRANE',/,'
     CAND IZ=IY:',2X, 'BONE',A8, 2X, 'C+D=', F6.2, 'L=', F6.2,
     C/)
      WRITE(6,647)
 647  FORMAT(/,' THE COLUMN HEADINGS ARE: X,P1,P2,P6,P7,P9,W6,
     CQ1,
     CQ2,Q3,ANS')
      DO 170 J=1,11
      WRITE(6,630) X(I,J),P1(I,J),P2(I,J),P6(I,J),P7(I,J),P9(I
     C,J),
     1W6(I,J),Q1(I,J),Q2(I,J),Q3(I,J),ANS4(I,J)
 630  FORMAT(1X,10F10.6,9X,F10.6,/)
 170  CONTINUE
```

```
100   CONTINUE
      DO 1805 I=1,6
      DO 1805 J=1,11
      E(I,J)=CYL(I,J)
1805  CONTINUE
      DO 1709 I=1,6,2
      DO 1709 J=1,11
      L=I+12
      E(I,J)=E(I,J)/FM(L)
      IF(I.EQ.1) ARM(J)=E(I,J)
      IF(I.EQ.1) GO TO  1709
      IF(I.EQ.3) YES(J)=E(I,J)
      IF(I.EQ.3) GO TO  1709
      CAN(J)=E(I,J)
1709  CONTINUE
      CALL PLOT(13.0,0.0,-3)
      CALL PICTUR(4.0,4.0,'   SECTION NUMBER  ',19,
     1'CYLINDER DA-DX  (L)',
     C19,AXI,ARM,11,.1,1,AXI,YES,11,.1,0,AXI,CAN,11,.1,2)
      DO 1710 I=2,6,2
      DO 1710 J=1,11
      L=I+12
      E(I,J)=E(I,J)/FM(L)
      IF(I.EQ.2) ARM(J)=E(I,J)
      IF(I.EQ.2) GO TO  1710
      IF(I.EQ.4) YES(J)=E(I,J)
      IF(I.EQ.4) GO TO  1710
      CAN(J)=E(I,J)
1710  CONTINUE
      CALL PLOT(13.0,0.0,-3)
      CALL PICTUR(4.0,4.0,'   SECTION NUMBER  ',19,
     1'CYLINDER DA-DX  (R)',
     C19,AXI,ARM,11,.1,1,AXI,YES,11,.1,0,AXI,CAN,11,.1,2)
      DO 1810 I=1,6
      DO 1810 J=1,11
      E(I,J)=ANS4(I,J)
```

```
 1810 CONTINUE
      DO 1715 I=1,6,2
      DO 1715 J=1,11
      L=I+18
      E(I,J)=E(I,J)/FM(L)
      IF(I.EQ.1) ARM(J)=E(I,J)
      IF(I.EQ.1) GO TO  1715
      IF(I.EQ.3) YES(J)=E(I,J)
      IF(I.EQ.3) GO TO  1715
      CAN(J)=E(I,J)
 1715 CONTINUE
      CALL PLOT(13.0,0.0,-3)
      CALL PICTUR(4.0,4.0,'   SECTION NUMBER  ',19,
     1'CYL DA-DX MEMB  (L)',
     C19,AXI,ARM,11,.1,1,AXI,YES,11,.1,0,AXI,CAN,11,.1,2)
      DO 1716 I=2,6,2
      DO 1716 J=1,11
      L=I+18
      E(I,J)=E(I,J)/FM(L)
      IF(I.EQ.2) ARM(J)=E(I,J)
      IF(I.EQ.2) GO TO  1716
      IF(I.EQ.4) YES(J)=E(I,J)
      IF(I.EQ.4) GO TO  1716
      CAN(J)=E(I,J)
 1716 CONTINUE
      CALL PLOT(13.0,0.0,-3)
      CALL PICTUR(4.0,4.0,'   SECTION NUMBER  ',19,
     1'CYL DA-DX MEMB  (R)',
     C19,AXI,ARM,11,.1,1,AXI,YES,11,.1,0,AXI,CAN,11,.1,2)
C
C
C
C        A     C     T     U     A     L
C
C
C
```

```
C CALCULATION OF DA/DX W/OUT MEMBRANE ,SO=SIII
C
C EQUATIONS USED ARE THE SAME AS THOSE FOR CYLINDER
C
      READ(5,555)  ((A(I,J),J=1,11),I=1,6),((DA(I,J),J=1,11),I=1,6),
     C((ZI(I,J),J=1,11),I=1,6),((YI(I,J),J=1,11),I=1,6)
 555  FORMAT(11F6.3,14X)
      DO 1000 I=1,6
      DO 999 K=1,2
      WRITE(6,16)
  16  FORMAT(//,3X,'A',3X,'C',3X,'T',3X,'U',3X,'A',3X,'L',//)
      WRITE(6,611) SPEC(I)
      WRITE(6,642)
 611  FORMAT(10X,'******',2X,A8,2X,'******',/)
      WRITE(6,666)  (A(I,J),J=1,11),(DA(I,J),J=1,11),(ZI(I,J),J
     C=1,11),
     1(YI(I,J),J=1,11)
 666  FORMAT(/,' DATA CHECK',/,4(11F6.3,/),/)
      DO 1111 J=1,11
C
C
C  CALCULATION OF TERMS:  ONLY IZ NEEDS TO BE CONSIDERED.
C  WITH NO MEMBRANE FORCE, THERE ARE NO FORCES IN THE X-Y
C  PLANE.  RECALL FROM THE THESIS TEXT (CHAPT.III) THAT STRESS
C  =FORCE/AREA+(THE RESULTANT MOMENT)*Y/(MOMENT OF INERTIA).
C
      W1(I,J)=R2(I,J)*DR2(I,J)/DX(I,J)+R1(I,J)*DR1(I,J)/DX(I,J
     C)
      W2(I,J)=(XL(I,J)*R2(I,J)*A(I,J)/(2.0*ZI(I,J)))*W1(I,J)
      W3(I,J)=(R2(I,J)+XL(I,J)*DR2(I,J)/DX(I,J))
      W4(I,J)=W3(I,J)-W2(I,J)
      W45(I,J)=(R1(I,J)**2.+R2(I,J)**2.)
      W5(I,J)=(A(I,J)**2.)*XL(I,J)*R2(I,J)*W45(I,J)*G(K)
      W6(I,J)=4.*ZI(I,J)**2.
      W7(I,J)=4.*ZI(I,J)*G(K)*(A(I,J)**2.)
      W21(I,J)=XL(I,J)*R2(I,J)*A(I,J)/(2.0*ZI(I,J))
```

```
      ANS1(I,J)=W7(I,J)*W4(I,J)/(W6(I,J)+W5(I,J))
      EXPTL(I,J)=DA(I,J)/DX(2,J)
C
C APPROXIMATIONS   W2=W5=0 ;  AR2 DOMINANT - NO MEMBRANE
C
      ANS2(I,J)=(4.*A(I,J)*W3(I,J)/W45(I,J))*G(K)
      ANS3(I,J)=20.*A(I,J)*R2(I,J)*G(K)
C
C GAMMA-YX FOR NO MEMBRANE : S0=SIII
C
      W8(I,J)=(ZI(I,J)/A(I,J)**2.)*DA(I,J)/DX(I,J)
      W9(I,J)=(XL(I,J)*R2(I,J)/A(I,J))*DA(I,J)/DX(I,J)
      GYX(I,J)=W8(I,J)/(W3(I,J)-W2(I,J)-W9(I,J))
 1111 CONTINUE
      WRITE(6,661) SPEC(I),M1(I),DL(I)
 661  FORMAT(/,' RESULTS FOR DA/DX COMPONENTS-NO MEMBRANE:',A8
     C,2F6.2,/)
      WRITE(6,6422)
 6422 FORMAT(/,' NO IY - NO MEMBRANE - USING BONE DATA')
      WRITE(6,648)
 648  FORMAT(/,' THE COLUMN HEADINGS ARE: X,W1,W2,W3,W4,W5,W6,W7,
     CW45,ANS')
      DO 1120 J=1,11
      WRITE(6,665) X(I,J),W1(I,J),W2(I,J),W3(I,J),W4(I,J),W5(I
     C,J),
     1W6(I,J),W7(I,J),W45(I,J),ANS1(I,J)
 665  FORMAT (/,1X,9F10.6,10X,F10.6,/)
 1120 CONTINUE
      WRITE(6,645)(EXPTL(I,J),J=1,11)
 645  FORMAT(/,1X,'EXPTL= ',11F10.6)
      WRITE(6,616) (ANS2(I,J),J=1,11),(ANS3(I,J),J=1,11)
 616  FORMAT(/,' APPROXIMATIONS: W2=0 , AR2 DOMT',/,2(11F10.6,
     C/,1X))
      WRITE(6,662) (W8(I,J),J=1,11),(W9(I,J),J=1,11),(GYX(I,J)
     C,J=1,11)
 662  FORMAT(' GAMMA-YX AND FACTORS',/,1X,'W8',2X,11F9.6,/,1X,
```

```
     C'W9',2X,
     111F9.6,/,1X,'GYX',1X,11F9.6,/)
 999  CONTINUE
C
C CALCULATION OF DA/DX WITHIN MEMBRANE
C CHANGES IN EQNS ARE A RESULT OF IZ NOT EQUAL TO IY
C
C
C CALCULATION OF TERMS
C
      DO 160 J=1,11
      W2(I,J)=(XL(I,J)*R2(I,J)*A(I,J)/(2.0*ZI(I,J)))*W1(I,J)
      P1(I,J)=W2(2,J)/XL(I,J)
      M(I)=C(I)+D(I)/2.
      M1(I)=C(I)+D(I)
      P3(I,J)=DR2(I,J)/DX(I,J)-P1(I,J)*ZI(I,J)/YI(I,J)
      Q4(I,J)=(4.*A(I,J)**2.)*(ZI(I,J)**2.)*YI(I,J)**2.
      Q5(I,J)=R2(I,J)*(1-(X(I,J)-C(I))/D(I))
      Q6(I,J)=(Q5(I,J)+Q1(I,J)*P3(I,J)/G(3))*G(3)/YI(I,J)
      Q7(I,J)=W4(I,J)*G(2)/ZI(I,J)
      Q8(I,J)=(XL(I,J)*YI(I,J)**2.)*G(2)
      Q9(I,J)=Q4(I,J)/A(I,J)**2.
      Q10(I,J)=(Q8(I,J)+Q1(I,J)*ZI(I,J)**2.)*P6(I,J)
      ANS5(I,J)=(Q7(I,J)-Q6(I,J))*Q4(I,J)/(Q9(I,J)+Q10(I,J))
 160  CONTINUE
      WRITE(6,655) SPEC(I),M1(I),DL(I)
 655  FORMAT(/,' RESULTS FOR DA/DX COMPONENTS WITHIN MEMBRANE:
     C',2X,
     1'BONE',A8,2X,'C+D=',F6.2,'L=',F6.2,/)
      WRITE(6,6428)
 6428 FORMAT(/,' THE COLUMN HEADINGS ARE: X,Q4,Q5,Q6,Q7,Q8,Q9,
     CQ10,P3,
     1ANS5',/)
      DO 175 J=1,11
      WRITE(6,660) X(I,J),Q4(I,J),Q5(I,J),Q6(I,J),Q7(I,J),Q8(I
     C,J),
```

```
    109(I,J),Q10(I,J),P3(I,J),ANS5(I,J)
660  FORMAT(1X,9F10.6,10X,F10.6,/)
175  CONTINUE
1000 CONTINUE
     DO 1815 I=1,6
     DO 1815 J=1,11
     E(I,J)=ANS5(I,J)
1815 CONTINUE
     DO 1719 I=1,6,2
     DO 1719 J=1,11
     L=I+24
     E(I,J)=E(I,J)/FM(L)
     IF(I.EQ.1) ARM(J)=E(I,J)
     IF(I.EQ.1) GO TO  1719
     IF(I.EQ.3) YES(J)=E(I,J)
     IF(I.EQ.3) GO TO  1719
     CAN(J)=E(I,J)
1719 CONTINUE
     CALL PLOT(13.0,0.0,-3)
     CALL PICTUR(4.0,4.0,'   SECTION NUMBER  ',19,
    U'BONE DA-DX MEMB (L)',
    C19,AXI,ARM,11,.1,1,AXI,YES,11,.1,0,AXI,CAN,11,.1,2)
     DO 1720 I=2,6,2
     DO 1720 J=1,11
     L=I+24
     E(I,J)=E(I,J)/FM(L)
     IF(I.EQ.2) ARM(J)=E(I,J)
     IF(I.EQ.2) GO TO  1720
     IF(I.EQ.4) YES(J)=E(I,J)
     IF(I.EQ.4) GO TO  1720
     CAN(J)=E(I,J)
1720 CONTINUE
     CALL PLOT(13.0,0.0,-3)
     CALL PICTUR(4.0,4.0,'   SECTION NUMBER  ',19,
    U'BONE DA-DX MEMB (R)',
    C19,AXI,ARM,11,.1,1,AXI,YES,11,.1,0,AXI,CAN,11,.1,2)
```

```
      DO 1820 I=1,6
      DO 1820 J=1,11
      E(I,J)=EXPTL(I,J)
 1820 CONTINUE
      DO 1725 I=1,6,2
      DO 1725 J=1,11
      L=I+30
      E(I,J)=E(I,J)/FM(L)
      IF(I.EQ.1) ARM(J)=E(I,J)
      IF(I.EQ.1) GO TO  1725
      IF(I.EQ.3) YES(J)=E(I,J)
      IF(I.EQ.3) GO TO  1725
      CAN(J)=E(I,J)
 1725 CONTINUE
      CALL PLOT(13.0,0.0,-3)
      CALL PICTUR(4.0,4.0,'   SECTION NUMBER  ',19,
     1'EXPERIMENTAL DA-DX ',
     C19,AXI,ARM,11,.1,1,AXI,YES,11,.1,0,AXI,CAN,11,.1,2)
      DO 1726 I=2,6,2
      DO 1726 J=1,11
      L=I+30
      E(I,J)=E(I,J)/FM(L)
      IF(I.EQ.2) ARM(J)=E(I,J)
      IF(I.EQ.2) GO TO  1726
      IF(I.EQ.4) YES(J)=E(I,J)
      IF(I.EQ.4) GO TO  1726
      CAN(J)=E(I,J)
 1726 CONTINUE
      CALL PLOT(13.0,0.0,-3)
      CALL PICTUR(4.0,4.0,'   SECTION NUMBER  ',19,
     1'EXPERIMENTAL DA-DX ',
     C19,AXI,ARM,11,.1,1,AXI,YES,11,.1,0,AXI,CAN,11,.1,2)
      DO 1830 I=1,6
      DO 1830 J=1,11
      E(I,J)=A(I,J)
 1830 CONTINUE
```

```
      DO 1729 I=1,6,2
      DO 1729 J=1,11
      L=I+36
      E(I,J)=E(I,J)/FM(L)
      IF(I.EQ.1) ARM(J)=E(I,J)
      IF(I.EQ.1) GO TO  1729
      IF(I.EQ.3) YES(J)=E(I,J)
      IF(I.EQ.3) GO TO  1729
      CAN(J)=E(I,J)
 1729 CONTINUE
      CALL PLOT(13.0,0.0,-3)
      CALL PICTUR(4.0,4.0,'   SECTION NUMBER  ',19,
     1'EXPERIMENTAL AREAS ',
     C19,AXI,ARM,11,.1,1,AXI,YES,11,.1,0,AXI,CAN,11,.1,2)
      DO 1730 I=2,6,2
      DO 1730 J=1,11
      L=I+36
      E(I,J)=E(I,J)/FM(L)
      IF(I.EQ.2) ARM(J)=E(I,J)
      IF(I.EQ.2) GO TO  1730
      IF(I.EQ.4) YES(J)=E(I,J)
      IF(I.EQ.4) GO TO  1730
      CAN(J)=E(I,J)
 1730 CONTINUE
      CALL PLOT(13.0,0.0,-3)
      CALL PICTUR(4.0,4.0,'   SECTION NUMBER  ',19,
     1'EXPERIMENTAL AREAS ',
     C19,AXI,ARM,11,.1,1,AXI,YES,11,.1,0,AXI,CAN,11,.1,2)
      DO 1835 I=1,6
      DO 1835 J=1,11
      E(I,J)=R1(I,J)
 1835 CONTINUE
      DO 1735 I=1,6,2
      DO 1735 J=1,11
      L=I+42
      E(I,J)=E(I,J)/FM(L)
```

```
      IF(I.EQ.1)  ARM(J)=E(I,J)
      IF(I.EQ.1)  GO TO  1735
      IF(I.EQ.3)  YES(J)=E(I,J)
      IF(I.EQ.3)  GO TO  1735
      CAN(J)=E(I,J)
 1735 CONTINUE
      CALL PLOT(13.0,0.0,-3)
      CALL PICTUR(4.0,4.0,'   SECTION NUMBER  ',19,
     1'INNER RADIUS AV (L)',
     C19,AXI,ARM,11,.1,1,AXI,YES,11,.1,0,AXI,CAN,11,.1,2)
      DO 1736 I=2,6,2
      DO 1736 J=1,11
      L=I+42
      E(I,J)=E(I,J)/FM(L)
      IF(I.EQ.2)  ARM(J)=E(I,J)
      IF(I.EQ.2)  GO TO  1736
      IF(I.EQ.4)  YES(J)=E(I,J)
      IF(I.EQ.4)  GO TO  1736
      CAN(J)=E(I,J)
 1736 CONTINUE
      CALL PLOT(13.0,0.0,-3)
      CALL PICTUR(4.0,4.0,'   SECTION NUMBER  ',19,
     1'INNER RADIUS AV (R)',
     C19,AXI,ARM,11,.1,1,AXI,YES,11,.1,0,AXI,CAN,11,.1,2)
      DO 1840 I=1,6
      DO 1840 J=1,11
      E(I,J)=R2(I,J)
 1840 CONTINUE
      DO 1739 I=1,6,2
      DO 1739 J=1,11
      L=I+48
      E(I,J)=E(I,J)/FM(L)
      IF(I.EQ.1)  ARM(J)=E(I,J)
      IF(I.EQ.1)  GO TO  1739
      IF(I.EQ.3)  YES(J)=E(I,J)
      IF(I.EQ.3)  GO TO  1739
```

```
      CAN(J)=E(I,J)
 1739 CONTINUE
      CALL PLOT(13.0,0.0,-3)
      CALL PICTUR(4.0,4.0,'   SECTION NUMBER  ',19,
     1'OUTER RADIUS AV (L)',
     C19,AXI,ARM,11,.1,1,AXI,YES,11,.1,0,AXI,CAN,11,.1,2)
      DO 1740 I=2,6,2
      DO 1740 J=1,11
      L=I+48
      E(I,J)=E(I,J)/FM(L)
      IF (I.EQ.2) ARM(J)=E(I,J)
      IF(I.EQ.2) GO TO  1740
      IF(I.EQ.4) YES(J)=E(I,J)
      IF (I.EQ.4) GO TO 1740
      CAN(J)=E(I,J)
 1740 CONTINUE
      CALL PLOT(13.0,0.0,-3)
      CALL PICTUR(4.0,4.0,'   SECTION NUMBER  ',19,
     1'OUTER RADIUS AV (R)',
     C19,AXI,ARM,11,.1,1,AXI,YES,11,.1,0,AXI,CAN,11,.1,2)
      DO 1806 I=1,6
      DO 1806 J=1,11
      E(I,J)=ZI(I,J)
1806  CONTINUE
      DO 1713 I=1,6,2
      DO 1713 J=1,11
      L=I+54
      E(I,J)=E(I,J)/FM(L)
      IF(I.EQ.1) ARM(J)=E(I,J)
      IF(I.EQ.1) GO TO  1713
      IF(I.EQ.3) YES(J)=E(I,J)
      IF(I.EQ.3) GO TO  1713
      CAN(J)=E(I,J)
1713  CONTINUE
      CALL PLOT(13.0,0.0,-3)
      CALL PICTUR(4.0,4.0,'   SECTION NUMBER  ',19,
```

```
     1'MOM OF INERTIA IZ L',
     C19,AXI,ARM,11,.1,1,AXI,YES,11,.1,0,AXI,CAN,11,.1,2)
      DO 1712 I=2,6,2
      DO 1712 J=1,11
      L=I+54
      E(I,J)=E(I,J)/FM(L)
      IF(I.EQ.2) ARM(J)=E(I,J)
      IF(I.EQ.2) GO TO  1712
      IF(I.EQ.4) YES(J)=E(I,J)
      IF(I.EQ.4) GO TO  1712
      CAN(J)=E(I,J)
1712  CONTINUE
      CALL PLOT(13.0,0.0,-3)
      CALL PICTUR(4.0,4.0,'   SECTION NUMBER  ',19,
     1'MOM OF INERTIA IZ R',
     C19,AXI,ARM,11,.1,1,AXI,YES,11,.1,0,AXI,CAN,11,.1,2)
      DO 1821 I=1,6
      DO 1821 J=1,11
      E(I,J)=YI(I,J)
1821  CONTINUE
      DO 1717 I=1,6,2
      DO 1717 J=1,11
      L=I+60
      E(I,J)=E(I,J)/FM(L)
      IF(I.EQ.1) ARM(J)=E(I,J)
      IF(I.EQ.1) GO TO  1717
      IF(I.EQ.3) YES(J)=E(I,J)
      IF(I.EQ.3) GO TO  1717
      CAN(J)=E(I,J)
1717  CONTINUE
      CALL PLOT(13.0,0.0,-3)
      CALL PICTUR(4.0,4.0,'   SECTION NUMBER  ',19,
     1'MOM OF INERTIA IY L',
     C19,AXI,ARM,11,.1,1,AXI,YES,11,.1,0,AXI,CAN,11,.1,2)
      DO 1718 I=2,6,2
      DO 1718 J=1,11
```

```
      L=I+60
      E(I,J)=E(I,J)/FM(L)
      IF(I.EQ.2) ARM(J)=E(I,J)
      IF(I.EQ.2) GO TO  1718
      IF(I.EQ.4) YES(J)=E(I,J)
      IF(I.EQ.4) GO TO  1718
      CAN(J)=E(I,J)
1718  CONTINUE
      CALL PLOT(13.0,0.0,-3)
      CALL PICTUR(4.0,4.0,'   SECTION NUMBER  ',19,
     1'MOM OF INERTIA IY R',
     C19,AXI,ARM,11,.1,1,AXI,YES,11,.1,0,AXI,CAN,11,.1,2)
      CALL ENDPLT(16.0,5.0,999)
      STOP
      END
```

ACKNOWLEDGEMENTS

"It is comforting to know that whatever happens, whether good or bad, there is a friend who will understand." Susan Polis Schutz

It is impossible for me to convey fully the warmth and gratitude I feel for my advisor, Professor Margaret Love Agnes MacVicar. Her support and encouragement, throughout the difficulties which I had undergone, went beyond that of an advisor. Her ability to stimulate people to strive for that which they most desire, has given me a positive outlook towards the past hardships and the new ones ahead. Thanks, Margaret.

There are many other individuals whom I would like to thank and acknowledge, and to have them share in my happiness and pride today by becoming a part of my thesis. Thanks to you all.....

Professor Judith Bostock
Professor Robert Rose
Mrs. Myra Rodriques
Maggie Lettvin
Special Fellowship Comm.
Keith Milkove
Jay, Walter, Juan, Mansour
Holly Carter, Bill, Benji
Carnel Hoover
Charlotte Simmonds
Shirley Jackson
Sherry Worley
Greg Smith
Margaret Browning
Fred Wilson
I. Puffer
Professor James Young
Dr. Mary Rowe
Dr. Clarence Williams
Paul Townsend & Family
The Hulsizers
Vicky Diaduik
Mary Hope
Monica Oliver
Violet Burch
Barbara Wyatt
Phil Jackman
Bill Westphal
Diane Eulian
Lucy Kelly
Art Gregor
Gunther Arndt

ACKNOWLEDGEMENTS (cont.)

Jinx Hinton
Jim Bishop
Pam Cameron
Rosa Hunt
Pat Garrison

Sam Nixon
John Turner
John Carney
St. Paul's

and FAMILY

Mom
Dad
Pop
Debbie
Rose
Pee Wee

Grandma Alene
Grandpa Jack
Grandma Maggie
Jackie
Sharon
Bea

Karl.....

And special, special thanks to you,

KEVIN